MAX-PLANCK-INSTITUT
FÜR METEOROLOGIE

Tropical Tropospheric Temperatures, Warming and Involved Mechanisms

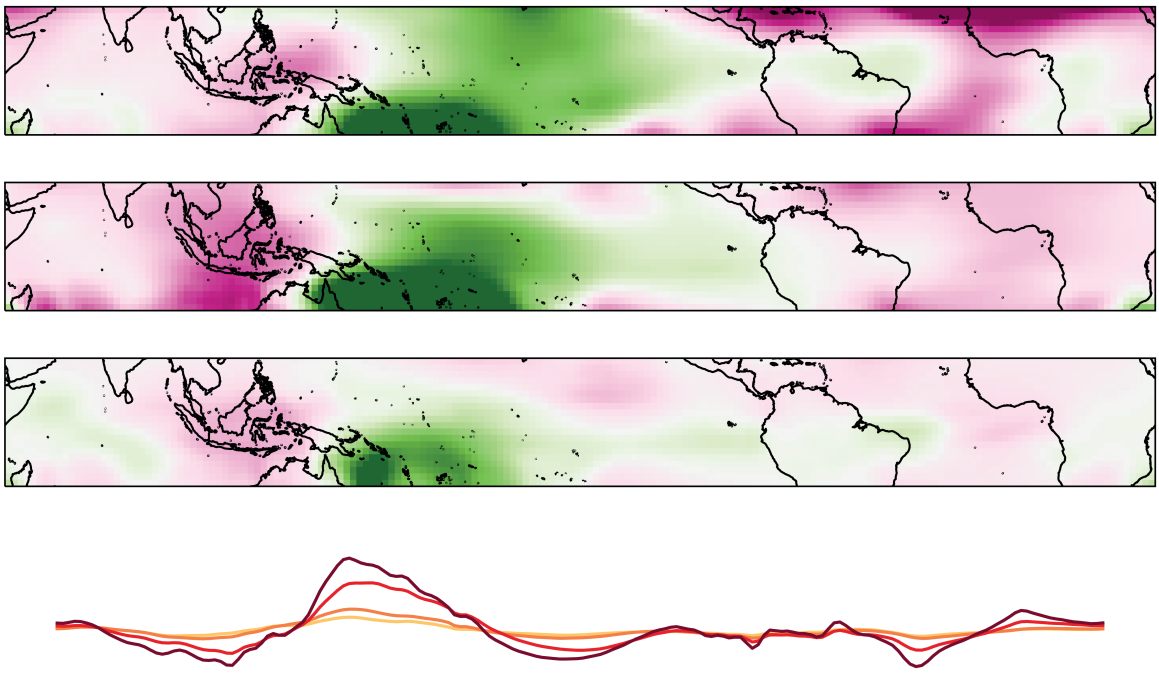

Paul Peter Keil

Hamburg 2023

Berichte zur Erdsystemforschung 268
Reports on Earth System Science 2023

Hinweis

Die Berichte zur Erdsystemforschung werden vom Max-Planck-Institut für Meteorologie in Hamburg in unregelmäßiger Abfolge herausgegeben.

Sie enthalten wissenschaftliche und technische Beiträge, inklusive Dissertationen.

Die Beiträge geben nicht notwendigerweise die Auffassung des Instituts wieder.

Die "Berichte zur Erdsystemforschung" führen die vorherigen Reihen "Reports" und "Examensarbeiten" weiter.

Anschrift / Address

Max-Planck-Institut für Meteorologie
Bundesstrasse 53
20146 Hamburg
Deutschland

Tel./Phone: +49 (0)40 4 11 73 - 0
Fax: +49 (0)40 4 11 73 - 298

name.surname@mpimet.mpg.de
www.mpimet.mpg.de

Notice

The Reports on Earth System Science are published by the Max Planck Institute for Meteorology in Hamburg. They appear in irregular intervals.

They contain scientific and technical contributions, including PhD theses.

The Reports do not necessarily reflect the opinion of the Institute.

The "Reports on Earth System Science" continue the former "Reports" and "Examensarbeiten" of the Max Planck Institute.

Layout

Bettina Diallo and Norbert P. Noreiks
Communication

Copyright

Tropical Tropospheric Temperatures, Warming and Involved Mechanisms

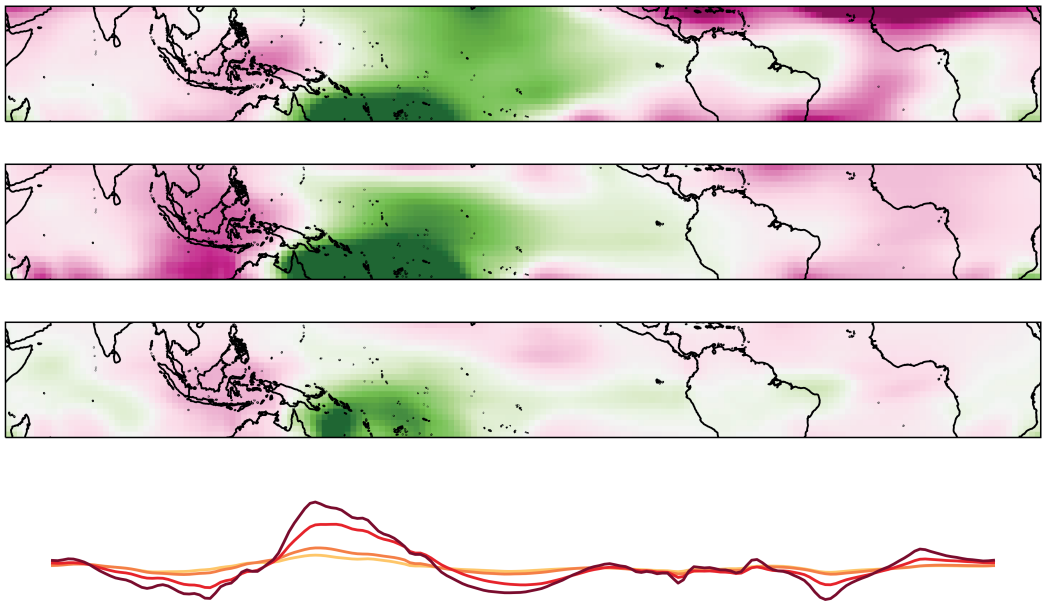

Paul Peter Keil

Hamburg 2023

Paul Peter Keil
aus Seeheim-Jugenheim, Deutschland

Max-Planck-Institut für Meteorologie
The International Max Planck Research School on Earth System Modelling
(IMPRS-ESM)
Bundesstrasse 53
20146 Hamburg

Tag der Disputation: 16. Dezember 2022

Folgende Gutachter empfehlen die Annahme der Dissertation:
Prof. Dr. Bjorn Stevens
Dr. Hauke Schmidt

Vorsitzender des Promotionsausschusses:
Prof. Dr. Hermann Held

Dekan der MIN-Fakultät:
Prof. Dr.-Ing. Norbert Ritter

Titelgrafik: *Warming pattern in the upper troposphere simulated by the ICON-A model and reproduced in a simple Gill model. The lines illustrate zonal temperature gradients along the equator for varying dissipation strength.* Credit: Paul Keil

Berichte zur Erdsystemforschung / Max-Planck-Institut für Meteorologie 268
Reports on Earth System Science / Max Planck Institute for Meteorology 2023

ISSN 1614-1199 - doi: 10.17617/2.3509472

To my Daughter Zoe

ACKNOWLEDGMENTS

The road leading up to this dissertation has been long and windy, and many people have helped me on this path, some of which I will unavoidably forget.

First of all, I would like to dearly thank Hauke Schmidt, my supervisor, colleague and football teammate. His ability to clear my confusion, identify what the missing link is and how we might find it, helped me countless times. Working with him made the daily business of this project considerably easier and more fun. If we did get stuck, Bjorn Stevens was there to pull us out of the mud, and I also owe many thanks to him. His vision to ask the big questions inspired many aspects of this project (the best day of the whole PhD was maybe the day he showed me the paper by A. Gill titled "Some simple solutions for heat-induced tropical circulation."). I learned so much from both of you. I would also like to thank my panel chair Dirk Notz for his encouraging words. If there had been graver problems, I am confident he could have helped me.

I also owe great thanks to Mike Byrne, who hosted me at the University of St Andrews, and made me feel very welcome. The opportunity to discuss my project with him and his group ultimately sparked a very fruitful collaboration.

I am grateful that Jiawei Bao and Hans Segura (fue papayita!) helped me out many times and allowed me to test my ideas on them. I would like to thank the writing club and others for their feedback, which helped me immensely. Special thanks to Luca Schmidt, Diego Jimenez, David Nielsen, Geet George, Fanny Lhardy, Laura Köhler, Marc Alessi. In addition, I need to thank Sebastian Rast, Thibaut Dauhut, Lukas Kluft, George Datseris, Matthias Retsch, Clarissa Kroll, Cathy Hohenegger, Arim Yoon, Abisha Gnanaraj, Dian Putrasahan, Moritz Günther, Christian Wengel, Claudia Stephan and everyone else from the GCC and PC groups. For emotional supoport and distraction I would like to thank the MPI football team, my fellow PhD reps Elliot and Mia, the Schlump zoom group for helping me keep my sanity during Covid and some great holidays afterwards. Antje Weitz and the IMPRS office also deserve special thanks for always being there and helping me through all of the bureaucracy.

Finally, this would not have been possible without my girlfriend Freddy. Thank you from the bottom of my heart for your unconditional support and providing distraction, even while you were carrying our baby for the final few months. I am also incredibly thankful to my parents for supporting me through all those years, and they are the reason I was able to get to this position in the first place.

ABSTRACT

In this dissertation I investigate the vertical and horizontal thermal structure of the tropical troposphere and its changes under greenhouse gas forcing. The vertical profile of tropospheric warming has been a controversial topic and received a lot of attention in recent years, as climate models show stronger upper tropospheric warming than suggested by observations. While progress has been made, it is still not entirely clear what mechanisms control lapse rates and the vertical profile of warming. In contrast, the horizontal thermal structure of the tropical troposphere has received less attention, as it is often assumed to be fairly uniform. The mechanisms behind the horizontal pattern of tropospheric warming remain unexplained until now.

In the first part of this dissertation I quantify the variations in tropical lapse rates in conventional climate models, represented here through the CMIP6 ensemble, and explore reasons for these variations. Because the vertical temperature structure in the tropics is primarily set by convection, I hypothesise that the representation of convection and associated small scale processes are responsible. I reproduce these variations in perturbed physics experiments with the global atmospheric model ICON-A, in which I vary autoconversion and entrainment parameters. For smaller autoconversion values, additional freezing enthalpy from the cloud water that is not precipitated warms the upper troposphere. Smaller entrainment rates also lead to a warmer upper troposphere, as convection and thus latent heating reaches higher altitudes. Furthermore, I show that according to most radiosonde datasets all CMIP6 AMIP simulations overestimate recent upper tropospheric warming. Additionally, all radiosonde datasets agree that climate models on average overestimate the amount of upper tropospheric warming for a given lower tropospheric warming. I demonstrate that increased entrainment rates reduce this overestimation, likely because of the reduction of latent heat release in the upper troposphere. These results suggest that imperfect convection parameterisations are responsible for a considerable part of the variations in tropical lapse rates and also part of the possible overestimation of warming compared to the observations. A rigorous assessment of the vertical profile of tropospheric warming remains challenging, because observations continue to disagree considerably with each other.

In the second part of this dissertation I demonstrate that projected tropospheric warming is horizontally inhomogeneous in CMIP6 models, as well as in a storm resolving climate model. I relate the upper tropospheric warming pattern to changes in the sea surface temperature pattern that reorganise convection and circulation, causing spatial shifts in convective heating. Using the classical Gill model for tropical circulation forced by the convective heating changes, the horizontal pattern of warming in climate models can be reproduced. Thus, the simple Gill model captures the mechanisms that determine the main features of the warming pattern. Close to the equator anomalous geopotential gradients are balanced by the dissipation term in the Gill model. The optimal dissipation timescale to reproduce the warming pattern varies depending on the climate model, and is between 1 and 10 days. This suggests that processes represented by the dissipation term that act on these timescales are essential for shaping the warming pattern. These processes likely include but are not limited to eddy momentum flux, advection and radiative cooling. While climate models show a large spread in projections of tropical sea surface temperature and precipitation changes, our results imply that once these predictions

improve, our confidence in the predicted upper tropospheric warming pattern should also increase.

ZUSAMMENFASSUNG

In dieser Dissertation untersuche ich die vertikale und horizontale thermische Struktur der tropischen Troposphäre und ihre Veränderungen unter Treibhausgasemissionen. Das vertikale Profil der Erwärmung der Troposphäre war in den letzten Jahren ein kontroverses Thema, da Klimamodelle die Erwärmung der oberen Troposphäre im Vergleich zu Observationsdaten oftmals überschätzen. Zwar wurden Fortschritte erzielt, aber es ist immer noch nicht vollständig klar, welche Mechanismen das Temperaturprofil und dessen Erwärmung beeinflussen können. Im Gegensatz dazu wurde der horizontalen thermischen Struktur der tropischen Troposphäre weniger Aufmerksamkeit gewidmet, da man oft davon ausgeht, dass sie ziemlich einheitlich ist. Die Mechanismen hinter dem horizontalen Muster der Erwärmung der Troposphäre sind bislang ungeklärt.

Im ersten Teil dieser Dissertation quantifiziere ich die Unterschiede der tropischen vertikalen Temperaturgradienten zwischen CMIP6-Modellen und untersuche die Gründe für diese Unterschiede. Da die vertikale Temperaturstruktur in den Tropen in erster Linie durch Konvektion bestimmt wird, stelle ich die Hypothese auf, dass die Darstellung der Konvektion und die damit verbundenen kleinskaligen Prozesse für die Unterschiede verantwortlich sind. Ich reproduziere diese Variationen in Experimenten mit veränderter Physik im globalen Atmosphärenmodell ICON-A, in denen ich Autokonversions- und Entrainmentparameter variiere. Bei kleineren Autokonversionswerten erwärmt die zusätzliche Gefrierenthalpie des nicht ausgefallenen Wolkenwassers die obere Troposphäre. Kleinere Entrainmentraten führen ebenfalls zu einer wärmeren oberen Troposphäre, da die Konvektion und damit die latente Erwärmung in größere Höhen reicht. Darüber hinaus zeige ich, dass alle CMIP6-AMIP-Simulationen die aktuelle Erwärmung der oberen Troposphäre gemäß den meisten Radiosondendatensätzen überschätzen. Außerdem stimmen alle Radiosondendatensätze darin überein, dass die Klimamodelle im Durchschnitt die Erwärmung der oberen Troposphäre bei einer gegebenen Erwärmung der unteren Troposphäre überschätzen. Erhöhte Entrainmentraten verringern diese Überschätzung, wahrscheinlich aufgrund der geringeren Freisetzung latenter Wärme in der oberen Troposphäre. Diese Ergebnisse legen nahe, dass unvollkommene Konvektionsparametrisierungen für einen beträchtlichen Teil der Unterschiede der tropischen vertikalen Temperaturgradienten und auch für einen Teil der möglichen Überschätzung der Erwärmung im Vergleich zu den Beobachtungen verantwortlich sind. Eine Bewertung des vertikalen Profils der Erwärmung der Troposphäre ist nach wie vor mit Unsicherheiten verbunden, da die Beobachtungen weiterhin erheblich voneinander abweichen.

Im zweiten Teil dieser Dissertation zeige ich, dass die projizierte Erwärmung der Troposphäre in CMIP6-Modellen sowie in einem sturmauflösenden Klimamodell räumlich inhomogen ist. Das Muster der Erwärmung der oberen Troposphäre steht mit Änderungen der Meeresoberflächentemperatur in Verbindung. Die Meeresoberflächentemperaturen verändern Konvektion und Zirkulation und versursachen dadurch räumliche Verschiebungen der konvektiven Heizraten. Mit Hilfe des klassischen Gill-Modells für tropische Zirkulation, das ich durch die Veränderungen der konvektiven Heizraten antreibe, können die unterschiedlichen Erwärmungsmuster, die von den globalen Klimamodelle simuliert werden, reproduziert werden. Dementsprechend beinhaltet das simple Gill Model die wesentlichen Prozesse, die das Erwärmungsmuster bestimmen. Das Antreiben des

Gill-Modells mit Veränderungen der Heizraten aus einer bestimmten Region zeigt, wie lokale troposphärische Temperaturänderungen von lokalen Änderungen der Konvektion abhängen. In der Nähe des Äquators werden Geopotentialgradienten durch den Dissipationsterm im Gill-Modell balanciert. Die optimale Dissipationszeitskala zur Reproduktion des Erwärmungsmusters variiert je nach Klimamodell und liegt zwischen 1 und 10 Tagen. Dies deutet darauf hin, dass nicht-lineare Prozesse, die auf diesen Zeitskalen wirken und im Gill-Modell durch den Dissipationsterm parameterisiert werden, für die Form des Erwärmungsmusters wichtig sind. Klimamodelle weisen große Unterschiede bei den Projektionen der Veränderungen der tropischen Meeresoberflächentemperatur und des Niederschlags auf, aber unsere Ergebnisse deuten darauf hin, dass, sobald sich diese Vorhersagen verbessern, auch unser Vertrauen in das vorhergesagte Erwärmungsmuster der oberen Troposphäre zunehmen sollte.

ACRONYMS

CMIP . . . . . Coupled Model Intercomparison Project
AMIP . . . . . Atmospheric Model Intercomparison Project
SSP . . . . . Shared Socioeconomic Pathway
piControl . . . . . Preindustrial Control
ECMWF . . . . . European Centre for Medium-Range Weather Forecasts
ERA5 . . . . . Fifth-generation ECMWF Atmospheric Reanalysis
ICON-ESM . . . . . Icosahedral Non-Hydrostatic Earth System Model
ICON-A . . . . . Atmospheric Component of the ICON-ESM Model
PJ . . . . . Perpetual January
SST . . . . . Sea Surface Temperatures
PRSST . . . . . Precipitation Weighted Sea Surface Temperatures
MSE . . . . . Moist Static Energy
WTG . . . . . Weak Temperature Gradient

CONTENTS

I UNIFYING ESSAY

1 INTRODUCTION AND MOTIVATION 3

2 BACKGROUND 5
- 2.1 The Vertical Temperature Structure of the Tropical Atmosphere 5
- 2.2 The Horizontal Temperature Structure of the Tropical Atmosphere 7
- 2.3 Research Questions 9

3 KEY RESULTS 10
- 3.1 Variations of Tropical Lapse Rates in Climate Models and Their Implications for Upper-Tropospheric Warming. 10
- 3.2 Tropical Tropospheric Warming Pattern Explained by Shifts in Convective Heating in the Matsuno-Gill Model 13

4 CONCLUSION 19
- 4.1 Answering the research questions 19
- 4.2 Remaining Uncertainties and Outlook 21

II APPENDICES

A APPENDIX A 27
- A.1 Introduction 30
- A.2 Methods 31
- A.3 Differences in Lapse Rates and Upper Tropospheric Temperatures in Conventional Climate Models 35
- A.4 Processes Influencing the Tropical Lapse Rate in ICON-A Simulations 37
- A.5 Upper Tropospheric Warming 39
- A.6 Summary and Discussion 42

B APPENDIX B 52
- B.1 Introduction 54
- B.2 Methods 55
- B.3 Tropical Tropospheric Warming Patterns and Precipitation Changes in Global Climate Models 58
- B.4 Interpreting the warming pattern using the Gill model 60
- B.5 Discussion and Conclusion 66

BIBLIOGRAPHY 71

Part I

UNIFYING ESSAY

1

INTRODUCTION AND MOTIVATION

Already in the 19th century, researchers observed how temperature changed with height and theorised what processes determine an air parcel's temperature as it changes its altitude. From the first law of thermodynamics, derivations of an *adiabatic lapse rate* were made. It describes how the temperature of an air parcel changes for decreasing pressure, as the volumetric expansion of the parcel draws its internal energy and thus decreases its temperature. In a lecture read before the Literary and Philosophical Society of Manchester in 1862, Lord Kelvin noted that the observed lapse rate (the rate at which temperature changes with pressure or altitude) is usually more stable, i.e. warmer air aloft than predicted by the adiabatic lapse rate (Kelvin, 1890). In this lecture, he was one of the first to theorise that the condensation of water vapour, which occurs as the air parcel cools during its ascent, releases heat to the air parcel, thereby reducing the rate of cooling and resulting in a lapse rate closer to observations. This idealised lapse rate is today referred to as the *moist adiabatic lapse rate*. In contrast, the adiabatic lapse rate without condensation is often referred to as *dry adiabatic lapse rate* by meteorologists. In the following decades, the importance of this moist adiabatic ascent was recognised, as Hann, 1874 notes that observations of the Föhn effect matched the theoretically calculated temperatures very well. Consequently, meteorologists started publishing look-up tables (Hann, 1874) and graphs (Hertz, 1884) of pre-calculated temperatures for different pressures or altitudes for practical use cases.

In the 20th century, the use of computers for numerical modelling allowed more detailed calculations of radiative transfer between layers of air by realistically representing radiative absorption and emission by atmospheric gases. These 1-dimensional models again produced a thermal equilibrium of the atmosphere with a vertical lapse rate that was steeper than observed, resulting in a too cold troposphere. This sets the scene for the groundbreaking studies of S. Manabe in the 1960s (Manabe and Strickler, 1964; Manabe and Wetherald, 1967), in which a critical lapse rate of 6.5 K/km was introduced to a radiative transfer model to represent convective heat transfer from the surface to the troposphere. This model produced a realistic vertical atmospheric structure and enabled an early estimate of the effect of increasing CO_2 in the atmosphere, which still holds up today. It laid the groundwork for understanding tropical climate, the greenhouse effect, climate feedbacks like the water vapour feedback and paved the road for further development of numerical climate models. This highlights the fundamental role that the lapse rate plays in earth's climate. Consequently, S. Manabe won the Nobel Prize for physics in 2021 for this work.

During this time, the spatial coverage of radiosonde measurements increased, allowing an examination of the horizontal temperature structure. It became apparent that lapse rates can be divided into an extratropical and a tropical regime (Stone and Carlson, 1979). While tropical lapse rates are close to the moist adiabat, the extratropical lapse rates are less stable and roughly lie between the moist and dry adiabat. In addition, the observations showed that the horizontal tropospheric temperature structure within the tropics is fairly uniform (Oort, 1983). This was also concluded from theoretical arguments, based on the scaling of the different terms in the equations of motion, in particular because of the small Coriolis force in the tropics (Charney, 1963). The mechanism by which horizontal temperature gradients are kept weak is the so called homogenisation by gravity

waves, which quickly communicate any anomalies that occur due to convective heating to the surrounding atmosphere (Bretherton and Smolarkiewicz, 1989). Consequently, many studies assumed horizontal temperature gradients to be weak or zero in the tropics, which is called the *weak temperature gradient approximation* or simply *WTG approximation* and facilitated modeling many aspects of tropical circulation (Sobel and Bretherton, 2000; Sobel et al., 2001).

Today, climate models typically include much more complexity than the studies by Manabe and broadly simulate a tropical lapse rate close to the moist adiabat. Nevertheless, differences between climate models continue to exist, and climate models often overestimate the recent observed tropical tropospheric warming (Santer et al., 2005; Fu et al., 2011; Mitchell et al., 2013; Santer et al., 2017b). And while it is useful to assume that horizontal temperature gradients in the tropical atmosphere are zero for many applications, both observations and climate models show that the warming of the tropical atmosphere is not horizontally uniform (Kamae et al., 2015), which is not well understood.

Beyond the fundamental role of the tropical thermal structure exposed by S. Manabe, more recent studies reveal additional mechanisms that crucially depend on the tropical thermal structure. In general, the stability of the atmosphere, which is given by the lapse rate, controls to what degree vertical motions occur, and if they occur how vigorous they are. For example, upper tropospheric temperatures have been shown to affect the strength of the Walker circulation and its evolution under greenhouse gas forcing (Sohn et al., 2016), as well as tropical cyclone intensity (Trabing et al., 2019). Midlatitude eddies and poleward heat transport are impacted by baroclinity which is set (in part) by upper tropospheric temperatures (Lu and Cai, 2010). Therefore, tropical upper tropospheric temperatures even impact the atmospheric moisture flux into the Arctic (Lee et al., 2019). In addition, the strength of the anvil cloud feedback, which directly impacts the strength of global warming given an increase in greenhouse gas forcing, depends on the change in the thermal stability (Zelinka and Hartmann, 2010). Even with the progress made in recent decades, the remaining uncertainties surrounding tropical tropospheric temperatures likely cascade to cause other uncertainties and diminish our understanding and simulation of global circulation, climate feedbacks, and other aspects of climate.

2

BACKGROUND

This chapter reviews the fundamentals of vertical and horizontal thermal structure of the tropical troposphere, and presents the current state of the research on what processes determine this structure and how this structure might change with greenhouse gas forcing. The vertical and horizontal structure are discussed in sections 2.1 and 2.2 respectively, and based on that section 2.3 presents the research questions to be answered in this dissertation.

2.1 THE VERTICAL TEMPERATURE STRUCTURE OF THE TROPICAL ATMOSPHERE

Vertical motions in the atmosphere occur if an air parcel's buoyancy is different to that of the surrounding atmosphere. These buoyancy anomalies are typically strongly related to temperature anomalies. When vertical motion occurs, the parcel's own temperature also changes, and therefore the parcel's lapse rate (the rate of temperature change for a give pressure change) together with the background atmosphere's lapse rate often provide sufficient information to predict and understand these motions. During the initial ascent close to the surface, which might be triggered by turbulence or orography, a parcel's temperature changes according to the *dry adiabatic lapse rate*, cooling as it expands. When the temperature reaches the dewpoint, where the parcel becomes saturated with respect to water vapour, condensation occurs. The condensation process liberates the enthalpy of vapourisation, a process also sometimes referred to as *condensation heating*. This reduces the adiabatic expansion cooling, and the subsequent temperature change follows the so called *moist adiabatic lapse rate* or *moist adiabat*. The atmosphere is unstable with respect to moist adiabatic ascent, meaning ascent can occur if the atmosphere's lapse rate is steeper than the moist adiabatic lapse rate, which makes the air parcel positively buoyant. To assess the atmosphere's stability, it can also be useful to employ moist static energy or the equivalent potential temperature (Bao and Stevens, 2021), since these quantities are approximately conserved along adiabatic ascent and thus can be easily compared across different heights.

Earth's atmosphere constantly loses heat through outgoing longwave radiation. In the tropics this radiative cooling is approximately uniform throughout the troposphere (Zelinka and Hartmann, 2010), while the surface constantly gains heat from short- and longwave radiation. Over time, this asymmetry in height causes the lapse rate to become unstable with respect to moist adiabatic ascent, and convection is triggered, heating the troposphere again. The resulting energy balance in the tropics is often referred to as *radiative-convective equilibrium* and explains why the observed tropical lapse rate is always close to a moist adiabat (Stone and Carlson, 1979; Betts, 1982; Xu and Emanuel, 1989). This holds even in regions where deep convection typically does not occur, because positive horizontal temperature anomalies produced by deep convection are communicated to surrounding areas through gravity waves (Charney, 1963; Bretherton and Smolarkiewicz, 1989). Therefore, the tropospheric lapse rate throughout the tropics is directly related to boundary layer entropy in regions of deep convection (Emanuel et al., 1994).

The moist adiabat describes the first order change in temperatures with decreasing pressure well, but is an idealised process which usually does not hold exactly. Mixing with surrounding drier air, so called *entrainment*, removes water vapour and therefore

condensation heating from the ascending parcel, leading to a slightly cooler lapse rate (Singh and O'Gorman, 2013; Zhou and Xie, 2019). Further, it is often assumed for simplicity that the condensed water precipitates immediately, which is referred to as the *moist pseudoadiabat*, but any condensate remaining in the air parcel provides additional heat capacity, which reduces the expansion cooling. This lapse rate is called the *reversible adiabat* or *saturated isentrope*. Another process to consider is the additional heat released when the condensate freezes, which typically occurs above 600hPa. Figure 2.1 illustrates the impact of these processes on the convective lapse rate and an overview of how these contributions can be considered in the calculation of the lapse rate is given in section A.2.4. In modern conventional climate models, such as the CMIP6 (Eyring et al., 2016, coupled model intercomparison project) ensemble, convection and the related processes described above are on a *subgrid-scale* and have to be parameterised instead of resolved explicitly by the basic laws of physics. The parameterisations are based on physical reasoning but often empirical, and are a major source of uncertainty for climate simulations, degrading their ability to realistically simulate tropical climate (Fiedler et al., 2020). In section 3.1, I can show how differences in the representation of these subgrid-scale processes can explain variations in tropical lapse rates among conventional climate models. Only recently the increase in computational power permitted *storm-resolving simulations*, in which convection is simulated explicitly, which should provide some added value to simulations of tropical climate (Stevens et al., 2020).

In recent decades, research focused on understanding observed tropospheric warming in response to greenhouse gas forcing. Considering the idealised moist adiabat, warming close to the surface under constant relative humidity produces amplified warming aloft, which at 200hPa amounts to around double the surface warming. This is because the cloud base saturation vapour pressure is a exponentially increasing function of temperature, and this additional condensation heating is realised by a disproportionate warming with height. The amplification of upper tropospheric warming is also predicted in complex climate models (Santer et al., 2005), but satellite as well as radiosonde measurements suggested that the observed tropospheric warming hardly showed any amplification at all (Santer et al., 2005; Thorne et al., 2007; Fu et al., 2011). This discrepancy triggered many follow-up studies as concerns were raised that a fundamental aspect of tropical climate was not well understood, and climate change sceptics often cited this particular problem in an effort to discredit climate science and delay action on climate change (Thorne et al., 2011). Today, these discrepancies have been greatly reduced, if not eliminated, and while some uncertainties remain, there is a robust understanding of why these discrepancies existed. Errors in satellite as well as radiosonde observations were reduced and now show stronger observed upper tropospheric warming (Haimberger et al., 2012; Po-Chedley et al., 2015; Zhou et al., 2021), the influence of the sea surface temperature pattern which is subject to the internal variability of the climate has been recognised (Mitchell et al., 2013; Fueglistaler et al., 2015; Tuel, 2019; Po-Chedley et al., 2021), and the fact that entrainment during the convective ascent reduces the amplification and needs to be simulated realistically has been demonstrated (Singh and O'Gorman, 2013; Miyawaki et al., 2020). Standing on the shoulders of giants, section 3.1 in this dissertation contains a contribution towards explaining and reducing the discrepancy between observed and simulated upper tropospheric warming.

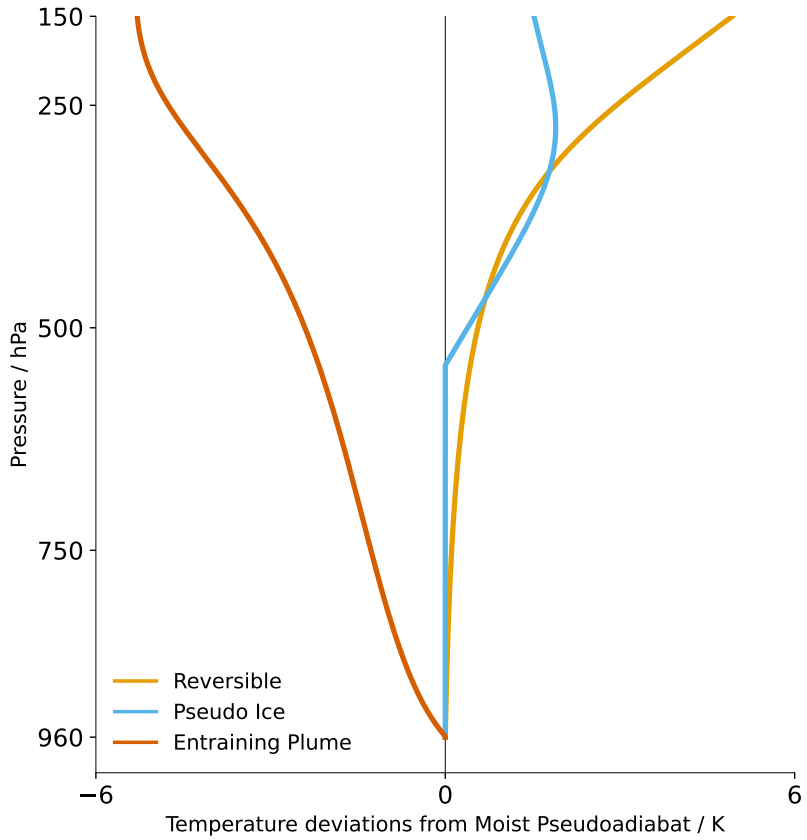

Figure 2.1: Temperature deviations of different versions of idealised moist adiabats from the moist pseudoadiabat in the troposphere. The idealised adiabats are calculated with the method given in the appendix section A.2.4. The vertical integration starts at 960hPa, a typical cloud base pressure level, and assumes saturation at that level.

2.2 THE HORIZONTAL TEMPERATURE STRUCTURE OF THE TROPICAL ATMOSPHERE

Convective ascent usually causes warm temperature and thereby positive buoyancy anomalies in the troposphere, which trigger so called gravity waves (Bretherton and Smolarkiewicz, 1989). The surrounding atmosphere is unsaturated and stable with respect to dry adiabatic motions, and vertical displacements triggered by neighbouring buoyancy anomalies result in oscillations. These gravity waves spread both horizontally and vertically and often travel far in the tropics, because they are not inhibited by the small Coriolis force. Thereby the gravity waves homogenise the horizontal temperature pattern throughout the tropics much faster than horizontal mixing could. Therefore, horizontal temperature gradients in the tropical troposphere are fairly weak compared to the extratropics (Figure 2.2), where the Coriolis force is stronger. For many studies of tropical circulation, it is useful to assume the horizontal temperature gradient is zero, which simplifies the problem and is often referred to as the *Weak Temperature Gradient Approximation* (Sobel and Bretherton, 2000; Sobel et al., 2001, WTG). Because temperature gradients are weak, the studies discussed above that focus on the vertical structure of

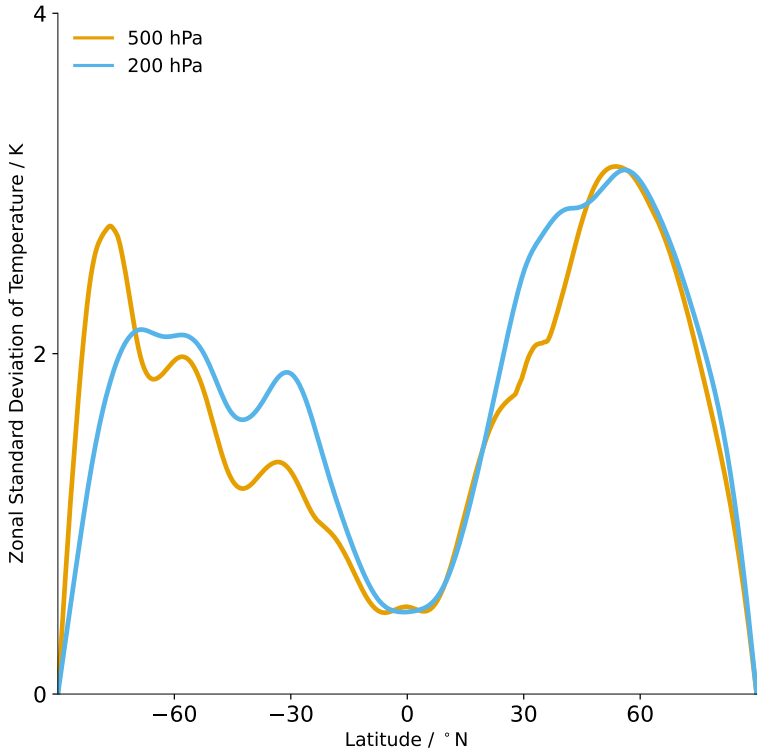

Figure 2.2: Zonal standard deviation of tropospheric temperatures at different pressure levels in the ERA5 reanalysis (Simmons et al., 2020). Calculated from monthly mean data for the period 1979-2014.

tropical warming usually only consider a horizontal mean value representative for the whole tropics.

Nevertheless, horizontal temperature gradients in the tropics can be observed especially in the upper troposphere (Wu et al., 2015; Bao and Stevens, 2021). In a simple model, Gill, 1980 demonstrated how the large scale tropical geopotential (and therefore temperature) and wind pattern respond to a localised convective heating. This model can successfully reproduce various aspects of tropical circulation, like the Walker Circulation and monsoon systems (Gill, 1980; Lau and Lim, 1982; Dias et al., 1983; Rodwell and Hoskins, 1996; Wu et al., 2015). Even if the Coriolis force is small, it has been shown that gradients in tropical geopotential can be balanced in the momentum equations by other processes. Especially in the upper troposphere, advection and eddy momentum flux are non-negligible (Lin et al., 2008; Bao et al., 2022), and thereby limit the influence of gravity waves at least to some degree. As a result, regions of frequent deep convection show a slightly warmer (a few degrees K) upper troposphere compared to regions with less deep convection. Strong temperature anomalies can be observed especially during monsoon conditions (Wu et al., 2015), or in relation to the El Niño Southern Oscillation (Bayr et al., 2014). The tropical tropospheric warming is also not completely uniform, and is related to the sea surface temperature (SST) pattern (Kamae et al., 2015), likely via changes in convective heating. Until now there are no studies that offer an explanation

for mechanisms that shape this pattern. This gap is addressed in section 3.2, where the mechanisms that shape the warming pattern are investigated.

2.3 RESEARCH QUESTIONS

The first part of this project focuses on the vertical structure of the tropical troposphere. Modern conventional climate models continue to simulate different tropical lapse rates and upper tropospheric warming rates among each other and still show a bias in upper tropospheric warming compared to most observations:

- Can differences in the representation of subgrid-scale processes alone, like freezing and entrainment, explain differences in tropical lapse rates and upper tropospheric warming among conventional climate models?
- Could an improved representation of these processes also help reduce the bias of climate models with regards to observational estimates of upper tropospheric warming?

The second part of this project investigates the horizontal warming pattern of the tropical troposphere. The pattern is likely related to changes in SST and convective heating, but the exact mechanisms are unclear:

- Can changes in convective heating, that influence the upper tropospheric warming pattern, be understood by purely thermodynamic arguments, or do circulation changes play a role in shaping this pattern?
- Can the warming pattern be reproduced in a simple model that is informative of the underlying mechanisms?
- In particular, what processes limit the homogenisation of the temperature pattern through gravity waves and sustain zonal warming gradients even at the equator?

The next chapter presents a comprehensive overview of the most important results that answer these questions.

3

KEY RESULTS

The first section of this chapter deals with the vertical structure of the atmosphere and is a summary of a publication in the *Journal of Climate* which is attached in Appendix A. The second section is a summary based on a manuscript that is submitted to the *Quarterly Journal of the Royal Meteorological Society* and is attached in Appendix B. For a more detailed presentation of methods and discussion of results refer to the appendices. The most important figures of the studies are presented here, sometimes with adaptations from the original figures to focus the key results.

3.1 VARIATIONS OF TROPICAL LAPSE RATES IN CLIMATE MODELS AND THEIR IMPLICATIONS FOR UPPER-TROPOSPHERIC WARMING.

In the first study (Appendix A) I examine differences in tropical lapse rates and tropical tropospheric warming and offer an explanation for why these differences exist, and why the warming might be overestimated by climate models. First, I document the spread of tropospheric temperatures and lapse rates in CMIP6 (coupled model intercomparison project, Eyring et al., 2016) models, which are typically used for a wide range of applications and studies in climate science. These are compared to radiosonde observations, which offer a high vertical resolution in comparison to satellite observations. Different radiosonde datasets exist, because the raw measurement data is processed in different ways, with the goal of reducing errors due to, e.g., changing instrument types over time (Free et al., 2005; Sherwood et al., 2005; Thorne et al., 2011; Haimberger et al., 2012; Sherwood and Nishant, 2015; Zhou et al., 2021).

For a given lower tropospheric temperature, CMIP6 models show a spread of more than 3 K in upper tropospheric temperatures, suggesting that lapse rates are indeed different among CMIP6 models (Figure A.1). Even for similar lower tropospheric temperatures, it is possible that differences in the spatial coupling of SSTs and convection might lead to differences in upper tropospheric temperatures among climate models. The coupling of SSTs and convection can be expressed through precipitation-weighted SSTs (PRSST). This metric has been used to explain differences upper tropospheric warming among climate models (Fueglistaler et al., 2015; Tuel, 2019), but I find that PRSSTs cannot explain the spread upper tropospheric temperatures in the mean state (Figure A.2). Therefore, I examine the variations of lapse rates among CMIP6 models more closely. Figure 3.1 shows how each climate model's lapse rate, the observed lapse rate, and idealised calculations of lapse rates deviate from the pseudoadiabat. While most models center around the pseudoadiabat, some model's lapse rates are considerably colder, suggesting a strong influence of entrainment. Other model's lapse rates are warmer, which might be due to a stronger impact of freezing enthalpy or a more reversible ascent. This causes the model's upper tropospheric temperature to deviate by more than 2 K from the value predicted by the pseudoadiabat. Therefore, I hypothesise that the effects of entrainment, reversible ascent and freezing enthalpy likely contribute to the spread of the lapse rates among CMIP6 models. While the pseudoadiabat seems like the best fit for many cases, this is likely because the effect of the other processes, which are all observed in reality, compensate each other to some degree.

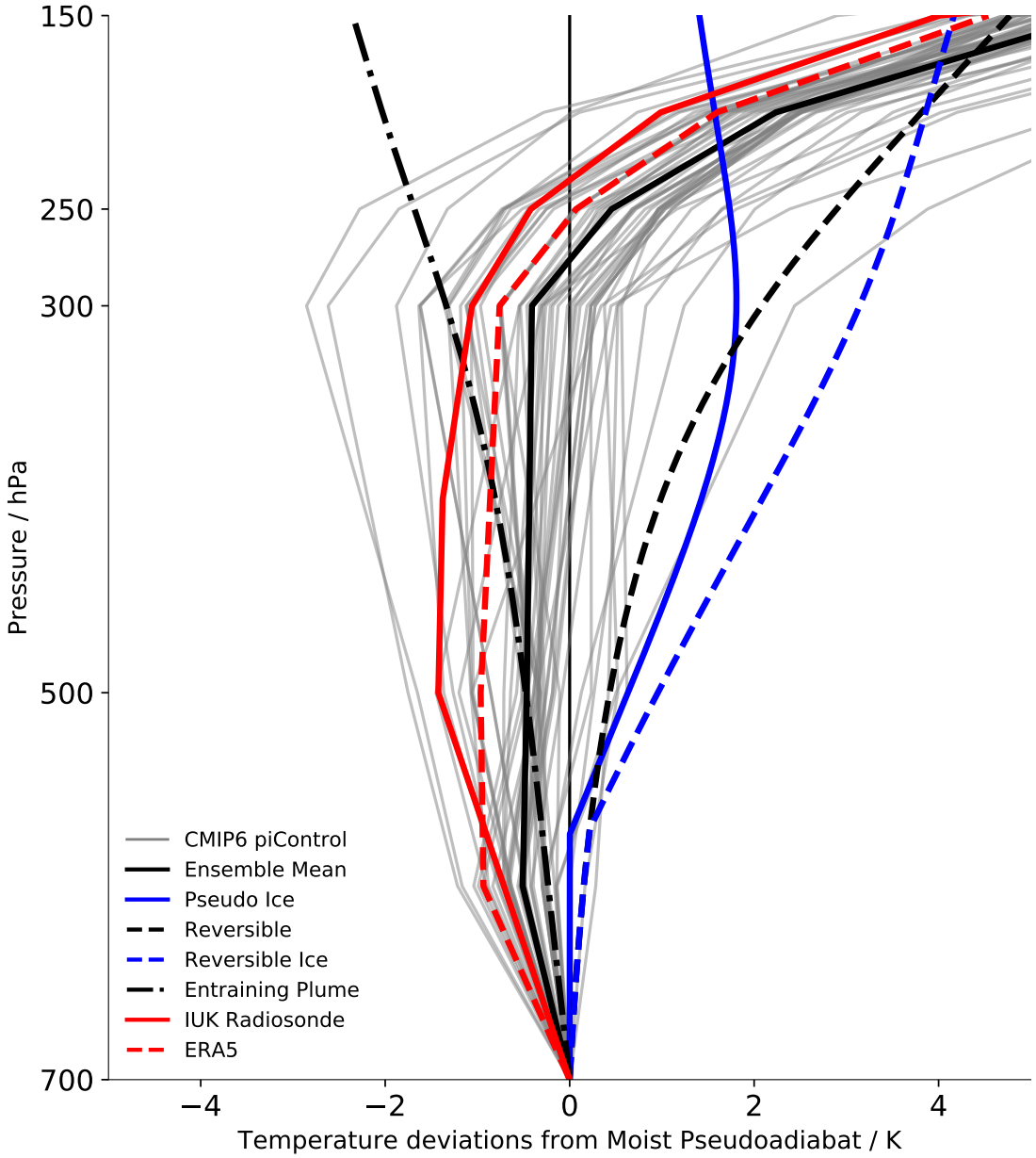

Figure 3.1: Deviations from the idealised moist pseudoadiabat for all CMIP6 piControl simulations and observations in the tropics (20°N-20°S), as well as some idealised cases. First, for every model and the observations an idealised moist pseudoadiabat is calculated based on the tropical mean temperature at 700 hPa assuming saturation. The deviations of the actually simulated (and measured) temperatures from each idealised moist pseudoadiabat are illustrated here. In addition, the deviations of the reversible adiabat, freezing pseudoadiabat, the freezing reversible adiabat, and the entraining plume with respect to the pseudoadiabat are shown.

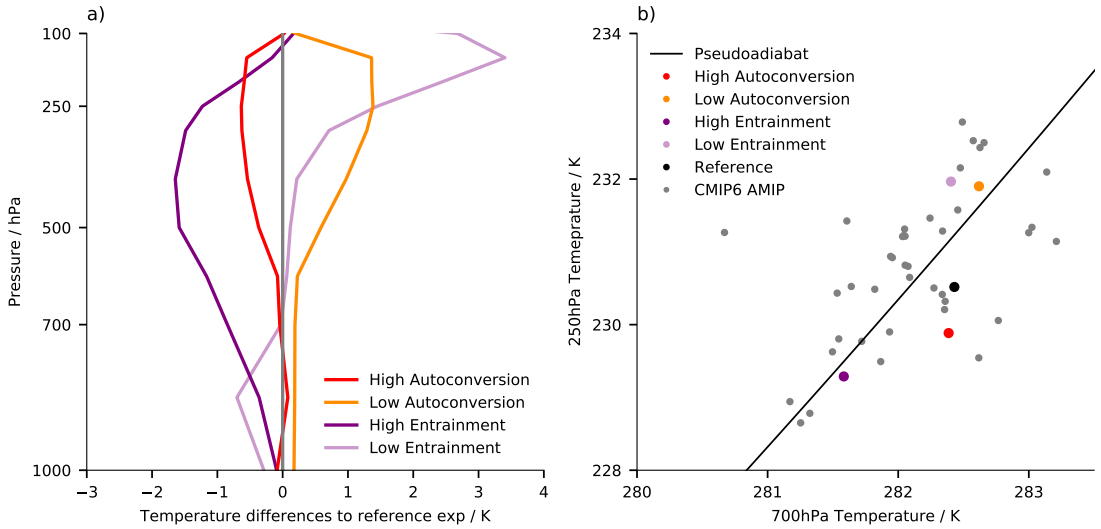

Figure 3.2: Changes in atmospheric temperatures in ICON-A perturbed physics experiments. Darker shading represents increased autoconversion (red/orange) and entrainment (purple). (a) Differences in tropical mean (20°N-20°S) temperatures to the reference experiment. (b) Lower vs. upper tropospheric tropical mean temperatures for ICON-A perturbed physics experiments, as well as CMIP6 AMIP simulations. The line represents the relationship expected from a pseudoadiabat.

Processes that cause the lapse rate to deviate from a pseudoadiabat occur on small spatial scales that are not explicitly resolved in CMIP6 models (i.e. the subgrid-scale). Instead, they have to be included in parameterisations, which differ among CMIP6 models. To demonstrate that these processes, and the way they are parameterised, cause variations in the lapse rates illustrated in Figure 3.1 I perform perturbed physics experiments with the ICON-A climate model. I perturb the conversion rate of cloud water to rainfall (autoconversion) and the turbulent entrainment rate for deep convection. In these experiments, tropical temperatures deviate by more than 2 K from the reference experiment, especially in the upper troposphere (Figure 3.2a), covering the spread of tropospheric temperatures in CMIP6 AMIP simulations (Figure 3.2b). A skill score for the evaluation of climate models (Reichler and Kim, 2008; Crueger et al., 2018) shows that the simulated climate of these experiments is broadly as realistic as simulated climates in the CMIP6 ensemble (Figure A.4).

In the experiments with decreased autoconversion, more condensate remains in the air parcel during the ascent. This allows a larger amount of condensate to freeze and the additional freezing enthalpy causes the warming above 600 hPa (orange line in Figure 3.2a). The condensate does not impact the parcel's heat capacity, as it should during reversible ascent which would cause additional warming, illustrating the shortcomings of the convection parameterisation. The upper troposphere is also warmer for the case of decreased entrainment (light purple line in Figure 3.2a). This is because the level of neutral buoyancy shifts to higher altitudes (Zhou and Xie, 2019), as less water vapour is mixed with the surrounding air and more condensation can occur. For increased entrainment, the troposphere becomes colder, as the condensation heating decreases. Enhanced evaporative cooling by detrained cloud water might also contribute to the cooling (Mauritsen et al., 2012).

Finally, I examine to what degree the subgrid-scale processes impact upper tropospheric warming rates. Upper tropospheric warming, shown here demonstratively at

250 hPa, is strongly connected to lower tropospheric warming throughout CMIP6 models (Figure 3.3a). Upper tropospheric warming in CMIP6 models is overestimated with respect to most radiosonde observations. The exact relationship between lower and upper tropospheric warming in the radiosonde observations and the ERA5 reanalysis is somewhat ambiguous, as they show a range of different estimates for both lower and upper tropospheric warming. Some (RATPAC and ERA5) show a similar relationship between lower and upper tropospheric warming as the CMIP6 models, but simulate weaker overall tropospheric warming, while others (especially Rich-Obs) show lower tropospheric warming on a similar magnitude as the CMIP6 models, but considerably weaker upper tropospheric warming, with hardly any amplification of the warming at all. Finally, the SUNY dataset agrees well with both lower and upper tropospheric warming of CMIP6 models. These differences in upper tropospheric warming cannot be resolved by considering differences in the spatial coupling of SSTs and convection: PRSSTs show a weak relationship to upper tropospheric warming differences among CMIP6 AMIP models and cannot explain differences to the ERA reanalysis (Figure A.8a).

To further investigate the amplification between lower and upper tropospheric warming I define an amplification factor as the slope of a linear regression of annual mean, tropical mean temperatures at 700 hPa versus those at 250 hPa (Figure 3.3b). CMIP6 models show an amplification between 1.5 and 1.8 K/K. The ICON-A model reference simulations cover almost half of this spread which indicates the impact of internal variability on the amplification. The radiosonde estimates on average show weaker amplification factors than almost all of the CMIP6 models. In experiments with increased entrainment rate, the amplification is smaller compared to the reference case, because the increased condensation heating due to the warming is reduced (Miyawaki et al., 2020). This effect is also demonstrated by theoretical calculations of the entraining plume. Entrainment alone could explain the spread in CMIP6 amplification factors, and thereby bridge the gap to the observed amplification rates. This suggests a part of the CMIP6 models' bias towards the observed warming is due to simulating entrainment too weakly (Romps, 2010).

3.2 Tropical tropospheric warming pattern explained by shifts in convective heating in the Matsuno-Gill model

In the second study (Appendix B) I explain the mechanisms that shape the upper tropospheric warming pattern and reproduce the pattern using a numerical Gill model (Matsuno, 1966; Webster, 1972; Gill, 1980). I examine upper tropospheric warming in CMIP6 simulations, forced by the SSP585 scenario (Eyring et al., 2016) and show differences between the late (2080-2099) and early 21st century (2015-2034) (Figure 3.4). The warming pattern is likely related to convection, which is arguably poorly represented in CMIP6 models (Fiedler et al., 2020). Consequently, I also present results for storm resolving simulations with 5 km gridspacing using the ICON-A model (Hohenegger et al., 2022). These simulations represent convection based on the laws of motion and do not rely on parameterisations, and therefore should simulate various aspects of convection more realistically (Stevens et al., 2020). I use eight months of data each from two storm resolving simulations, one forced by present day January SSTs, while the other uses January SSTs from a 4 K warmer world. Hence they are called Perpetual January (PJ) simulations. The warming pattern is given by the difference between these two simulations.

Upper tropospheric warming shows deviations of more than 2 K from region to region in the PJ simulations (Figure 3.4b). In CMIP6 models, patterns have a similar magnitude as in the PJ simulations, but differ in terms of their shape among each other. This results

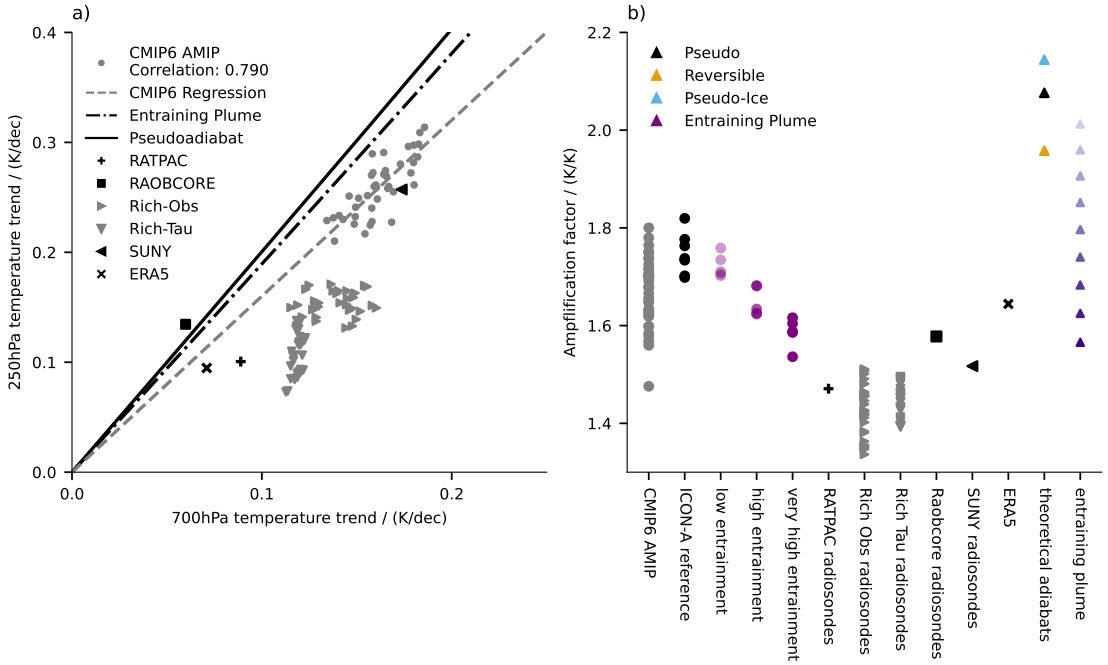

Figure 3.3: a) Tropical (20°N-20°S) trends in 700 hPa versus trends in 250 hPa temperatures for radiosondes, CMIP6 AMIP simulations and the ERA5 reanalysis. Cross-model correlation and a regression line is given for CMIP6 models. Trends are calculated over the 1979-2012 period. Theoretical values for the pseudoadiabat and the entraining plume using $\epsilon_0 = 0.3$ are also given. b) Amplification factor of tropical mean 250 hPa vs 700 hPa warming for years 1979-2012. Shown are CMIP6 AMIP simulations, ICON-A perturbed physics experiments (black and purple circles), radiosonde observations, ERA5 reanalysis and the amplification expected from theoretical moist adiabats. In the case of the entraining plume, the amplification is calculated for entrainment rates ϵ_0 from 0.1 to 0.9 in steps of 0.1.

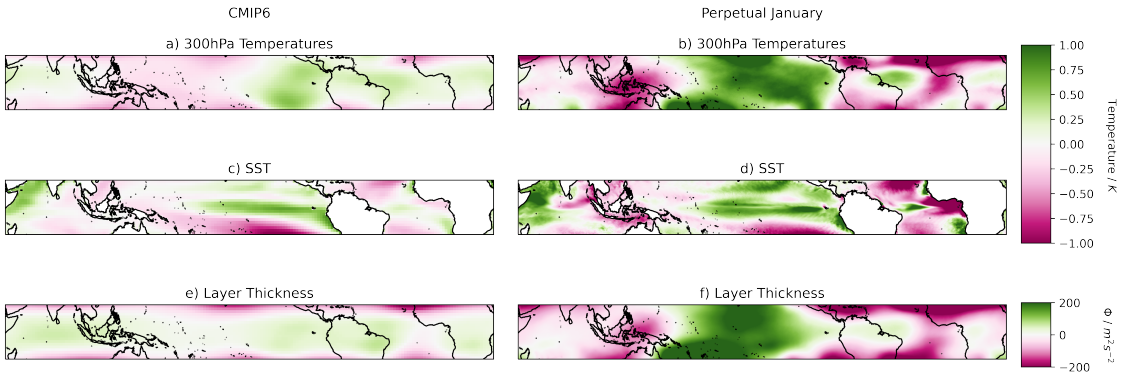

Figure 3.4: Anomalies from tropical mean (20°N-20°S) changes between the early and late period in CMIP6 SSP585 models and the warm and cold simulation in the PJ simulations. Shown are temperatures at 300 hPa (a,b), sea surface temperatures (c,d) and 400-150 hPa layer thickness (e,f).

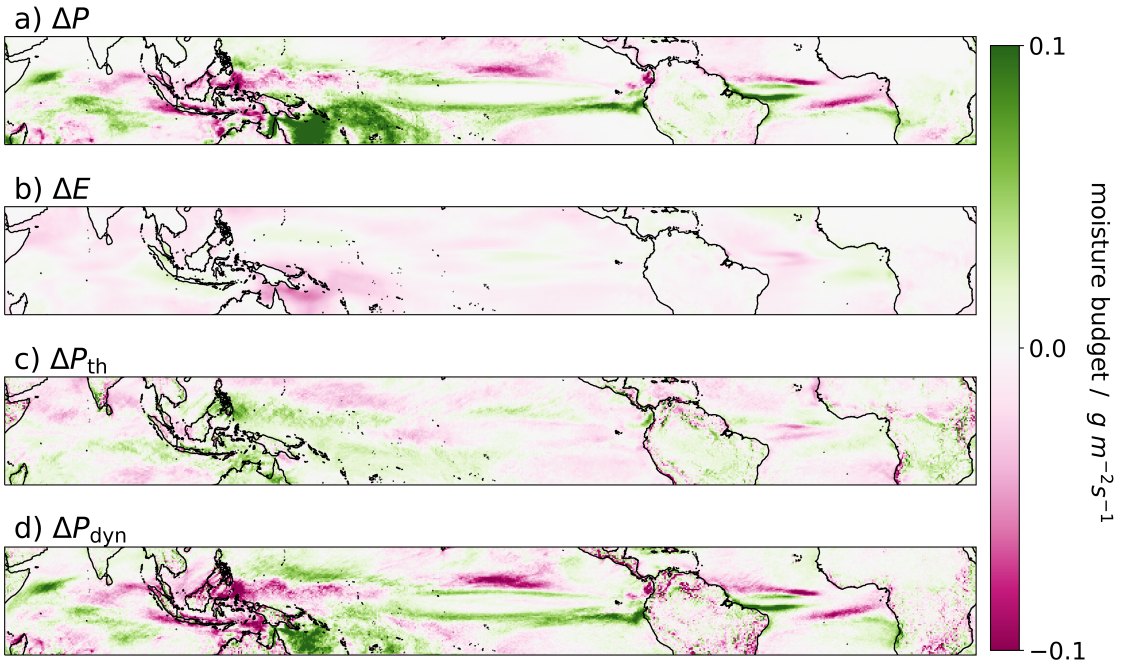

Figure 3.5: Precipitation changes (ΔP, a) in the PJ Simulations decomposed into thermodynamic (ΔP_{th}, c) and dynamic (ΔP_{dyn}, d) changes. b) shows evaporation changes (ΔE). The signs are such that they are positive for atmospheric moisture loss.

in a more uniform ensemble mean upper tropospheric warming pattern (Figure 3.4a). Upper tropospheric layer thickness changes (Figure 3.4e-f) are overall very similar to the temperature changes. In addition, regions with a above average upper tropospheric warming tend to have above average warming of SSTs, confirming that SSTs probably play a role in shaping the pattern (Kamae et al., 2015). The likely mechanism by which the SST pattern causes upper tropospheric warming anomalies is through impacting precipitation and thereby latent heating in the troposphere.

An increase in precipitation could either be related to an increase of humidity that occurs due to the warmer SSTs, and is transported by the mean circulation to the regions of deep convection. This can be characterised as thermodynamic changes in convection (Held and Soden, 2006). Alternatively, precipitation changes could be related to dynamic changes triggered by the SST pattern (Lindzen and Nigam, 1987), where an increase in moisture convergence would be associated with an increase of horizontal convergence of the winds or increased moisture advection. To investigate this mechanism in the PJ simulations I decompose the changes of precipitation into dynamic changes ΔP_{dyn} and thermodynamic changes ΔP_{th} (Seager et al., 2010). The dynamic precipitation changes ΔP_{dyn} dominate the thermodynamic changes ΔP_{th} (Figure 3.5), and closely resemble the full precipitation changes ΔP. Thus, the precipitation and thereby convective heating changes cannot be understood by thermodynamic arguments alone but are coupled to circulation changes, which are in turn induced by the SST pattern.

To understand the warming pattern and the related circulation changes, I employ the Gill model (Matsuno, 1966; Gill, 1980) that directly relates convective heating to circulation and layer thickness changes. In this configuration the three prognostic variables are the wind shear between an upper and a lower pressure level in zonal direction u and meridional direction v and the thickness of the layer Φ:

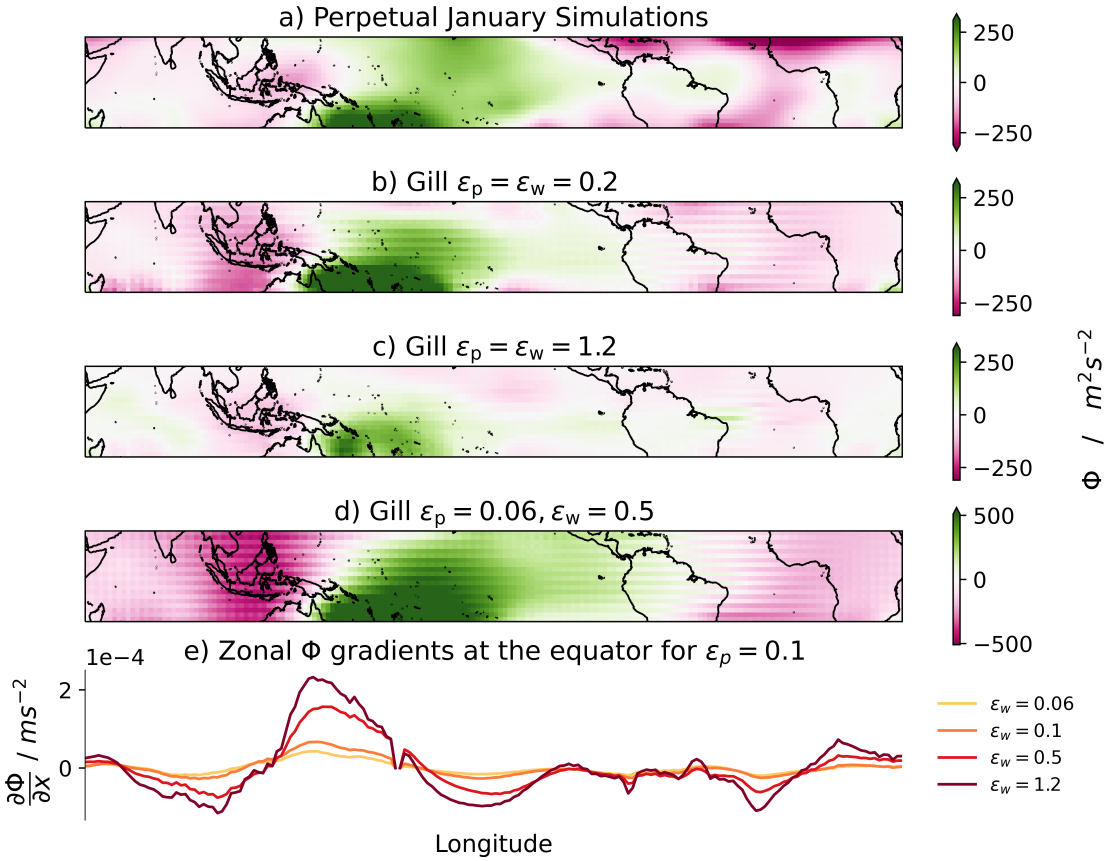

Figure 3.6: Panel a) shows anomalies from the tropical (20°N-20°S) average layer thickness changes from the PJ simulation (as Figure 3.4e), and panels b-d show anomalies from the tropical (20°N-20°S) average layer thickness produced by the Gill model forced by the PJ precipitation changes. Panel e) shows zonal layer thickness gradients for different Gill simulations.

$$\begin{aligned} \frac{\partial u}{\partial t} + \epsilon_w u - \frac{1}{2} y v &= -\frac{\partial \Phi}{\partial x} \\ \frac{\partial v}{\partial t} + \epsilon_w v + \frac{1}{2} y u &= -\frac{\partial \Phi}{\partial y} \\ \frac{\partial \Phi}{\partial t} + \epsilon_p \Phi + \frac{\partial u}{\partial x} + \frac{\partial v}{\partial y} &= Q \end{aligned} \tag{3.1}$$

Here x and y are the horizontal coordinates, Q is the convective forcing and the terms $\epsilon_w u$, $\epsilon_w v$ represent the momentum dissipation, and $\epsilon_p \Phi$ the thermal dissipation. The dissipation terms are needed from a numerical point of view to converge to a stable solution, but also physically to represent more complex processes like advection, eddy momentum flux ($\epsilon_w u$ and $\epsilon_w v$) and radiative cooling ($\epsilon_p \Phi$). ϵ can be thought of as an inverse dissipation timescale, and a larger value for ϵ will cause a signal to dissipate over a shorter time. Because it is unclear what value ϵ should have exactly, I present an ensemble of Gill simulations using different values for ϵ. Q is derived from the precipitation changes in CMIP6 models or the PJ simulations, under the assumption that precipitation changes closely resemble convective heating changes. Thus, u,v and Φ can be interpreted as the circulation and layer thickness changes that arise due to greenhouse gas forcing.

The Gill model forced by the PJ precipitation changes is able to reproduce the main features of the warming pattern in the PJ simulations (Figure 3.6), such as the above average warming in the Pacific and the below average warming over the Maritime Continent. For larger values of ϵ more small scale features like the warming patch in the Atlantic become more pronounced, illustrating the influence the dissipation has on the warming pattern. The thermal dissipation $\epsilon_p \Phi$ controls how far a signal can travel before it dissipates, and a large value for ϵ_p leads to a warming pattern that resembles the convective heating pattern Q (and thus the precipitation changes in Figure 3.5a). The momentum dissipation $\epsilon_w u$ can balance strong zonal gradients of Φ close to the equator (Figure 3.6e). The largest correlation (0.88) between the PJ layer thickness pattern and the Gill simulation is found for a configuration of $\epsilon_p \approx 0.1$ and $\epsilon_w \approx 0.3$, corresponding to a dissipation timescale of 1-2 days. Correlations of the pattern produced by the Gill model are generally higher with the 400-150 hPa layer thickness than the 700-200 hPa layer thickness changes in the PJ simulations, likely because the bulk of the additional warming related to the convective heating is realised in the upper troposphere.

In some more idealised Gill simulations that are only forced by precipitation changes from one region (Figure B.7), I demonstrate that the warming over the whole Pacific can be reproduced by only using western Pacific precipitation changes. To reproduce the pattern in the Atlantic, it is necessary to use the Atlantic precipitation changes, illustrating that local convective heating can have locally confined effects on upper tropospheric temperatures.

Finally, I demonstrate that the numerical Gill model also reproduces the warming pattern simulated by CMIP6 models. To be concise, here I present results for the December, January, February season, but results are very similar for the June, July, August season (see Appendix B). For the vast majority of CMIP6 models, a corresponding Gill simulation exists where the correlation between the layer thickness in the Gill simulation and the CMIP6 simulation is above 0.5 (Figure 3.7a). In many cases correlations of 0.8 or higher are achieved. Using these Gill simulations, I can determine which values for ϵ are most skilful for reproducing the tropospheric warming pattern (Figure 3.7b). The values of ϵ_p that achieve the highest correlation generally lie between 0.02 (corresponding to a dissipation timescale of 10 days) and 0.3 (18 hours). The ϵ_w distribution centers around slightly smaller values of 0.02 (10 days) to 0.1 (2 days). This suggests processes like advection and eddy momentum flux are indeed representative for the momentum dissipation term, as they have similar dissipation timesclaes (Lin et al., 2008). For the thermal dissipation radiative cooling, as well as horizontal temperature advection (Bao et al., 2022), are processes that have corresponding dissipation timescales. The fact that there are a range of suitable values for ϵ points towards different physics and different large scale momentum balances in the CMIP6 models.

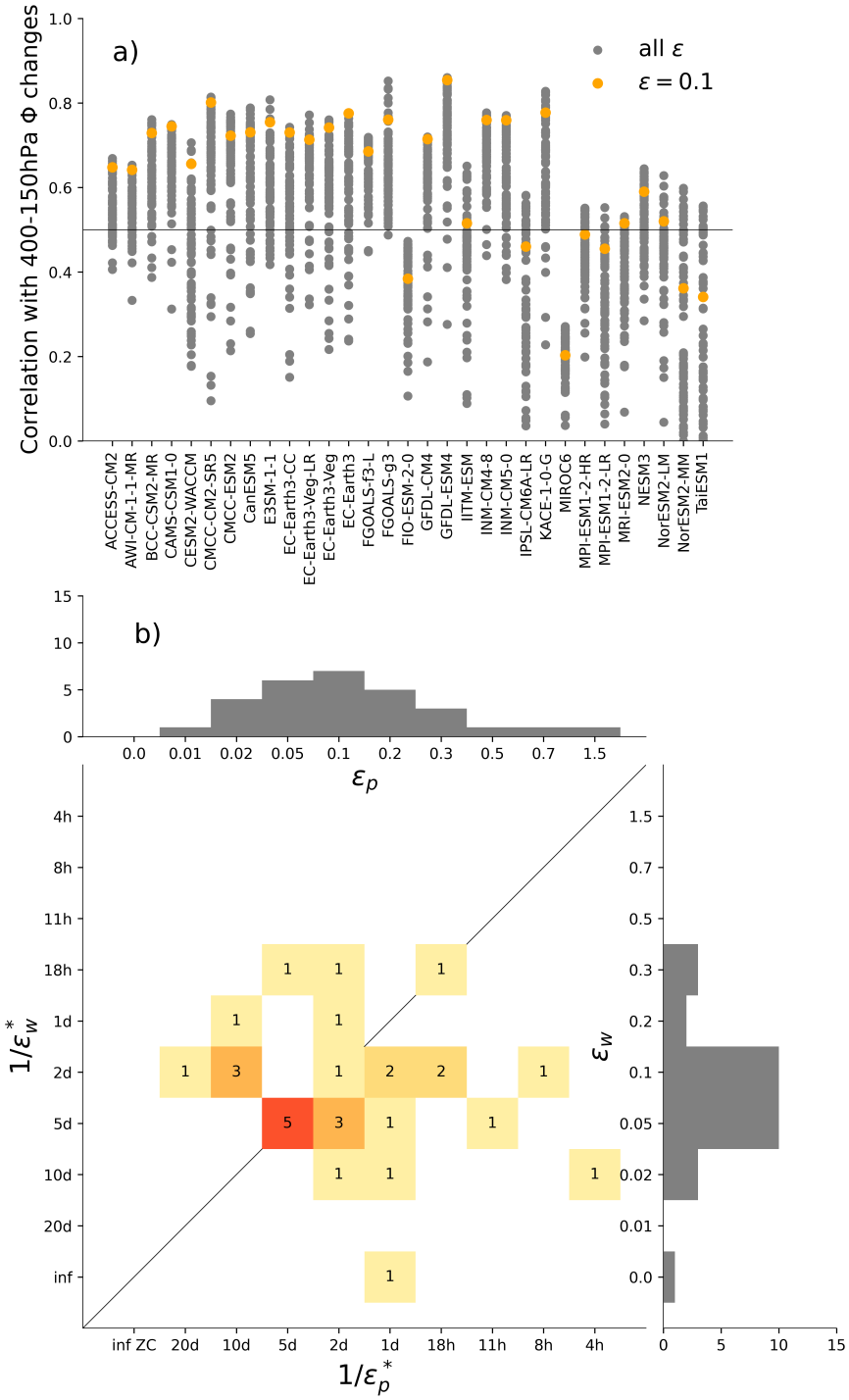

Figure 3.7: a) Correlation of Gill simulations for a range of ϵ_p and ϵ_w values with the 400-150 hPa layer thickness anomalies in every CMIP6 SSP585 model (grey dots). Orange dots show the simulations with $\epsilon_p = \epsilon_w = 0.1$. b) Histogram of cases with highest correlation. This plot counts the amount of cases in which certain ϵ_p and ϵ_w values achieve the best correlation for every CMIP6 model, given there is a Gill simulation that exceeds a correlation of 0.5. The dissipation is shown in its non-dimensional value for the histogram plots. The corresponding timescales (the inverse of the dimensional dissipation value ϵ^*) are given on the lowermost and leftmost axis. Here d refers to day and h to hour. "inf" refers to the infinite timescale for $\epsilon = 0$. For the case $\epsilon_p = 0$, the forcing Q is zonally compensated (indicated by "ZC"), following Bretherton and Sobel, 2003. Both panels show results for the December, January, February period.

4

CONCLUSION

4.1 ANSWERING THE RESEARCH QUESTIONS

This section provides comprehensive answers to the key research questions posed in section 2.3. The answers are divided into two parts, that deal with the vertical and the horizontal temperature structure, respectively, corresponding to sections 3.1 and 3.2, as well as the two manuscripts in the appendix.

1. Variations of Tropical Lapse Rates in Climate Models and Their Implications for Upper-Tropospheric Warming.

Differences in lapse rates among conventional climate models, represented here through CMIP6 ensemble, have the same order of magnitude as temperature deviations one would expect from subgrid-scale processes like the release of freezing enthalpy and entrainment. In addition, upper tropospheric warming rates also differ among CMIP6 models, and are generally overestimated compared to radiosonde observations. To investigate the impact of subgrid-scale processes on the lapse rate and upper tropospheric warming, I perform perturbed physics experiments with the convection parameterisation of the ICON-A climate model. I change the values of the turbulent entrainment rate and autoconversion (the conversion rate of cloud water to rain), which allows for answering the research questions:

a) Can differences in the representation of subgrid-scale processes alone, like freezing and entrainment, explain differences in tropical lapse rates and upper tropospheric warming among conventional climate models?

   Yes. For decreased autoconversion, the upper troposphere is warmer. This is because additional condensate is retained in the updraft and freezes instead of being precipitated, which releases additional freezing enthalpy. In simulations with decreased entrainment the upper troposphere is warmer, because less moisture is detrained to the environment and instead condensates in the updraft. This releases additional latent heating, which results in a lapse rate closer to a moist adiabat. These experiments cover the spread in upper tropospheric temperatures found in CMIP6 models, while still showing a broadly realistic climate overall. Therefore, the representation of subgrid-scale processes alone can be responsible for the variations in lapse rates among CMIP6 models.

   The amplification of lower to upper tropospheric warming is also impacted by entrainment. I can reproduce the spread of amplification among CMIP6 models by increasing the entrainment rate. This is because the amplification depends on the amount of additional latent heating that happens with warming, which decreases for increasing entrainment.

b) Could an improved representation of these processes also help reduce the bias of climate models with regards to observational estimates of upper tropospheric warming?

Yes, although the answer partly depends on the radiosonde product one chooses as reference, because they considerably disagree in their estimates of upper tropospheric warming. The implications of these uncertainties are discussed in section 4.2. For strong entrainment rates, the amplification of lower to upper tropospheric warming decreases and becomes close the radiosonde estimates. It has been suggested that the effect of entrainment is indeed simulated too weakly in conventional climate models (Romps, 2010). Therefore I conclude that improving the representation of entrainment in climate models should benefit estimates of upper tropospheric warming. With the simulations used here, I can show that this effect is not just relevant for future tropospheric warming, but strong enough that it is likely important for simulations of the recently observed warming.

Biases in upper tropospheric temperatures and warming rates likely impact the representation of global circulation in climate models, like the moisture flux into the arctic (Lee et al., 2019). In addition, it has been suggested that stronger entrainment and a colder upper troposphere is related to higher clear-sky equilibrium climate sensitivities (Bao et al., 2021). Therefore, improving the representation of subgrid-scale processes in climate models remains an important task that should benefit our understanding of many aspects of climate.

2. Tropical Tropospheric Warming Pattern Explained by Shifts in Convective Heating in the Matsuno-Gill Model

Most conventional climate models, storm resolving models, as well as observations show a non-uniform tropical upper tropospheric warming that differs horizontally by more than 2 K from region to region. This pattern is also reflected in the layer thickness changes of the upper troposphere. To investigate the mechanisms behind this pattern I use the simulations of a future warming scenario from two types of global climate models: the CMIP6 ensemble and a storm resolving model (the PJ simulations). Since the upper tropospheric warming pattern likely depends on convection, using a storm resolving model that arguably simulates convection more realistically than conventional climate models makes the analysis more robust. In the PJ simulations, the horizontal pattern of upper tropospheric warming somewhat resembles the changes in SSTs (Kamae et al., 2015) and precipitation, indicating that patterns at the surface and the upper troposphere could indeed be coupled by convective heating.

a) Can the changes in convective heating, that influence the upper tropospheric warming pattern, be understood by purely thermodynamic arguments, or do circulation changes play a role in shaping this pattern?

   The circulation changes are essential for shaping changes in convective heating. By decomposing the changes to the atmospheric moisture budget into dynamic and thermodynamic changes, it is evident that the changes of precipitation, and thereby convective heating, are mainly coupled to circulation changes. This results in horizontal shifts in convective heating. In contrast, the thermodynamic changes in the moisture budget have a weaker effect on the changes in convection. This analysis is limited to the storm resolving model, but past studies agree that the dynamic changes are at least as important as the thermodynamic changes (Seager et al., 2010; Bony et al., 2013).

b) Can the warming pattern be reproduced in a simple model that is informative of the underlying mechanisms?

   Yes. The warming pattern simulated by global climate models can be reproduced in a simple numerical Gill model, that couples tropospheric layer thickness and circulation to convective heating. The changes in convective heating that I derive from the precipitation changes in the global climate models are taken as input to force the Gill model. The Gill model reproduces the main features of the warming pattern simulated by the global climate models, and the representation of some of the more detailed features depends on the dissipation parameter. For the vast majority of global climate models, a corresponding Gill simulation exists that produces a skilful warming pattern. Therefore, I conclude that the mechanisms that shape the upper tropospheric warming pattern are described to a large degree by the balances retained in the Gill model.

c) In particular, what processes limit the homogenisation of the temperature pattern through gravity waves and sustain zonal warming gradients even at the equator?

   In the Gill model, increased momentum dissipation leads to increased zonal gradients of layer thickness at the equator, illustrating how the momentum dissipation can balance the pressure gradient force. The dissipation parameter values which most skilfully reproduce the warming patterns correspond to the dissipation timescales of advection and eddy momentum flux. This suggests that these processes are essential in shaping the warming pattern.

Upper tropospheric temperature anomalies are often associated with water vapour anomalies in the tropical tropopause layer, (Fueglistaler et al., 2009), which implies that the warming pattern could modulate the transport of water vapour into the stratosphere. An upper tropospheric warming pattern with considerable horizontal gradients is a robust feature in most climate models, but the CMIP6 models disagree on the shape of the pattern. This disagreement is likely because CMIP6 models currently represent tropical convection poorly (Fiedler et al., 2020) and therefore disagree considerably on how tropical precipitation will change under global warming. Once climate models improve their representation of tropical precipitation, projections of upper tropospheric warming patterns should also improve and become more consistent across different models.

4.2 REMAINING UNCERTAINTIES AND OUTLOOK

Over the recent decade, the discrepancy between observed and simulated upper tropospheric warming has been considerably reduced. On the one hand, this is because the impact of entrainment (Miyawaki et al., 2020, and this study), as well as internal variability expressed through SSTs (Mitchell et al., 2013; Tuel, 2019; Po-Chedley et al., 2021), on upper tropospheric warming is better understood. On the other hand, observations of upper tropospheric temperatures have been revised (Haimberger et al., 2012; Po-Chedley et al., 2015; Zhou et al., 2021) and now show stronger estimates of upper tropospheric warming. Nevertheless, radiosonde observations still disagree among each other (see section 3.1), as do satellite observations (Santer et al., 2017b). In particular, it remains unclear

- whether upper tropospheric warming is overestimated mainly because the models too strongly amplify a correctly simulated lower tropospheric warming,

- whether the warming throughout the troposphere is overestimated (Mitchell et al., 2013) and the bias already appears at 700 hPa,
- or the CMIP6 AMIP ensemble actually simulates lower and upper tropospheric warming well, as the SUNY dataset (and a recent analysis of satellite data, Po-Chedley et al., 2021) suggests.

As a consequence the assessment of upper tropospheric warming in climate models remains ambiguous. Earlier estimates of upper tropospheric warming from climate models (Santer et al., 2005; Fu et al., 2011) now hold up much more favourable. It seems that some of the controversy could have been avoided by trusting climate models more and critically assessing observations. After all, the procedure of measuring and processing radiosonde and satellite data contains maybe as many empirical assumptions as a convection parameterisation.

As for climate models, the CMIP6 ensemble shares no common bias with regards to the mean lapse rate, likely because they are tuned to best represent the present day climate. However, it is possible that errors related to parameterisations are compensated by tuning other parameters (Mauritsen et al., 2012). This becomes obvious in the ICON-A convection parameterisation, where the condensate does not enter the calculation of the heat capacity. This makes the lapse rate more pseudoadiabatic and thereby colder. One way to compensate for this would be to decrease the turbulent entrainment rate, but this would also cause an overestimation of upper tropospheric warming. This is indeed what might have happened here, because the ICON-A model simulates upper tropospheric amplification of warming that is stronger than most CMIP6 models, let alone observations. Therefore the development of these parameterisations is perhaps driven too strongly by the goal of correctly simulating present day climate instead of taking a physics based approach (Emanuel, 2020).

The new generation of storm resolving models promises to improve the representation of many aspects of tropical climate, especially precipitation (Stevens et al., 2020; Hohenegger et al., 2022), by not relying on a convection parameterisation. Whether this translates into improved upper tropospheric temperatures and warming is yet unclear, as many of the subgrid-scale processes, especially microphyiscal processes, remain parameterised. Organised entrainment and detrainment are represented explicitly, at least to some degree, but smaller scale turbulent entrainment is accounted for in the turbulence parameterisation. During the development of these new storm resolving models, errors that were compensated among the parameterisations before, suddenly appear in the storm resolving models, and the remaining parameterisations have to be retuned. As a result, the promise of simulating an improved climate is not instantly fulfilled for every aspect. Considering climate models with convection parameterisations will be needed for simulations of longer time periods, I think that continued understanding and physics based improvement of convection parameterisations in parallel to developing a new generation of storm resolving models is necessary. An improved understanding of convection and its implementation in climate models could prove to be beneficial for the storm resolving models further down the line (Emanuel, 2020). Once some of the initial problems are solved, in the long term storm resolving models will likely be an extremely important leap forward for climate science.

Finally, it is still somewhat unclear which near-surface variables are useful to determine and predict upper tropospheric temperature anomalies. Boundary layer moist static energy should be a good indicator of convection, but has not been used to assess upper tropospheric temperatures. PRSSTs (Fueglistaler et al., 2015; Tuel, 2019), that account for

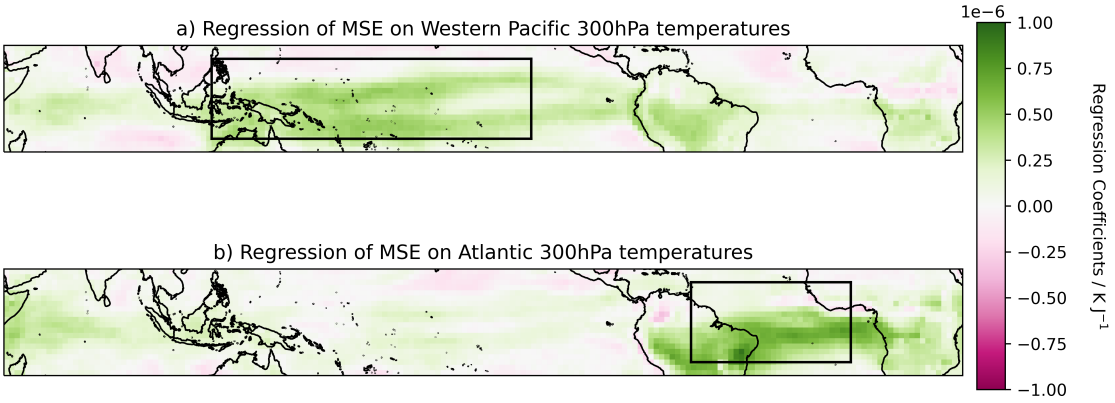

Figure 4.1: Linear Regression coefficients of 925 hPa moist static energy (MSE) at every grid point on horizontally averaged 300 hPa temperatures. The areas over which 300 hPa are averaged are indicated as boxes. Shown are the multi-model mean regression coefficients over 31 CMIP6 models, using the SSP585 scenario. The regression is done with detrended monthly mean January values.

the spatial coupling of SSTs and convection, work well for CMIP5 models, but not necessarily for CMIP6 models, as shown in section 3.1. Instead it has been suggested that the El Niño index explains upper tropospheric warming differences among CMIP6 models (Po-Chedley et al., 2021). This would imply that convection occurring in a single region (the region represented by the El Niño index) sets the tropospheric temperatures throughout the tropics. In contrast, the results presented in section 3.2 demonstrate that the influence of convective heating on upper tropospheric temperatures can be locally confined. This would suggest that a spectrum of convective plumes throughout the tropics contributes to setting the tropical mean lapse rate and thereby upper tropospheric warming.

The questions of what near-surface variables are useful to explain upper tropospheric temperature anomalies and to which degree different regions contribute to setting upper tropospheric temperatures could be tackled by a machine learning approach: Surface and boundary layer variables from climate models could be used to train a neural network to predict upper tropospheric temperature anomalies. By using an *explainableAI algorithm* (Mamalakis et al., 2022; Retsch et al., 2022), one can gain insight into which variables and which regions are most important for the neural network's predictions. Figure 4.1 shows a preliminary and simplified implementation of this method. A linear regression of boundary layer moist static energy with different areas of upper tropospheric temperatures reveals that regional coupling of the boundary layer and the upper troposphere indeed seems to be substantial. Further, convective coupling over land, especially over South America, also seems important, which is often not considered in other studies. These results encourage the further development of this method, especially because a machine learning approach should be even more skilful than a simple linear regression. This approach could also reveal if the relationship between the surface and the upper troposphere is fundamentally different between conventional climate models, storm resolving climate models, and reanalysis datasets, and could aid our understanding of how the upper troposphere and the surface are connected. Here, climate models and analysis of their output could lead to new theories and simple models.

These simple models, like the idealised calculations of moist adiabats and the numerical Gill model, are incredibly valuable for understanding complex processes and have been the key to progressing and completing this project. Especially today, as climate

scientists struggle to analyse large amounts of data produced by storm resolving models, and to interpret results from novel machine learning approaches, taking a physics based approach with simple models is maybe more important than ever.

Part II

APPENDICES

A

APPENDIX A

The work in this appendix has been published as:

Keil, P., Schmidt, H., Stevens, B., & Bao, J. (2021). "Variations of Tropical Lapse Rates in Climate Models and Their Implications for Upper-Tropospheric Warming." *Journal of Climate*, 34(24), 9747-9761.

Variations of Tropical Lapse Rates in Climate Models and Their Implications for Upper-Tropospheric Warming.

Paul Keil[1,2], Hauke Schmidt[1],Bjorn Stevens[1],Jiawei Bao[1]

[1] Max Planck Institute for Meteorology, Hamburg, Germany
[2] International Max Planck Research School on Earth System Modelling, Max Planck Institute for Meteorology, Hamburg, Germany

Manuscript submitted 10 March 2021, in final form 8 September 2021

ABSTRACT

The vertical temperature structure in the tropics is primarily set by convection and therefore follows a moist adiabat to first order. However, tropical upper tropospheric temperatures differ among climate models and observations, as atmospheric convection remains poorly understood. Here, we quantify the variations in tropical lapse rates in CMIP6 models and explore reasons for these variations. We find that differences in surface temperatures weighted by the regions of strongest convection cannot explain these variations and therefore we hypothesise that the representation of convection itself and associated small scale processes are responsible. We reproduce these variations in perturbed physics experiments with the global atmospheric model ICON-A, in which we vary autoconversion and entrainment parameters. For smaller autoconversion values, additional freezing enthalpy from the cloud water that is not precipitated warms the upper troposphere. Smaller entrainment rates also lead to a warmer upper troposphere, as convection and thus latent heating reaches higher.
Furthermore, we show that according to most radiosonde datasets all CMIP6 AMIP simulations overestimate recent upper tropospheric warming. Additionally, all radiosonde datasets agree that climate models on average overestimate the amount of upper tropospheric warming for a given lower tropospheric warming. We demonstrate that increased entrainment rates reduce this overestimation, likely because of the reduction of latent heat release in the upper troposphere. Our results suggest that imperfect convection parameterisations are responsible for a considerable part of the variations in tropical lapse rates and also part of the overestimation of warming compared to the observations.

SIGNIFICANCE STATEMENT

A major criticism of climate model simulations has been their overestimation of warming in the tropical upper troposphere, between 8 and 13 km altitude, compared to observations. We show that climate models already disagree on the mean upper tropospheric temperatures, even before warming. We demonstrate that the process of how much a convective cloud mixes with its surroundings, so called entrainment, significantly influences upper tropospheric temperatures and their rate of warming. Increasing entrainment decreases the heat released by condensation, which in turn reduces upper tropospheric

warming to resemble the observed warming. Improving the representation of this process in climate models, as well as other aspects of convection, should therefore be beneficial for the simulation of upper tropospheric temperatures.

Air parcels undergoing deep convection change their temperature during their ascent according to the moist adiabatic lapse rate. In the tropics any horizontal temperature gradients produced by deep convection are quickly reduced by gravity waves (Bretherton and Smolarkiewicz, 1989), resulting in a fairly weak temperature gradient (WTG). Thus, the lapse rate throughout the tropical troposphere is set by deep convection and follows a moist adiabat closely (Stone and Carlson, 1979).

However, this is a simplified picture, and neglects some crucial details. For starters, the effect of entrainment is important, since undiluted ascent is very rare (Romps and Kuang, 2010), and entrainment has been shown to influence upper tropospheric stratification by regulating latent heating in the convecting plumes (Singh and O'Gorman, 2013). Also, the lapse rate is likely not set by the single warmest and deepest convective plume, but rather a spectrum of entraining convective plumes (Zhou and Xie, 2019; Bao and Stevens, 2021). Further, it is not clear to what degree the ascent follows an idealised moist pseudoadiabat, which assumes instant removal of condensate (all cloud water precipitates), or a reversible moist adiabat, which assumes no removal of condensate at all (no precipitation), or something in between (Bao and Stevens, 2021). Another aspect to be considered is the fusion enthalpy, which is a source of cloud buoyancy (Romps and Kuang, 2010). Finally, at some level in the upper troposphere, the radiative-convective equilibrium starts to transition to a purely radiative equilibrium (Folkins, 2002). Since the WTG approximation holds reasonably well, and the mean tropical lapse rate is indeed primarily set by deep convection (Bao and Stevens, 2021), all of these processes should have an influence on the mean observed lapse rate in the tropics. Due to deficient resolutions climate models usually parameterise many of these processes, and do so in a range of different ways (Plant and Yano, 2016). It should be noted that the WTG assumption applies to the virtual temperature and thus drier regions of the tropical troposphere should be slightly warmer.

Uncertainties have also been reported in relation to global warming. Under greenhouse gas forcing, the tropical upper troposphere is expected to warm more than the surface and lower troposphere, since cloud base saturation vapor pressure is a strongly increasing function of temperature, and this additional vaporization enthalpy is realized by a disproportionate warming with height (Santer et al., 2005). However, the observed warming in the early 21st century is significantly weaker than predicted by climate models and basic theory (Santer et al., 2005; Thorne et al., 2007; Fu et al., 2011; Mitchell et al., 2013; Santer et al., 2017a,b; Suárez-Gutiérrez et al., 2017), although results depend on the exact time period (Thorne et al., 2007; Suárez-Gutiérrez et al., 2017), and observations also hold uncertainties (Sherwood et al., 2005; Thorne et al., 2007, 2011; Po-Chedley et al., 2015). It has been suggested that deficiencies in the post-2000 forcing (Santer et al., 2017b), as well as a wrong representation of SSTs and their coupling to deep convection (Flannaghan et al., 2014; Fueglistaler et al., 2015; Tuel, 2019) might impact upper tropospheric warming rates. Indeed, the bias is smaller in atmospheric models that use observed SSTs, compared to coupled atmosphere-ocean models (Mitchell et al., 2013; Po-Chedley et al., 2021). Furthermore, entrainment dampens the warming of the tropical troposphere by reducing the additional vaporization enthalpy (Singh and O'Gorman, 2013) which is likely one reason why the overestimation of warming by climate models is not as drastic as expected from the theoretical adiabats (Miyawaki et al., 2020).

Increasing the conceptual understanding of what processes determine the tropical upper tropospheric lapse rate and reducing these uncertainties in climate models could

be beneficial for the representation of many other aspects of global circulation and climate. For example, the strength of the Walker Circulation and its evolution under greenhouse gas forcing (Sohn et al., 2016), the atmospheric moisture flux into the Arctic (Lee et al., 2019) as well as tropical cyclone intensity (Trabing et al., 2019) have been shown to depend on the tropical upper tropospheric stratification. Because tropical mid- to upper tropospheric temperature affects baroclinity in the midlatitudes it also impacts midlatitude eddies and poleward heat transport (Lu and Cai, 2010; Wu et al., 2011). In addition, the response of tropical anvil clouds to greenhouse gas warming likely depends on upper tropospheric static stability (proportionally higher anvil temperature hypothesis, PHAT, Zelinka and Hartmann, 2010), and may result in a cloud feedback that impacts equilibrium climate sensitivity.

In this study we investigate the diverse representations of tropical lapse rates across climate models. In section A.3 we document differences in the mean lapse rates and upper tropospheric temperatures among CMIP6 models. We find that precipitation weighted sea surface temperatures (PRSSTs, Fueglistaler et al., 2015; Tuel, 2019) do not explain the variation of upper tropospheric temperatures in the mean state better than lower tropospheric temperatures. Therefore, in section A.4 we demonstrate how differences in the way climate models parameterise precipitating deep convection itself has a large influence on upper tropospheric temperatures. We do this by changing parameters in the convection and microphysics parameterisations in AMIP experiments with the atmospheric component of the climate model ICON-ESM (hereafter, ICON-A). Finally, in section A.5 we examine recent upper tropospheric warming in our ICON-A experiments, CMIP6 models and radiosonde observations and investigate how the warming from the lower troposphere is transferred to the upper troposphere.

A.2 METHODS

A.2.1 *CMIP6*

To study variations in upper tropospheric temperatures we use the preindustrial control (piControl) and the atmospheric model intercomparison project (AMIP) experiments of CMIP6 (coupled model intercomparison project, Eyring et al., 2016). In section A.3 we analyse tropical lapse rates in the CMIP6 piControl and AMIP simulations. In sections A.4 and A.5 we use the AMIP simulations to compare to the ICON experiments and analyse historical warming rates respectively. In the piControl experiments the climate is equilibrated, which is ideal to study the time mean properties of tropical lapse rates. In contrast, the AMIP experiments are forced by observed sea surface temperature and therefore do not represent the stationary state (i.e. the mean state), but provide a somewhat realistic framework to analyse historical warming. Also, the warming trend should be less conflated with uncertainties arising from internal variability compared to a coupled simulation (e.g. a RCP scenario), in which SSTs vary substantially (Mitchell et al., 2013). We use the first ensemble member of every model ('r1i1p1f1') and the entire available timespan, which differs from model to model in the piControl case, and the years 1979-2012 in the AMIP case, since some radiosonde products do not extend beyond 2012. 51 models provide air temperature, and of those 50 provide surface temperature and precipitation in the piControl case. In the AMIP case 40 models provide air temperature, while 38 models provide air temperature, surface temperature and precipitation.

A.2.2 *Observations*

Recent studies analysing upper tropospheric temperatures have primarily made use of satellite data which provides spatially complete measurements in the tropics. Radiosonde data have been used less frequently, perhaps because the spatial coverage is sparse and they have been suggested to be error prone (Sherwood et al., 2005; Thorne et al., 2011). However temperatures inferred from satellites have also been shown to underestimate tropical tropospheric warming rates and have been continuously corrected (Po-Chedley et al., 2015). Radiosonde data have the advantage of higher vertical resolution, and therefore we make use of various different radiosonde products in this study to analyse tropical lapse rates. As we will show, the radiosondes products are overall in reasonable agreement amongst each other and with the ERA5 reanalysis, which strengthens our confidence in the radiosonde data.

For the analysis of the mean state in subsections A.3 and A.5, we use the Iterative Universal Kriging version 2 (IUKv2, Sherwood and Nishant, 2015) radiosonde dataset to compare models with observations. The IUKv2 addresses many of the issues identified as limitations in the past, as it considers time-changing instrument biases. Unlike the other radiosonde products, it provides absolute temperatures, which makes it suitable to assess the time mean tropical lapse rates. However, it provides no estimate of a tropical average, only data for individual stations. We use data from 69 stations in the tropics (20°N-20°S) over the 1979-2014 period. Tropical means that are shown refer to simple averaging over all stations. When subsampling the model data to the gridpoints of the radiosonde locations, results in subsection A.3 are very similar.

For the analysis of upper tropospheric warming in subsection A.5 we also include radiosonde data from various other sources, namely the HADAT (Thorne et al., 2005), RATPAC (Free et al., 2005), Rich-obs, Rich-tau and Raobcore (Haimberger et al., 2012), and SUNY-Albany (Zhou et al., 2021) datasets. These datasets provide temperature anomalies as a tropical mean (20°N-20°S) or as gridded data, from which we calculate the tropical mean. Homogenisation over time, as in the IUKv2 case, is also applied in different manners for all of these products. We show perturbed parametric ensemble estimates for Rich-obs and Rich-tau until the year 2012, which indicate the range of uncertainty in these products.

In addition to the radiosondes we also use the ERA5 reanalysis (Hersbach et al., 2020) as an estimate for the lapse rate and upper tropospheric warming. For air temperature in years 2000-2006 we use ERA5.1 that shows more realistic stratospheric temperatures (Simmons et al., 2020).

A.2.3 *ICON-A Experiments and Convection Parameterisation*

We employ the atmospheric component of the ICON earth system model ICON-A (Giorgetta et al., 2018) to investigate the sensitivity of the tropical lapse rate to perturbations in the convection scheme. We choose the R2B4 AMIP configuration (160km horizontal gridspacing and 47 vertical levels) for various reasons: ICON-A produces a realistic climate in the tropics in this configuration (Crueger et al., 2018), the resolution is representative of those in the CMIP6 ensemble and it is computationally feasible to perform many experiments over the AMIP time period (1979-2014) to investigate the role of different parameters and also account for internal variability. We simulate a reference climate with seven ensemble members and experiments with perturbed autoconversion

and turbulent entrainment with five ensemble members for each parameter value. The chosen parameter values are given in Table A.1.

The convection parameterisation in ICON-A is based on the scheme proposed by Tiedtke, 1989 with some adaptations by Nordeng, 1994. A comprehensive summary of the scheme as implemented in ICON-A is given by Möbis and Stevens, 2012. It is based on the bulk equations that calculate the convective mass flux M_u as a function of homogeneous entrainment E_u and detrainment D_u. The subscript u denotes the updraft variables.

$$\frac{\partial M_\mathrm{u}}{\partial z} = E_\mathrm{u} - D_\mathrm{u} \tag{A.1}$$

The convective fluxes of dry static energy, moisture, cloud water and momentum are calculated in a similar manner, including processes like condensation and precipitation. Besides detrainment, the cloud water l_u depends on the condensation rate c of water vapour to cloud water and conversion of cloud water to rain (or autoconversion) K. The overbar indicates the resolved large-scale variables.

$$\frac{\partial (M_\mathrm{u} l_\mathrm{u})}{\partial z} = -D_\mathrm{u} l_\mathrm{u} + \bar{\rho} c - \bar{\rho} l_\mathrm{u} K \tag{A.2}$$

Here $\bar{\rho}$ is the large-scale air density. K will be one of the parameters varied for the perturbed physics experiments. The condensation heating includes fusion enthalpy. However, the heat capacity does not consider the liquid or frozen condensate.

Entrainment and detrainment are assumed to consist of an organised and turbulent part.

$$E_\mathrm{u} = E_\mathrm{u,turb} + E_\mathrm{u,org} \tag{A.3}$$

$$D_\mathrm{u} = D_\mathrm{u,turb} + D_\mathrm{u,org} \tag{A.4}$$

The organised entrainment and detrainment rates are calculated from large-scale and updraft variables and are only applied at certain levels. The turbulent entrainment and detrainment acts on all levels and depends on the mass flux and the entrainment rate parameter ϵ_u and detrainment rate parameter δ_u:

$$E_\mathrm{u,turb} = \epsilon_\mathrm{u} M_\mathrm{u} \tag{A.5}$$

$$D_\mathrm{u,turb} = \delta_\mathrm{u} M_\mathrm{u} \tag{A.6}$$

Shallow and deep convection have different entrainment rates, in this study we focus on the entrainment rate for deep (or penetrative) convection. It is assumed that $\epsilon_\mathrm{u} = \delta_\mathrm{u} = L^{-1}$ for $p > p^*$ and $\epsilon_\mathrm{u} = 0$, $\delta_\mathrm{u} = L^{-1}$ otherwise, where L is the characteristic length scale with the standard value $L = 5\,\mathrm{km}$, which is also used for our reference experiments, and p^* is either the arithmetic centre of the cloud base and cloud top pressure, or the pressure of maximum updraft velocity (see Möbis and Stevens, 2012 for more information). It is usually situated somewhere in the mid-troposphere. Therefore the mass flux decreases between p^* and the level of the cloud top, at which the organised detrainment is applied. In the following, we will refer to both ϵ_u and δ_u as the turbulent entrainment parameter.

A.2.4 *Theoretical Moist Adiabats*

We calculate some theoretical moist adiabats under different assumptions: the pseudoadiabat, which assumes all condensate precipitates immediately, the reversible (or isentropic) adiabat, which assumes that no condensate is removed, and their respective ice versions that include the fusion enthalpy. We follow the method of Stevens and Siebesma, 2020 (section 2.2.2) and start with the enthalpy form of the First Law of Thermodynamics for an adiabatic process

$$0 = \mathrm{d}h - v\mathrm{d}p \tag{A.7}$$

where dh is the change in specific enthalpy, v is the specific volume and dp is the change in pressure. The specific enthalpy depends on temperature T, saturation water vapour mixing ratio q_s, specific heat capacity c_p and the phase change enthalpy l:

$$h = c_p T + l q_\mathrm{s} \tag{A.8}$$

l and q_s in turn also depend on pressure and temperature and the heat capacity can also change during the ascent. Direct analytical calculation for some types of moist adiabats is possible, but here we take a numerical approach for all. We define

$$\mathrm{d}X = \mathrm{d}h - v\mathrm{d}p \tag{A.9}$$

and determine $\frac{\partial X}{\partial T}$ and $\frac{\partial X}{\partial p}$. With this we can compute the lapse rate

$$\frac{\mathrm{d}T}{\mathrm{d}p} = -\frac{\frac{\partial X}{\partial p}}{\frac{\partial X}{\partial T}} \tag{A.10}$$

which can be integrated along p to obtain a temperature profile. The $\frac{\partial X}{\partial T}$ and $\frac{\partial X}{\partial p}$ terms are calculated according to the chosen adiabat. For the pseudoadiabat the specific heat capacity is calculated from the specific heat capacity of dry air and water vapour which decreases with ascent, while for the isentropic adiabat the specific heat capacity of the condensate is also used. The phase change enthalpy l is simply the condensation enthalpy for the pseudoadiabat and the isentropic adiabat, whereas for their ice-counterparts the fusion enthalpy is added at temperatures below the freezing level. Thus, in the case of freezing we assume that all condensate freezes above the freezing level (and then precipitates in the case of the pseudo-ice adiabat). The saturation water vapour pressure is calculated with respect to ice in these cases. We start the integration at a certain level in the lower troposphere (usually 700 hPa) where we assume saturation. For the isentropic adiabats we need to specify the total water content in the parcel, for which we chose 15 $\mathrm{g\,kg^{-1}}$. This is larger than the saturation specific humidity at this level since it is likely that the parcel already contains condensate.

In addition, we calculate a lapse rate that considers entrainment using a zero-buoyancy entraining plume model based on the calculation of Singh and O'Gorman, 2013 with reference to the pseudoadiabat. In this model, it is assumed that cloud buoyancy is negligible, which in this case means uniform horizontal temperature (virtual temperature effects are not considered). The environmental air is entrained at a rate $\epsilon = \epsilon_0/z$ and has uniform relative humidity r, where z is height above ground. If not stated otherwise, we set $\epsilon_0 = 0.3$ and $r = 0.8$. The vertical profile of the temperature difference to the pseudoadiabat is calculated as

$$\Delta T(z) = \frac{(1-r)}{1 + \frac{l^2 q_\mathrm{v}^*}{R_\mathrm{v} T^2 c_p}} \int_{z_\mathrm{b}}^{z} \frac{\epsilon l q_\mathrm{v}^*}{c_p} dz' \tag{A.11}$$

where q_v^* is the saturation specific humidity of the environment and R_v is the gas constant for water vapour. The integration is started from the cloud base height z_b to some height z. We use 960 hPa as cloud base level (starting the integration at 700hPa underestimates the effect of entrainment on the temperature profile). In the following, the zero-buoyancy entraining plume will be referred to as 'entraining plume'.

A.3 Differences in lapse rates and upper tropospheric temperatures in conventional climate models

First, we provide an overview of the relationship of lower tropospheric and upper tropospheric temperatures in the tropics (defined as 20°N-20°S, including both land and ocean). We use the 700hPa level as proxy to represent the lower free troposphere, since the horizontal temperature variations are small around this level (Bao and Stevens, 2021). The WTG approximation holds fairly well and we expect tropospheric temperatures throughout the tropics at and above 700 hPa to be primarily set by deep convection and thus follow a moist adiabatic lapse rate. Consequently, we should be able to infer the upper tropospheric temperatures from their lower tropospheric values. In CMIP6 models, this is indeed the case (Figure A.1a), as a model with a warmer lower troposphere tends to have a proportionally warmer upper troposphere and the linear fit across CMIP6 models is at 1.19 K/K. Overall, the models are close to the line that would indicate a pseudoadiabatic relation (moist adiabatic ascent where all condensate precipitates immediately) between 700 and 250 hPa, but the upper tropospheric temperatures in individual models deviate by up to 1.7 K from the theoretical line. Only very few models are closer to the line that indicates reversible adiabatic relation (convective ascent with no precipitation) than the pseudoadiabatic relation. Despite the robust correlation, there is considerable variability of more than 3 K in the upper tropospheric temperatures of CMIP6 models for the same lower tropospheric temperatures. Similar behaviour is found in the AMIP simulations (Figure A.1b), which are forced by observational SST datasets (Flannaghan et al., 2014) and, therefore, show less spread in their lower tropospheric temperatures. However, for a given lower tropospheric temperature the spread in the upper troposphere has approximately the same magnitude as in the coupled case, resulting in a reduced correlation of lower and upper tropospheric temperatures. As in the piControl case, the AMIP experiments can deviate considerably from the temperatures expected from a theoretical pseudoadiabat (up to 1.8 K in the upper troposphere), and even more from the reversible adiabat, while the IUK radiosondes and the ERA5 reanalysis are fairly close to a pseudoadiabatic relationship (this does not hold for the whole troposphere, as we will show below). The slopes of the regression in both cases in Figure A.1 demonstrate that the cross model-relationship of a proportionally warmer upper troposphere for models with a warmer lower troposphere does not follow the moist adiabat, as the pseudoadiabatic and the reversible relationships have larger slopes of 1.99 K/K and 1.89 K/K respectively. Note that the slopes of the piControl and the AMIP case are within one standard error of each other, while the theoretical adiabats are clearly outside of the standard error range. Figure A.1 demonstrates that lower tropospheric temperatures are useful for predicting upper tropospheric temperatures, but only to a certain degree. Pseudoadiabatic ascent is a decent approximation for the tropical lapse rate in CMIP6 models but the variation in upper tropospheric temperatures and the cross-model regression suggests that it is influenced by additional processes that will be discussed in this section.

Above, we have examined the tropical atmosphere in a horizontal mean view. However, only the convective plumes with strong enough buoyancy reach the upper troposphere,

which usually originate over warmer SSTs. This coupling of SSTs and convection likely varies across models and has been quantified with precipitation weighted SSTs (PRSST) which show a relationship to upper tropospheric warming in CMIP5 models (Fueglistaler et al., 2015; Tuel, 2019). Here, we apply this methodology to the CMIP6 piControl ensemble using monthly means of SSTs and precipitation to investigate whether this can explain the variations in upper tropospheric temperatures in the mean state. Additionally, we calculate precipitation weighted 700 hPa temperature (PRTA) in a similar manner, but also include gridpoints over land in this case, to facilitate the comparison to Figure A.1. We find that PRSSTs cannot explain differences in the mean state (Figure A.2a) any better than plain tropical mean 700 hPa temperatures (Figure A.1a). Instead, the correlation between PRSSTs and upper tropospheric temperatures is even slightly worse than in Figure A.1a and the spread in upper tropospheric temperatures also remains similar at around 4 K for a given value of PRSST. The PRTA (Figure A.2b) shows a better correlation than the PRSST (0.75 vs 0.68), but worse than the unweighted 700 hPa temperatures (0.79). Therefore, the temperatures in the convecting regions, whether SSTs or 700 hPa air temperatures, do not seem to be a better indicator of upper tropospheric temperatures than the simple tropical mean at 700hPa. This is likely because the 700 hPa temperatures are homogenised quite effectively to the convecting temperatures by gravity waves (Bao and Stevens, 2021) and thus the spatial coupling is naturally included in the tropical mean 700 hPa (or even to some extent in a single radiosonde station). Consequently, we will focus on differences in tropical mean lapse rate behaviour above 700 hPa to explain the spread in upper tropospheric temperatures, given a certain lower tropospheric temperature.

To illustrate the diversity in tropical lapse rates we assume the moist pseudoadiabat as the closest option to reality (Figure A.1) and show how the tropical lapse rates deviate from the moist pseudoadiabat in individual piControl simulations (AMIP simulations yield similar results). We calculate the pseudoadiabat with the tropical mean 700 hPa temperature as basis and assume saturation at this level. The same calculation was done for radiosonde data from the IUKv2 dataset, as well as the ERA5 reanalysis. CMIP6 models deviate both positively and negatively from their idealised moist pseudoadiabat (Figure A.3). The maximum deviations increase with height, and reach a range from approximately 3 K colder to 2 K warmer than predicted by the moist pseudoadiabat in the upper troposphere. The observations lie within the model spread, but show stronger deviations from the idealised pseudoadiabat than the ensemble mean, especially in the middle troposphere around 500 hPa. Although the reanalysis does not match the observations perfectly, it provides further indication that the real tropical lapse rate is colder than the pseudoadiabat for most of the troposphere. Models and observations systematically become warmer than their idealised pseudoadiabat above 250 hPa, indicating the transition from the radiative-convective equilibrium to a purely radiative equilibrium (Folkins, 2002).

While the pseudoadiabatic ascent seems to reasonably explain the vertical temperature structure in the tropics at first glance, the impact of subgrid-scale processes that alter the diabatic response of the air parcel to the ascent is less clear. In the following we will discuss how some of these processes impact the tropical lapse rate and thereby attempt to explain the spread in lapse rates in CMIP6 models. For example, an air parcel following a reversible adiabat will end up being warmer than one following a pseudoadiabat because of the additional heat reservoir of the condensate contributing to the heat capacity. What happens in reality is somewhere in between these two processes, although it has been suggested that the lapse rate is closer to the pseudoadiabat in the middle and upper

troposphere (Bao and Stevens, 2021). Figure A.3 shows the deviation of the reversible adiabat from the pseudoadiabat (again using the ensemble mean 700 hPa temperature of CMIP6 models) and reveals that the majority of models are closer to the pseudoadiabat. Furthermore, fusion enthalpy causes additional warming during the ascent, which we illustrate with the pseudo-ice adiabat. Again, the standard pseudoadiabat seems a better fit for most models, but not all. A further process to consider is the entrainment of dry air from outside the cloud that has a cooling effect (Singh and O'Gorman, 2013), since it decreases the available moisture and thereby reduces latent heating. The entraining plume approximation, that takes this process into account in a simplified manner (methods), agrees fairly well with a considerable amount of models and the observations. Note that the exact values of the reversible adiabats and the entraining plume are somewhat arbitrary, since they depend on the specified total water content for the parcel and the entrainment rate, respectively.

It is not clear whether the good agreement of the lapse rates to the pseudoadiabat and the entraining plume means that these processes dominate in tropical convection or whether the lapse rates are determined by all of the discussed processes and as a result are close to the moist pseudoadiabat because of compensation. The latter option seems more likely since processes like freezing and (partly) reversible ascent can be observed in reality. In addition, tropospheric temperatures are most likely not set by a single plume with a determined behaviour, but rather a spectrum of convecting plumes, that penetrate to different heights and vary in their entrainment rate (Zhou and Xie, 2019; Bao and Stevens, 2021). We conclude that all of the discussed processes likely impact the lapse rates in CMIP6 models and thereby explain a considerable part of the spread. Since all of these processes happen on subgrid scales, conventional climate models like those in the CMIP6 ensemble parameterise them in a range of different manners. And even if two models use the same convection parameterisation, the parameters might be tuned to different values to best compensate errors from other assumptions, which differ across models (Mauritsen et al., 2012). Also, CMIP6 models might contain a common bias related to assumptions made in the convection parameterisations, especially considering the observed lapse rate almost falls outside of the CMIP6 spread at 500hPa. To demonstrate the impact these subgrid-scale processes have on lapse rates simulated in conventional climate models, we perform experiments with perturbed convection parameterisation, which we present in the next section.

A.4 Processes influencing the tropical lapse rate in ICON-A simulations

We use the atmosphere component ICON-A from the ICON general circulation model in experiments where we perturb the conversion of cloud water to rainfall (autoconversion) and the turbulent entrainment rate for penetrative convection (the reasoning behind these choices are described in the respective subsections below). The values of the tuning parameters are given in Table A.1. In the model development process these parameters are set so as to simulate the overall climate as well as possible, hence changing them is generally expected to degrade the climate, at least for those quantities which the tuning process targeted. Nonetheless, by using a skill score for climate models (Reichler and Kim, 2008) we demonstrate that all of our experiments but one lie within the skill range of CMIP6 models, and one experiment just outside the range (Figure A.4). The temperature response in both sets of experiments is shown in Figure A.5. Temperatures deviate by more than 2 K from the reference experiment, especially in the upper troposphere (Figure A.5a). With these experiments we can reproduce the spread in temperatures in CMIP6

AMIP simulations (Figure A.5b). The temperature responses in individual experiments and the reasons behind them will be discussed in the following subsections. In this section we present ensemble mean values for our ICON-A experiments, since the differences among ensemble members of one type of experiment are small.

A.4.1 *Conversion of Cloud Water to Rain*

First, we examine the experiments with perturbed autoconversion in comparison to the reference experiment. Increasing autoconversion decreases temperatures in the upper troposphere (Figure A.5) and vice-versa. Lower tropospheric temperatures are unchanged, which means that the lapse rate is different to that of the reference experiment only above 700 hPa. In the case of the low autoconversion, the upper troposphere is more than 1 K warmer than the reference experiment.

We analyse the reason behind the temperature changes for the case of low autoconversion: Figure A.6a shows the expected increase of cloud water and cloud ice mixing ratio for decreased autoconversion, as less condensate is precipitated. This increase in condensate points towards two processes that could explain the warming: 1) The condensate contributes to the heat capacity of the air parcel and therefore the expansion cooling is reduced (ascent which is closer to the reversible adiabat than the pseudoadiabat), and 2) the additional cloud water freezes, which produces additional fusion enthalpy. Since the additional condensate heat capacity is not accounted for in the ICON-A convection parameterisation, the fusion enthalpy is responsible for the warming. This is supported by the fact that the temperature deviations occur only above 600 hPa level, which is approximately the freezing level (Figure A.5a). We further illustrate the effect of the fusion enthalpy by calculating the temperature deviations from the theoretical pseudoadiabat above 600 hPa (Figure A.6b), with the same method as in Figure A.3. For small values of autoconversion, the lapse rate agrees with the pseudo-ice adiabat between 600 and 500 hPa before becoming colder, but still remain substantially warmer than the pseudoadiabat. Above 250 hPa, the transition to the purely radiative equilibrium begins, and the idealised moist adiabats become less relevant for understanding the lapse rate. We observe the opposite behaviour for increased autoconversion: Cloud condensate decreases, indicating less freezing of condensate cloud water (Figure A.6a), which cools upper tropospheric temperatures (Figure A.6b).

We conclude that fusion enthalpy can have a considerable impact on upper tropospheric temperatures and thereby explain some of the spread in CMIP6 models. These experiments demonstrate how the parameterisation of autoconversion controls the tropical lapse rate, while also showing a deficiency of the convection parameterisation used here, to not consider the effect of the condensate on the heat capacity. In similar experiments with parameterisations that include this effect, even larger temperature deviations can be expected.

A.4.2 *Turbulent Entrainment*

Changing the entrainment rate for deep convection has substantial effects on the lapse rate and, therefore, upper tropospheric temperatures (Figure A.5). For increased entrainment we observe a cooling throughout the troposphere with a peak between 500 and 300 hPa. This cooling appears as a shift along the pseudoadiabat at 700 hPa and 250 hPa, (Figure A.5b), but is stronger at around 500 hPa. In contrast, for the case of decreased

entrainment, we can observe a warming that is confined to the uppermost troposphere and the tropopause layer (Figure A.5a), and does not change the lapse rate in the mid-troposphere. The mechanisms behind these changes can be illustrated by changes in cloud amount and the heating rates from the convection parameterisation (Figure A.7), which will be referred to as convective heating rates.

For small turbulent entrainment rates, the lower troposphere becomes drier, while the upper troposphere moistens, since less moisture from within the convective plumes is mixed with the surroundings. This is reflected in the cloud fraction changes (Figure A.7a): the lack of entrainment reduces the cloud amount drastically throughout the troposphere and only the anvil cloud amount increases. Weakening entrainment shifts the level of neutral buoyancy higher (Zhou and Xie, 2019) since the ascent is closer to a moist adiabat and, therefore, the convective heating rates (Figure A.7b) increase in the upper troposphere and in the tropopause layer, causing the warming there. Note that at 250 hPa and higher levels, convective heating rates are at least tripled with respect to the reference experiment. Another aspect here could be that reduced entrainment decreases the degree of convective organisation (Becker et al., 2017), which also happens in these experiments (not shown) and thereby the upper troposphere, where the WTG approximation holds less well (Bao and Stevens, 2021), is more uniformly heated by deep convection. Additional fusion enthalpy might also contribute to the warming, since more cloud water is available to freeze in the convective plume, and indeed there is a small positive temperature deviation at around 600 hPa (approximately the freezing level). The cooling in the boundary layer is likely because for reduced entrainment, deep convection can occur at lower temperatures. For large entrainment rates, cloud fraction increases in the lower troposphere and decreases in the upper troposphere, since moisture is detrained to the environment earlier during the ascent. As a result, less condensation heating occurs during the ascent (Singh and O'Gorman, 2013). The reduced convective heating rates are balanced by increased heating rates from the cloud parameterisation (not shown), which means that mechanisms outside the convective parameterisation, like large scale ascent, control a substantial part of the tropical energy balance in this case. The resulting temperature profile is colder likely because of the reduced latent heating and increased evaporation of detrained cloud water (Mauritsen et al., 2012). This difference in behaviour by the parameterisations explains why the vertical temperature response is structured asymmetrically for low and high entrainment rates (Figure A.5a).

We conclude that the entrainment rate also has a substantial impact on tropical lapse rates, demonstrating that the representation of entrainment in convection parameterisations is likely one reason behind the spread in upper tropospheric temperatures in CMIP6 models. The shift of the level of neutral buoyancy illustrates how the levels at which the transition from a convective-radiative equilibrium to a purely radiative equilibrium takes place might be different across models, which has important implications for middle and upper tropospheric temperatures. Moreover, increasing entrainment results in temperature anomalies in the middle troposphere that resemble the observed temperature profile (Figure A.3), suggesting that CMIP6 models underestimate the effect of entrainment as suspected by Romps, 2010.

A.5 Upper tropospheric warming

Above, we have demonstrated how the mean tropical lapse rate is influenced by small scale processes like autoconversion and entrainment. Here, we investigate whether these processes could also impact the rate at which the upper troposphere warms under green-

house gas forcing. In a warmer climate the temperature profile is expected to change to a warmer moist adiabat, thereby amplifying the warming in the upper troposphere with respect to the surface warming. A peak amplification is expected in the upper troposphere around 200 hPa (Santer et al., 2005). However, as for the mean tropical lapse rates investigated in the previous sections, the response to global warming varies across climate models (Santer et al., 2005). More importantly, observations show a substantially weaker warming in the upper troposphere compared to what is simulated by climate models (Santer et al., 2005; Fu et al., 2011; Santer et al., 2017a,b). Here, we assess how coupling of convection and SSTs (Fueglistaler et al., 2015; Tuel, 2019; Po-Chedley et al., 2021), and the representation of autoconversion and especially entrainment (Singh and O'Gorman, 2013; Zhou and Xie, 2019; Miyawaki et al., 2020) impact upper tropospheric warming in CMIP6 AMIP simulations and our ICON-A experiments. We show results for the 250 hPa level and the time period of 1979-2012 in this section, because some radiosonde products are only available until 2012. Results are similar for 300 hPa and the 1979-2014 period. There is a considerable influence of internal variability on temperature trends and therefore, unlike in the previous section, we present individual ensemble members for the reference case as well as the autoconversion and entrainment experiments.

Following Fueglistaler et al., 2015 we examine whether the trend in PRSST, which incorporates the coupling of SSTs to convection, explains the different trends in upper tropospheric warming in CMIP6 models, our ICON-A experiments, and ERA5 reanalysis (Figure A.8a). We find a large spread in upper tropospheric temperature and PRSST trends in CMIP6 AMIP simulations but only a weak relationship with a correlation coefficient of 0.403. For our ICON experiments, the relationship is more robust, independent of the parameter experiments. However, the ERA5 upper tropospheric warming is clearly outside the CMIP6 range, while the PRSST are very similar between ERA5 and CMIP6. Therefore, we conclude that PRSSTs are of limited usefulness in explaining differences in upper tropospheric warming rates in single realisations of CMIP6 AMIP simulations and cannot explain the difference to the observed upper tropospheric warming (although the observations also show considerable uncertainty, which will be discussed below). Nevertheless, stronger differences of spatial SST-convection coupling, that occur in coupled ocean-atmosphere simulations, are important for explaining even stronger upper tropospheric warming in these simulations (Tuel, 2019; Po-Chedley et al., 2021).

In CMIP6 simulations and our ICON experiments the upper tropospheric warming is strongly connected to the warming in the lower troposphere (Figure A.8b). As in the case of the mean state (Figures A.1 and A.2) lower tropospheric temperature trends have a stronger correlation to upper tropospheric temperatures than the PRSST trend has (0.79 vs 0.40). This relationship also seems to roughly hold for all ICON-A experiments in general and the reference experiments in particular, indicating that variations of trends due to internal variability are vertically consistent throughout the troposphere.

The warming in the upper troposphere shown throughout the models in Figure A.8b is weaker than expected from the theoretical moist adiabats. For stronger entrainment rates ($\epsilon_0 \approx 0.8$) the entraining plume is able to predict the same relationship as the CMIP6 regression suggests (not shown). Most radiosonde estimates show weaker warming trends than the models at both levels, 700 and 250 hPa, with some noteable exceptions. The SUNY dataset agrees remarkably well with CMIP6 models and suggests, that there is no real discrepancy at all, and the IUK dataset at least shows the same upper tropospheric warming, but stronger than predicted by the theoretical adiabats. While the other datasets provide gridded data or tropical means, the value for IUK radiosondes shown here is simply the mean over all IUK stations in the tropics (methods). This is a minor issue

at 700 hPa (if at all), but apparently produces unrealistically strong upper tropospheric warming, where the WTG assumption holds less well (Bao and Stevens, 2021). In contrast, the HADAT data shows very weak warming, which is also unrealistic, and therefore we will not analyse the IUK and HADAT datasets further. The remaining datasets agree that the upper tropospheric warming is weaker than simulated by the CMIP6 models, even considering the uncertainties illustrated for the Rich-Obs and Rich-Tau products. However, the radiosondes disagree substantially on the lower tropospheric warming. For example, the RAOBCORE data suggests that models overestimate the warming in the whole troposphere, suggesting the discrepancy in the upper troposphere is due to the bias at lower altitudes. This contrasts with the Rich-Obs ensemble, according to which CMIP6 models simulate lower tropospheric warming reasonably well, but the amplification of warming in the upper troposphere is overestimated. It's unclear which radiosonde product is the most trustworthy, but most datasets indicate that the models overestimate recent upper tropospheric warming. This could be due to a misrepresentation of lower tropospheric warming, or due to how the warming is amplified from lower to upper troposphere.

Consequently, to quantify the relation of warming in the upper and lower troposphere we calculate an amplification factor which is the slope of a linear regression of yearly mean, tropical mean temperatures at 700 hPa vs those at 250 hPa. We assess the CMIP6 AMIP ensemble, our ICON-A experiments, observations, the ERA5 reanalysis, and the amplification expected from theoretical adiabats (Figure A.9). For CMIP6 AMIP experiments, lower tropospheric temperature increases (700 hPa) are amplified by a factor of approximately 1.5 to 1.8 K/K in the upper troposphere (250 hPa). The RATPAC, Rich-Obs, Rich-Tau and SUNY radiosonde estimates fall outside of the CMIP6 range, except for one model, with amplification factors between 1.35 and 1.55 K/K. The Raobcore radiosondes show a larger amplification of 1.6 K/K, and amplification in the ERA reanalysis is even larger, consistent with the CMIP6 ensemble.

While the CMIP6 AMIP ensemble on average overestimates the amplification seen in the radiosonde observations, the prediction by the theoretical adiabats is even stronger and outside of the model range. For the pseudoadiabat and the pseudo-ice adiabat the amplification is stronger than 2 K/K. We also show the amplification based on the entraining plume model for a range of entrainment rates from $\epsilon_0 = 0.1$ to $\epsilon_0 = 0.9$. This illustrates how entrainment tends to decrease the amplification due to the regulation of latent heating.

As indicated before, our ICON-A reference experiments show that the amplification is impacted substantially by natural variability. The spread in the reference experiments demonstrates how internal variability, that is purely driven by the atmosphere in these experiments, covers approximately a third of the CMIP6 spread and is therefore important to consider over the fairly short AMIP observational period. While Suárez-Gutiérrez et al., 2017 have excluded internal variability as sole cause of the lack of upper tropospheric warming in radiosonde data, Po-Chedley et al., 2021 showed that natural variability can explain a large part of the difference between coupled simulations and satellite data. For our experiments, internal variability alone is unlikely to be the reason for the gap to the weak observed amplification, although the variability is surprisingly strong, considering SSTs are identical across the experiments.

The behaviour of the theoretical adiabats is mirrored to some extent by our ICON-A experiments. We can reproduce the spread in the CMIP6 models and close the gap to the observations in our experiments with increased turbulent entrainment rates. The experiments with high entrainment fall just outside the range of the reference experi-

ments. To obtain an even clearer signal, we present experiments with further increased entrainment rates (by a factor of ten, called "very high entrainment", Table A.1), which clearly fall outside of the reference experiment spread and agree well with the Raobcore and SUNY radiosonde datasets, while still producing a climate that is approximately as realistic as the CMIP6 average (Figure A.4). Thus, the entrainment experiments cover almost the complete range of amplification factors in the CMIP6 ensemble and a substantial range of the theoretical entraining plume. The behaviour in the autoconversion experiments is less clear. The additional fusion enthalpy should increase amplification slightly, illustrated by the idealised pseudo-ice adiabat. However, the low autoconversion experiments, in which more condensate freezes, show a slightly weaker amplification than the high autoconversion case (although they both largely fall within the spread of the reference experiments). Overall, changes in autoconversion do not seem to have a substantial effect on the amplification of the historical warming.

The behaviour of the entrainment experiments can be understood in a broader context of other recent studies: It has been shown that the entraining plume model gives a more realistic picture of tropical lapse rates and cloud buoyancy for strong warming in idealised radiative-convective equilibrium simulations because it considers reduction in condensation heating through entrainment (Singh and O'Gorman, 2013). In addition, Miyawaki et al., 2020 suggest that one reason for weaker warming than predicted by the theoretical moist adiabat in CMIP5 experiments with a quadrupling of CO_2 is the presence of entrainment, and stronger entrainment weakens upper tropospheric warming. Our results show that this effect is already relevant for the historically observed (lack of) warming. Recently, Zhou and Xie, 2019 developed a spectral plume model, in which a plume's entrainment rate depends level of neutral buoyancy the plume reaches. This conceptual model reproduces the tropical lapse rate for colder (last glacial maximum) and warmer (RCP 8.5) simulations of general circulation models even more realistically than the single entraining plume. This emphasises the need to understand the structure of tropical temperatures through convection as a spectrum of entraining plumes with varying characteristics (Bao and Stevens, 2021; Becker and Hohenegger, 2021).

A.6 SUMMARY AND DISCUSSION

Conventional climate models, represented here through the CMIP6 ensemble, show a range of tropical lapse rates and, therefore, models with the same lower tropospheric temperature can have a spread in their upper tropospheric temperatures of more than 3 K. Models with similar PRSSTs, that incorporate the spatial coupling of SSTs (or lower tropospheric temperatures) with convection, show a similar spread spread in upper tropospheric temperatures, with a slightly worse correlation than for lower tropospheric temperatures. Therefore, we focus on explaining the variations in upper tropospheric temperatures with differences in lapse rates especially between 700 and 250 hPa. While the pseudoadiabatic ascent and the entraining plume provide the best fit to the multi-model mean, individual models can deviate up to 3 K from the latter in the upper troposphere. Since entrainment, freezing and heat capacity effects all likely play a role, some of these effects could compensate each other to produce a lapse rate close to the pseudoadiabat. In our ICON perturbed physics experiments we demonstrate how the freezing enthalpy, modified here via the precipitation efficiency or autoconversion, and entrainment substantially alter tropical lapse rates. As these processes are typically used for tuning climate models it suggests that they contribute to the spread in CMIP6 models.

Unlike the mean state, the pseudoadiabat (or any of the other theoretical adiabats) does not predict the recent upper tropospheric warming well in models or observations, further indicating that tropical lapse rates are influenced by a multitude of processes. The coupling of convection and SSTs does not explain inter-model differences in upper tropospheric temperature trends in the AMIP setup, nor the difference to the ERA5 dataset in upper tropospheric warming. In the CMIP6 ensemble upper tropospheric warming is closely related to lower tropospheric warming, but overestimated compared to almost all radiosonde datasets. Furthermore, we can show that most CMIP6 AMIP models fall outside of the observed range of lower to upper tropospheric amplification, meaning that the upper troposphere warms too strongly for a given lower tropospheric warming. By increasing entrainment in the convection scheme the amplification falls within the range of observed values, and with varying entrainment rates almost the entire range of amplification factors simulated by CMIP6 models can be covered, which shows that an inadequate representation of entrainment in CMIP6 models likely contributes to the bias between simulated and observed upper tropospheric warming. However, since the radiosondes disagree amongst themselves it is not entirely clear whether a) upper tropospheric warming is overestimated mainly because the models too strongly amplify a correctly simulated lower tropospheric warming (as the Rich-Obs dataset indicates), whether b) in addition to the overestimation of amplification, the overall warming throughout the troposphere is overestimated (Mitchell et al., 2013) and the bias already appears at 700hPa, or c) the CMIP6 AMIP ensemble actually simulates lower and upper tropospheric warming well, as the SUNY dataset (and to some extent the most recent analysis of satellite data, Po-Chedley et al., 2021) suggests. If the warming is indeed already too weak in the lower troposphere, the question remains what causes this bias. In a nutshell, according to most radiosonde products, CMIP6 models overestimate upper tropospheric warming, and according to all radiosonde products on average overestimate the amplification from lower to upper troposphere, which depends on the representation of convective entrainment.

Our results suggest that various small scale processes that occur in moist convection impact tropical lapse rates, but the exact contribution of each process remains unclear. Consequently, climate models not capturing the weak upper tropospheric warming is no surprise considering our lack of understanding in what determines the tropical lapse rate. With the results presented here, that emphasise the important role of entrainment, we connect the theoretical, more idealised work by Singh and O'Gorman, 2013 and Zhou and Xie, 2019 to studies analysing the weak observed warming (Santer et al., 2005; Fu et al., 2011; Santer et al., 2017a,b) and show that entrainment dampens the recent warming in a realistic AMIP setup. While comparing turbulent entrainment used here and in other parameterisations to real observed entrainment is difficult, it has been suggested that entrainment in models is often underestimated (Romps, 2010). We can only speculate that CMIP6 models have not been tuned with higher entrainment rates, because that leads to a worse representation of the overall climate (the energy balance in the tropics changes substantially in our high entrainment experiments, see section A.4.2. A more realistic representation of convection and entrainment could be achieved by applying a more sophisticated spectral cumulus parameterisation, in which the entrainment rate depends cloud characteristics (Zhou and Xie, 2019), as in Baba and Giorgetta, 2019. The deficiencies of convection parameterisations are also highlighted in the autoconversion experiments, in which the variation of cloud water and cloud ice should affect the heat capacity and therefore temperatures, but this process is simply not included in the parameterisation used in the ICON-A model.

While the relationship between PRSSTs and upper tropospheric warming is seemingly weak in our results, unlike for Fueglistaler et al., 2015, we only present individual ensemble members, and use CMIP6 instead of CMIP5. The relationship for individual ensemble members is more robust in CMIP5, likely because CMIP5 uses two different SST datasets which increases the spread in PRSST (see Figure 1 in Fueglistaler et al., 2015). Also, we omit any analysis of ensemble means, and therefore would argue that our results are not directly comparable to those of Fueglistaler et al., 2015. Especially for stronger variations in PRSSTs that occur in coupled atmosphere-ocean models, the coupling of convection and SSTs is an important factor to explain differences in upper tropospheric warming among models (Mitchell et al., 2013; Tuel, 2019; Po-Chedley et al., 2021). CMIP6 AMIP models seem to simulate a realistic trend in PRSSTs, which should be more reliably observed than upper tropospheric warming. Therefore, if there is a bias in upper tropospheric warming in CMIP6 AMIP models, as most radiosonde products suggest, then this bias originates from other misrepresented processes, of which entrainment is likely one.

A large part of the presented analysis was also done for CMIP5 models, but overall did not differ much from the CMIP6 results presented here. While CMIP5 models include some stronger outliers for tropical mean lapse rates, the spread in the amplification factor is virtually identical, suggesting that conventional climate models have not significantly improved in this regard over the past decade, even though our understanding of the problem with regards to the role of entrainment (Singh and O'Gorman, 2013; Miyawaki et al., 2020), and the coupling of SSTs and convection (Fueglistaler et al., 2015; Tuel, 2019; Po-Chedley et al., 2021) has increased and errors in satellite as well as radiosonde observations have reduced. Therefore, we propose to tackle this problem in the future with high resolution storm resolving models, that do not rely on parameterised convection (Stevens et al., 2019). While cloud microphysical properties will always have to be parameterised, at least an improvement in the representation of entrainment and overall tropical circulation can be expected (Stevens et al., 2020). Nevertheless, long term or large ensemble simulations will likely rely on convection parameterisations for the near future, and therefore further development in this area (Baba and Giorgetta, 2019) should be beneficial for the representation of global circulation in climate models.

ACKNOWLEDGEMENTS

The research is supported by public funding to the Max Planck Society. The authors also acknowledge support from the European Union's Horizon 2020 Research and Innovation368Programme under grant agreement No. 820829 (CONSTRAIN Project). The authors would like to thank C. Wengel, C. Hohenegger, T. Dauhut, and L. Kluft for valuable discussion and feedback.

DATA AVAILABILITY STATEMENT

Run scripts for the ICON experiments and code to produce the figures are available here: https://github.com/pkeil7/tropical_lapse_rates . CMIP6 data is available at DKRZ or from the Earth System Grid Federation (ESGF) (https://esgf-node.llnl.gov/projects/cmip6/). Rich and RAOBCORE radiosonde data are avaliable here: https://www.univie.ac.at/theoret-met/research/raobcore/. SUNY-Albany radiosonde dataset is available here: ftp://aspen.atmos.albany.edu/HRD/ . RATPAC: https://www.ncdc.noaa.gov/data-access/weather-balloon/radiosonde-

	entrainment ϵ_u	autoconversion K
reference	2e-4	2.5e-4
low	0.4e-4	0.5e-4
high	10e-4	12.5e-4
very high	20e-4	-

Table A.1: Parameter variations in the ICON-A experiments.

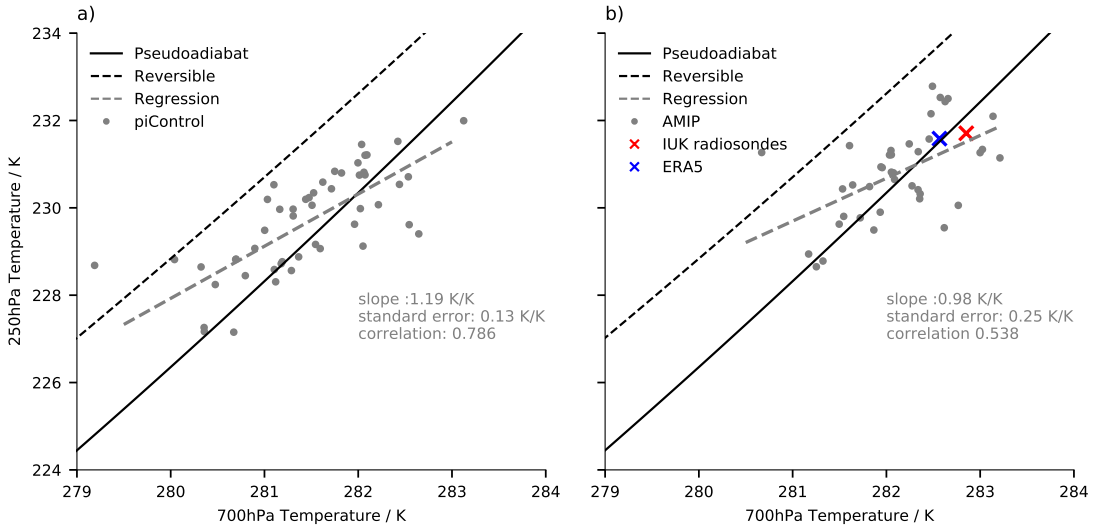

Figure A.1: Tropical (20°N-20°S) temperatures in CMIP6 models in the lower and upper troposphere. Shown are preindustrial control simulations (a) and AMIP simulations as well as IUKv2 radiosonde observations (red cross) and ERA5 reanalysis (blue cross) averaged over years 1979-2014 (b). The black line represents the relationship of 700 hPa to 250 hPa temperatures under the assumption of a moist pseudoadiabatic ascent and the black dashed line the same for a reversible adiabat. The grey dashed line indicates an ordinary least squares linear regression, with the slope and standard error given in grey text. The cross-model Pearson correlation coefficient is also given.

atmospheric-temperature-products-accessing-climate. IUK: https://www.ccrc.unsw.edu.au/professor-steven-sherwood/research-steven-sherwood/iuk-radiosonde-analysis-project-now-updated . ERA5 data is available on the Copernicus Climate Change Service Climate Data Store (CDS). https://cds.climate.copernicus.eu/cdsapp#!/home.

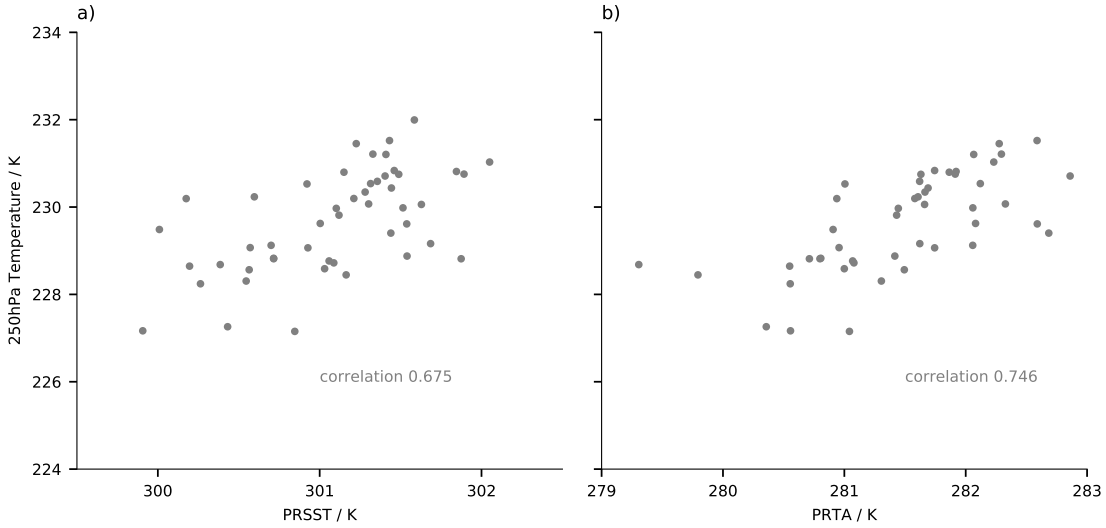

Figure A.2: Tropical (20°N-20°S) PRSST and PRTA versus upper tropospheric temperatures. Both panels show time averages of preindustrial control simulations over the whole available timespan. The cross-model Pearson correlation coefficient is also given.

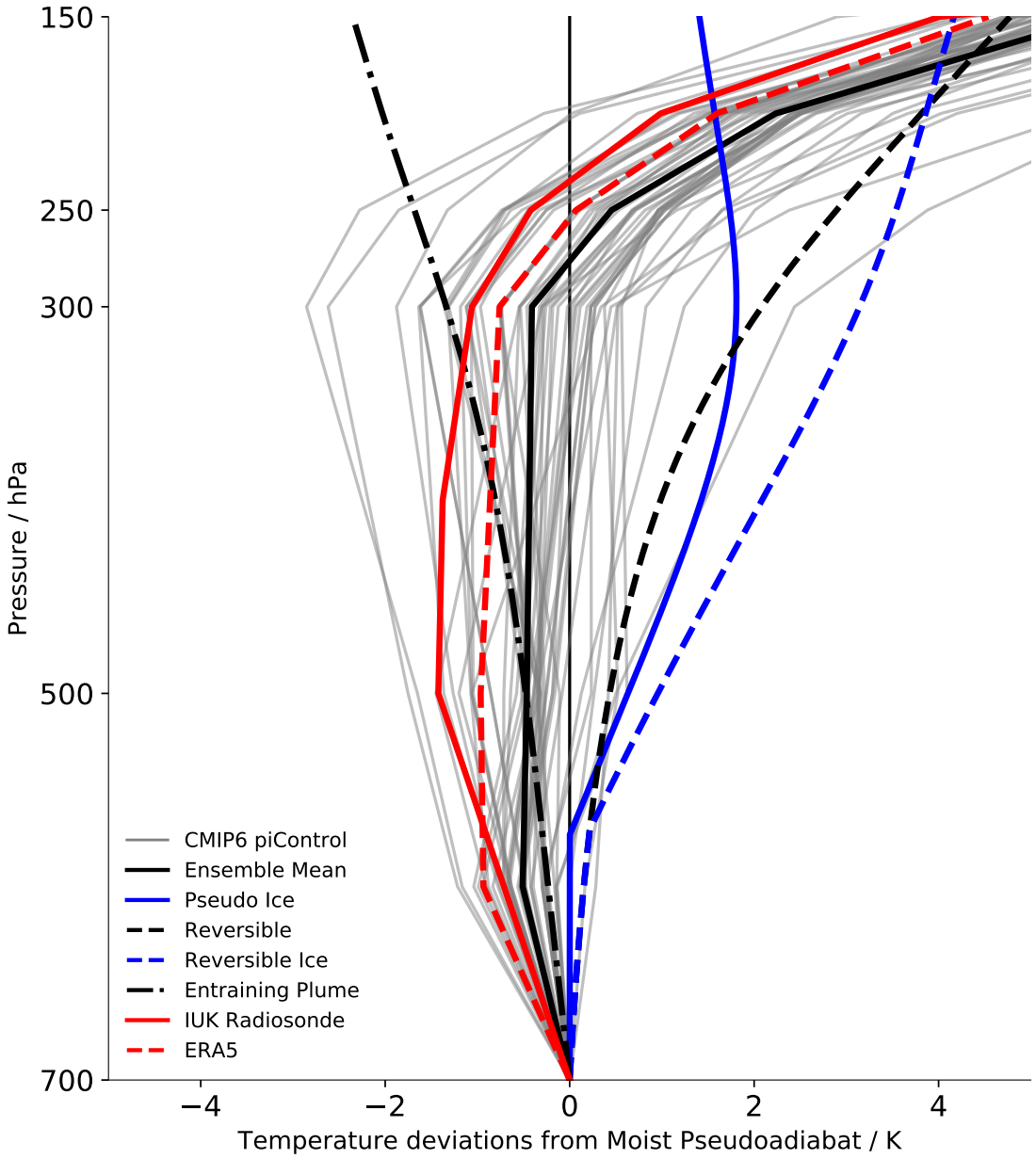

Figure A.3: Deviations from idealised moist pseudoadiabats for all CMIP6 piControl simulations and observations in the tropics (20N-20S), as well as some idealised cases. First, for every model (and the observations) an idealised moist pseudoadiabat is calculated based on the tropical mean temperature at 700 hPa assuming saturation. The deviations of the actually simulated (and measured) temperatures from each idealised moist pseudoadiabat are illustrated here. In addition, the deviations of the reversible adiabat, freezing pseudoadiabat (assuming fusion above the freezing level), the freezing reversible adiabat, and the entraining plume with respect to the pseudoadiabat are shown.

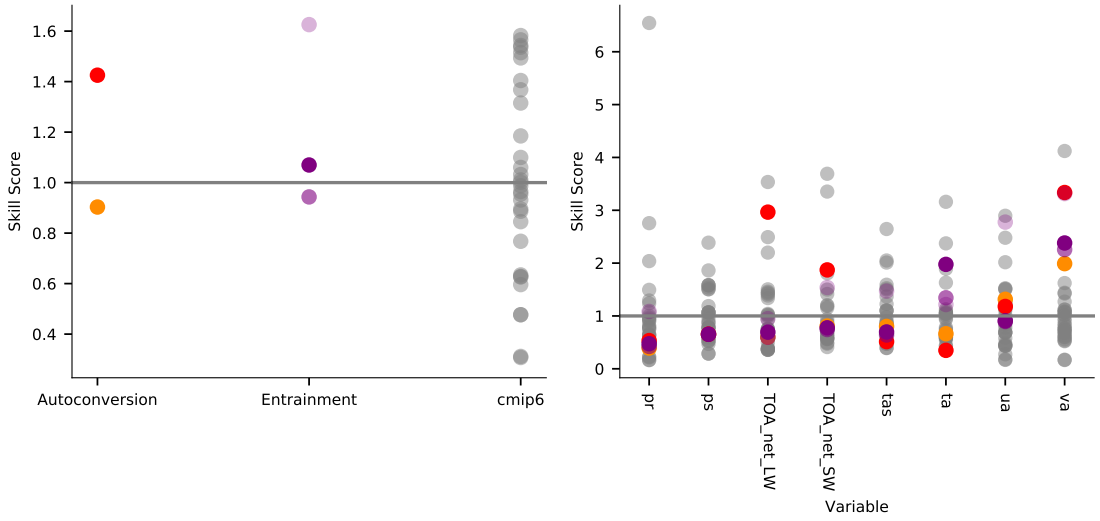

Figure A.4: Skill score of ICON experiments and CMIP6 models in the tropics (30°N-30°S). Grey dots represent CMIP6 AMIP simulations, dots with red shading autoconversion experiments and dots with purple shading entrainment experiments. Darker shading indicates stronger autoconversion/entrainment. A skill score of 1 indicates the average CMIP6 AMIP skill score. Variable abbreviations are as follows: pr : precipitation, ps : surface pressure, TOA_net_LW : Top of the atmosphere net long wave flux, TOA_net_SW : Top of the atmosphere net short wave flux, tas : surface temperature, ta : zonal mean temperature, ua : zonal mean zonal wind, va : zonal mean meridional wind.

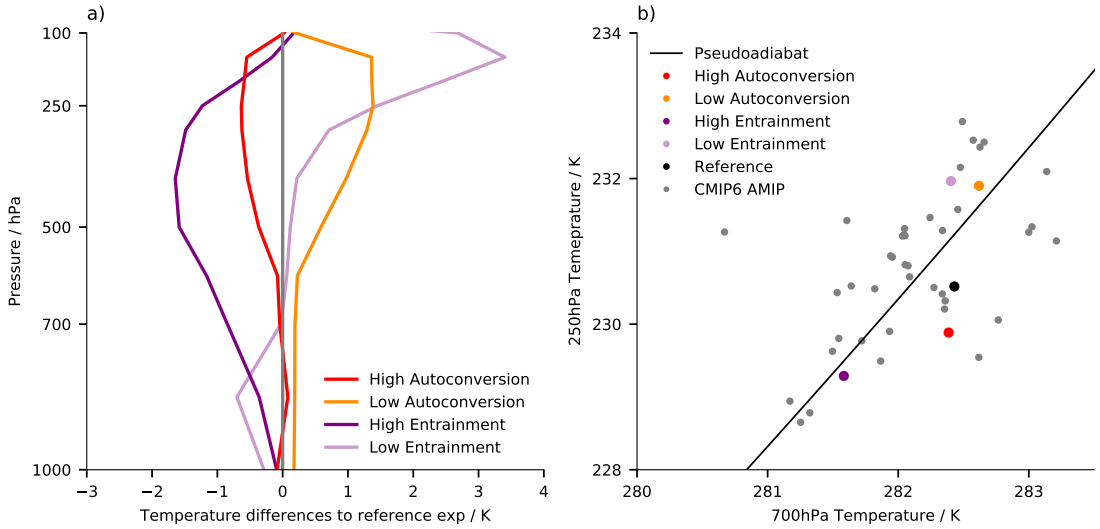

Figure A.5: Changes in atmospheric temperatures in ICON-A parameter sensitivity experiments. Darker shading represents increased autoconversion (red) and entrainment (purple). (a) Differences in tropical mean (20N-20S) temperatures to the reference experiment. (b) Lower vs. upper tropospheric tropical mean temperatures for all AMIP experiments as well as CMIP6 AMIP simulations. The line represent the relationship expected from a pseudoadiabat.

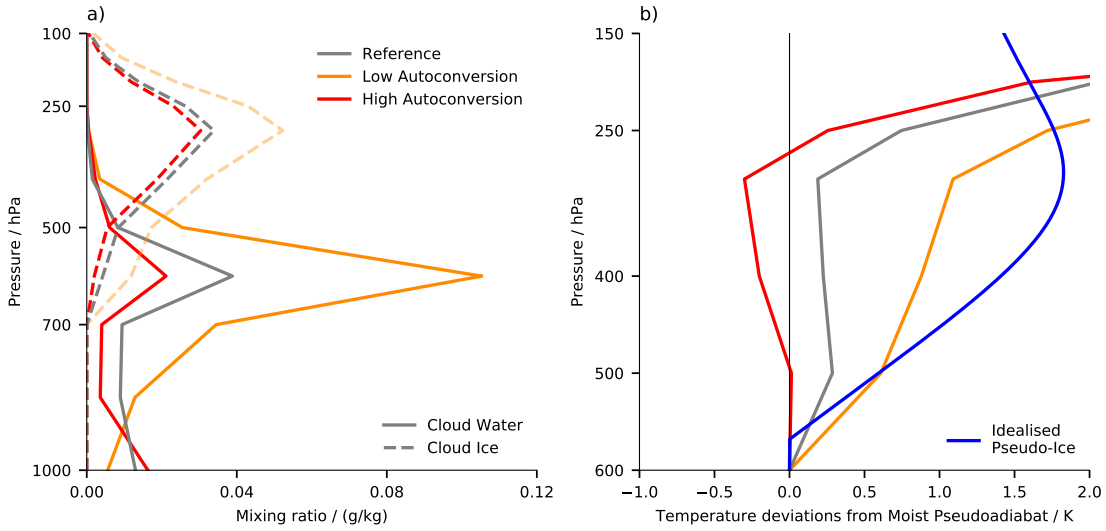

Figure A.6: Cloud water and ice mixing ratio (a), as well as temperature deviations from the pseudoadiabat (b) in the autoconversion experiments. Darker shading represents increased autoconversion and grey the reference experiments. (a) shows an average over the convecting regions (gridpoints above the 90th percentile of precipitable water) and (b) the tropical mean (20°N-20°S). Deviations from the pseudoadiabat were calculated as in Figure A.3.

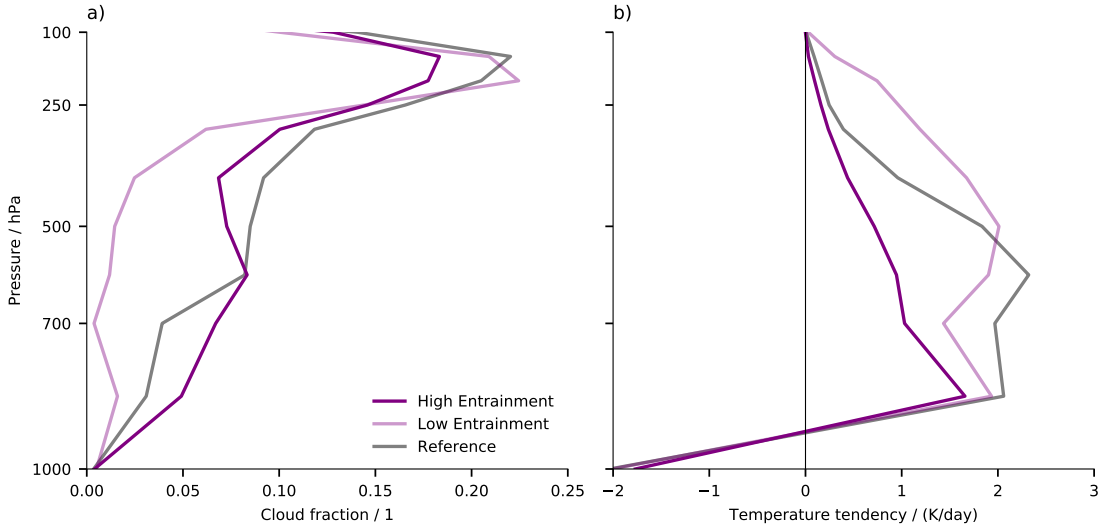

Figure A.7: Tropical (20°N-20°S) mean cloud fraction (a) and convective heating rates (b) in the turbulent entrainment experiments. Darker shading represents increased entrainment and grey the reference experiments.

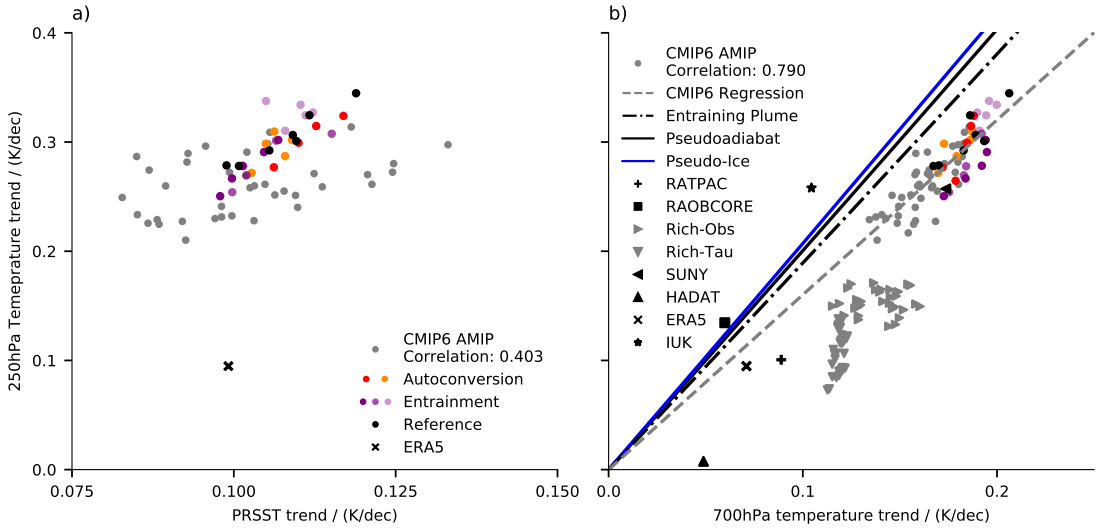

Figure A.8: Tropical (20°N-20°S) trends in PRSST (a) and 700 hPa (b) versus trends in 250 hPa temperatures for ICON experiments and CMIP6 AMIP simulations. Darker shading indicates increased autoconversion or entrainment as in Figure A.5. Cross-model correlation is given for CMIP6 models. Trends are calculated over the 1979-2012 period.

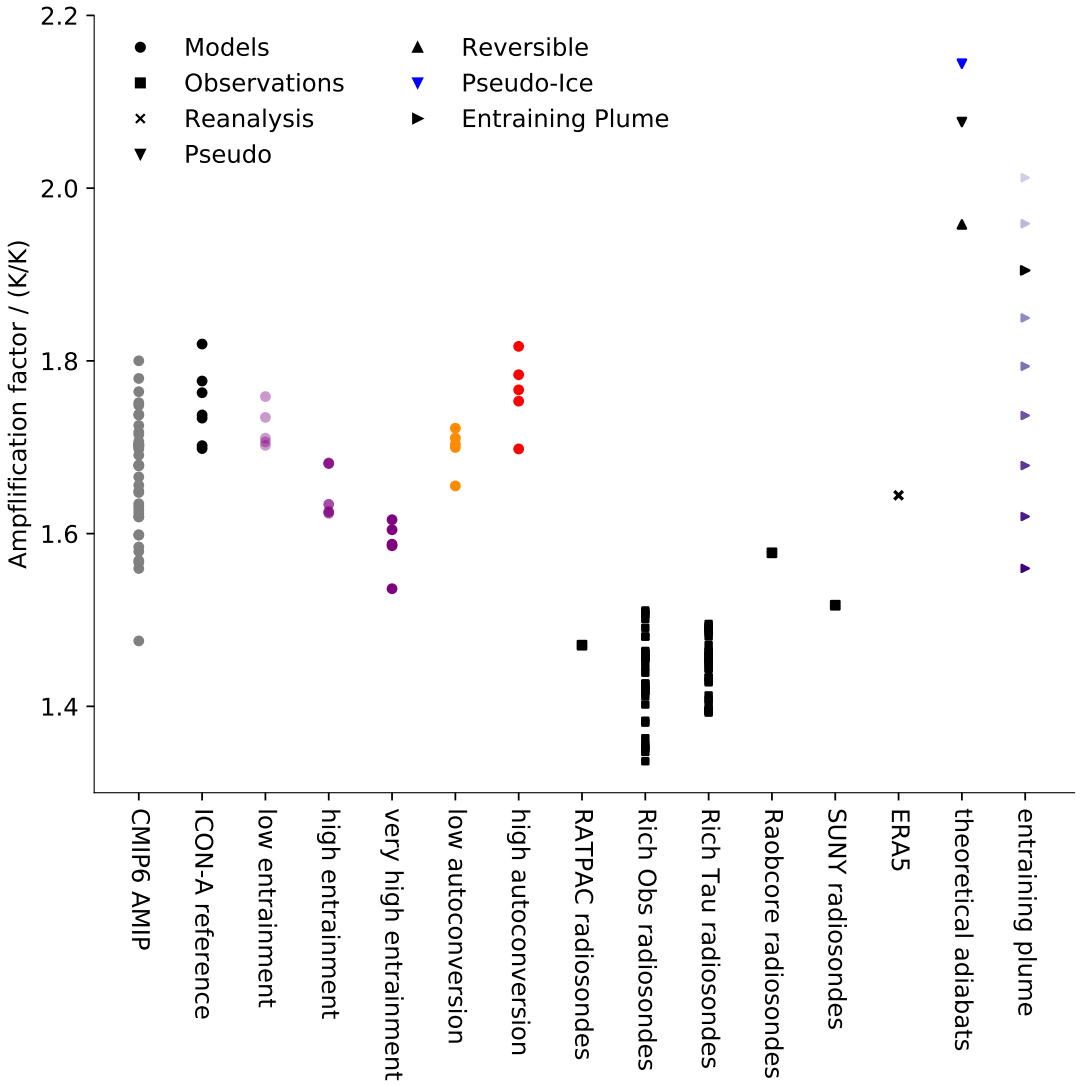

Figure A.9: Amplification factor of tropical mean 250 hPa vs 700 hPa warming for years 1979-2012. Circles show CMIP6 AMIP simulations and ICON experiments, darker colour shading indicates stronger entrainment/autoconversion. Black squares tropical mean radiosonde data. The cross represents the ERA5 reanalysis and the triangles show the amplification expected from theoretical moist adiabats. In the case of the entraining plume, the amplification is calculated for entrainment rates ϵ_0 from 0.1 to 0.9 in steps of 0.1.

B

APPENDIX B

The work in this appendix has been submitted to the *Quarterly Journal of the Royal Meteorological Society* as

Keil, P., Schmidt, H., Stevens, B., Byrne, M.P., Segura, H. & Putrasahan "Tropical Tropospheric Warming Pattern Explained by Shifts in Convective Heating in the Matsuno-Gill Model"

Tropical Tropospheric Warming Pattern Explained by Shifts in Convective Heating in the Matsuno-Gill Model.

Paul Keil[1,2], Hauke Schmidt[1],Bjorn Stevens[1],Micheal P. Byrne[3,4], Hans Segura[1], Dian Putrasahan[1]

[1] Max Planck Institute for Meteorology, Hamburg, Germany
[2] International Max Planck Research School on Earth System Modelling, Max Planck Institute for Meteorology, Hamburg, Germany
[3] School of Earth and Environmental Sciences, University of St Andrews, St Andrews, UK
[4] Department of Physics, University of Oxford, Oxford, UK

Manuscript submitted 29 September 2022

ABSTRACT

Horizontal temperature gradients in the free troposphere are fairly weak, and tropical tropospheric warming is usually treated as uniform. However, here we show that projected tropospheric warming is spatially inhomogeneous in CMIP6 models, as well as in a storm resolving climate model. We relate the upper tropospheric warming pattern to sea surface temperature changes that reorganise convection and thereby cause spatial shifts in convective heating. Using the classical Gill model for tropical circulation forced by precipitation changes that arise due to greenhouse gas warming we can understand and reproduce the different warming patterns simulated by a range of global climate models. Forcing the Gill model with precipitation changes from a certain region demonstrates how local tropospheric temperature changes depend on local changes in convective heating. Close to the equator anomalous geopotential gradients are balanced by the dissipation term in the Gill model. The optimal dissipation timescale to reproduce the warming pattern varies depending on the CMIP6 model, and is between 1 and 10 days. This suggests that processes acting on these timescales, such as the eddy momentum flux, advection or radiative cooling, are important for determining the warming pattern. While climate models show a large spread in projections of tropical sea surface temperature and precipitation changes, our results imply that once these predictions improve, our confidence in the predicted upper tropospheric warming pattern should also increase.

In the tropical free troposphere horizontal buoyancy gradients produced by deep convection are quickly reduced by gravity waves due to the absence of a strong Coriolis force (Bretherton and Smolarkiewicz, 1989), resulting in weak geopotential gradients. Thus, the temperature throughout the tropical free troposphere is approximately horizontally uniform and set by the boundary layer regions with the highest moist static energy via convection. Consequently, in a warming climate increased boundary layer temperatures lead to approximately horizontally homogeneous warming throughout the free troposphere. This warming is amplified with respect to the boundary layer since the warmer air can hold additional water vapour and thus additional latent heating occurs in the troposphere (Santer et al., 2005). While climate models continue to show biases in various aspects of tropical climate, maybe most striking for precipitation (Fiedler et al., 2020), estimates of horizontal mean upper tropospheric warming are arguably within the range of measurement errors and internal variability (Santer et al., 2017b; Po-Chedley et al., 2021).

The weak temperature gradient (WTG) approximation is valid in the tropics, and is both conceptually powerful and useful for many applications [e.g. Bretherton and Sobel (2002)]. Nevertheless, horizontal temperature gradients of several degrees Kelvin do exist in the free troposphere. These temperature gradients persist over months and develop in response to strong local convective heating, e.g. during the Indian Summer Monsoon (Wu et al., 2015) and in response to the El Niño-Southern Oscillation (Bayr et al., 2014). Especially in the upper troposphere temperature gradients are substantial and not explained by the virtual temperature effect (Bao and Stevens, 2021). Observed recent tropospheric warming is also inhomogeneous, and possibly linked to sea surface temperature (SST) patterns (Kamae et al., 2015), which in turn organise convection (Lindzen and Nigam, 1987). In addition, in climate simulations under greenhouse gas forcing, upper tropospheric warming shows deviations of more than 2 K from region to region in most CMIP6 [Coupled Model Intercomparison Project, Eyring et al. (2016)] models. The pattern differs among the models, resulting in a more uniform ensemble mean upper tropospheric warming pattern (Figure B.1a). In simulations using storm resolving models that represent convection based on the laws of motion and not on a parameterisation (Stevens et al., 2020), the warming also differs by up to 2 K horizontally (Figure B.1b). Horizontal differences in tropospheric warming have implications for how observed warming is sampled by sparsely distributed radiosonde stations and, by impacting upper tropospheric static stability, could be an important influence on tropical circulation systems like the Pacific Walker circulation (Sohn et al., 2016) and on tropical cyclone intensity (Trabing et al., 2019). While the SST pattern seems to play an important role (Kamae et al., 2015), likely by impacting deep convection, what mechanisms exactly govern the upper tropospheric warming pattern is unclear.

Here we use the Matsuno-Gill model (Matsuno, 1966; Webster, 1972; Gill, 1980), from now on referred to as the Gill model, for tropical circulation to understand the pattern of tropospheric warming. While the Gill model cannot capture the full dynamics of the tropical atmosphere, especially at smaller spatial and temporal scales, it has proven very useful to describe the large scale tropical circulation and geopotential characteristics (Gill, 1980; Lau and Lim, 1982; Dias et al., 1983; Rodwell and Hoskins, 1996; Lin et al., 2008; Shaw and Boos, 2012). We show that the warming pattern is related to horizontal changes in convection, by only using precipitation to force the Gill model and thereby reproduce these patterns. Besides the pressure gradient force and Coriolis force, it includes a dissipa-

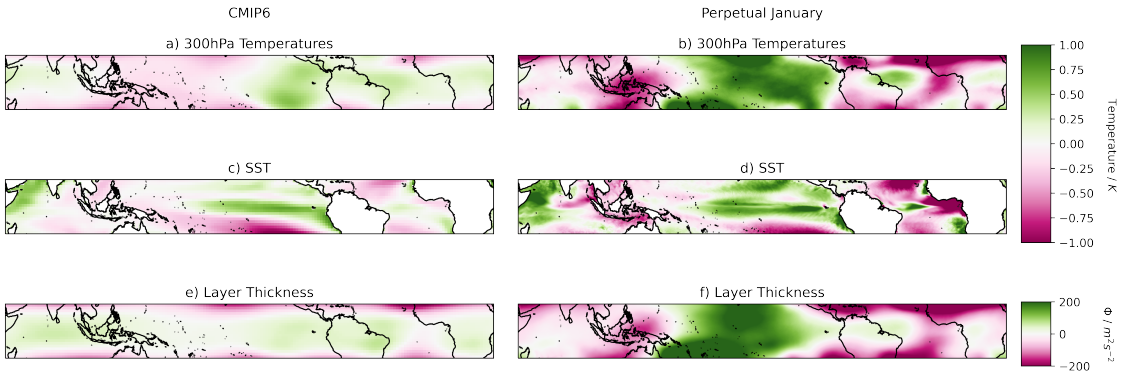

Figure B.1: Anomalies from tropical mean (20°N-20°S) changes between the early and late period in CMIP6 SSP585 models and the warm and cold simulation in the PJ simulations. Shown are temperatures at 300 hPa (a,b), sea surface temperatures (c,d) and 400-150 hPa layer thickness (e,f).

tion term which can be understood as a contribution from more complicated, non-linear processes such as advection and convective momentum transport in the momentum equations (Sardeshmukh and Held, 1984; Lin et al., 2008), as well as radiative cooling. Although the magnitudes of these processes are typically small compared to, e.g., the Coriolis force in the extratropics, they are essential to balance the geopotential gradients close to the equator (Bao et al., 2022). We will show that this dissipation term is essential to understand and reproduce the tropospheric warming pattern.

Section 2 describes the methods, including the global climate model data and the implementation of the Gill model. Section 3 documents the spatial anomalies in surface warming and upper tropospheric warming in different global climate models and shows the mechanisms behind precipitation and convective heating changes. In section 4 we demonstrate how the Gill model can reproduce large scale changes in upper tropospheric temperatures using the changes in precipitation as forcing and discuss the dependence of the results on the dissipation term. The method is also applied to reproduce warming patterns in the vast majority of CMIP6 models. We use these results to determine the most skilful values for the dissipation term to reproduce the warming pattern, which elucidates what processes are likely represented by the dissipation term. Section 5 contains a conclusion and further points of discussion.

B.2 METHODS

B.2.1 *Climate Models*

B.2.1.1 *Perpetual January*

We analyse upper tropospheric warming patterns, layer thickness changes and precipitation changes in two so-called Perpetual January (PJ) simulations. These simulations are performed with the ICON-A model at a storm-resolving horizontal resolution (5 km) and thus do not rely on convection and gravity wave parameterisations (Hohenegger et al., 2022), thereby improving many aspects of the simulated tropical climate in comparison to conventional climate models (Stevens et al., 2020). Since the computational cost of these simulations is quite high, two simulations with eight months each are analysed, both using only January boundary conditions for all months, hence the name Perpetual

January. SSTs and sea ice boundary conditions are taken from simulations with the MPI-ESM-ER model that use approximately 10 km resolution in the ocean model and 1° in the atmosphere (Gutjahr et al., 2019). One PJ simulation uses boundary conditions averaged over 40 Januaries from a MPI-ESM-ER control simulation with 1950 levels of greenhouse gases, while the other uses the average over 40 Januaries from two ensemble members from the timeperiod 2080-2099 using the SSP585 scenario in the MPI-ESM-ER model (Putrasahan et al., 2021). Throughout the study we present temperature, layer thickness and precipitation changes as differences between the warm and the cold simulation.

B.2.1.2 *CMIP6*

We also present upper tropospheric warming patterns and layer thickness changes in the SSP585 simulations performed by 31 CMIP6 models (Eyring et al., 2016). We analyse one ensemble member ('r1i1p1f1') for every model and show differences between the late (2080-2099) and early 21st century (2015-2034).

B.2.2 *Numerical Gill Model*

To understand the warming pattern produced in the climate models and identify the relevant processes, we employ the Gill model that can reproduce the large scale characteristics of the tropical circulation (Matsuno, 1966; Webster, 1972; Gill, 1980). The equations were first derived and their wave-like solutions presented by Matsuno Matsuno, 1966, and the first numerical solutions to a steady forcing investigated by Webster Webster, 1972. It was Gill's elegant analytic solutions which made the steady state behaviour of the equations, something we approximate by integrating under steady forcing, first clearly apparent. We use the momentum equations with the β-plane approximation and a thermodynamic equation that includes a stationary forcing $Q(x, y)$ as a starting point [e.g. Matsuno, 1966]:

$$\begin{aligned} \frac{\partial u}{\partial t} - \beta y v &= -\frac{\partial \Phi}{\partial x} \\ \frac{\partial v}{\partial t} + \beta y u &= -\frac{\partial \Phi}{\partial y} \\ \frac{\partial \Phi}{\partial t} + \alpha \left(\frac{\partial u}{\partial x} + \frac{\partial v}{\partial y} \right) &= Q \end{aligned} \tag{B.1}$$

Mathematically, this model is equivalent to a shallow water model, but we interpret it slightly differently. Here, Φ, u and v are the differences in geopotential, zonal and meridional winds between the upper layer (in this case 150 hPa) and lower layer (in this case 400 hPa), and β is the Rossby parameter for the β-plane approximation [see discussion in, e.g., Matsuno, 1966]. We use these pressure levels, since the bulk of the additional warming due to the release of condensation heating is realised in the upper troposphere (Figure B.2). Thus Φ can be interpreted as a layer thickness proportional to upper tropospheric temperatures in this layer and u and v are the wind shears. Then $\alpha = Sa$, where S is the static stability $S = \frac{\partial \Phi}{\partial p} \frac{\partial log(\theta)}{\partial p}$ and a is a parameter related to the chosen vertical levels. For typical values using the 750-250 hPa layer, which is perhaps the most common use case, $\alpha \approx 4500 \frac{m^2}{s^2}$, which is equivalent to the values used by Gill, 1980. Here we are mostly interested in the tropical upper troposphere, and therefore mostly use values for the 400-150 hPa layer, resulting in $\alpha \approx 2800 \frac{m^2}{s^2}$.

The geopotential source Q can be related to thermal heating rate $\overline{Q}$ (in K/s):

$$Q = R\overline{Q}\ln\left(\frac{p_t}{p_b}\right), \tag{B.2}$$

where R is the gas constant and p_t and p_b are the upper and lower pressure layers, respectively. See the appendix for a complete derivation of the thermodynamic equation.

Following Gill, 1980, the typical length scale is $L = \sqrt{\frac{\sqrt{\alpha}}{2\beta}}$, corresponding to about 10 degrees of latitude, which is roughly the tropical deformation radius, and the typical time scale is $T = \sqrt{\frac{1}{2\sqrt{\alpha}\beta}}$, corresponding to about 6 hours, which is roughly the convective timescale. Even though the estimate used for α is somewhat different, the resulting values for L and T are very similar to the ones used in Gill, 1980. Now the equations can be non-dimensionalised:

$$\begin{aligned}
\frac{\partial u}{\partial t} + \epsilon_w u - \frac{1}{2}yv &= -\frac{\partial \Phi}{\partial x} \\
\frac{\partial v}{\partial t} + \epsilon_w v + \frac{1}{2}yu &= -\frac{\partial \Phi}{\partial y} \\
\frac{\partial \Phi}{\partial t} + \epsilon_p \Phi + \frac{\partial u}{\partial x} + \frac{\partial v}{\partial y} &= Q.
\end{aligned} \tag{B.3}$$

Here the dissipation terms $\epsilon_w u$ and $\epsilon_w v$ are introduced which parameterise additional, more complex processes, like advection or eddy momentum flux (Lin et al., 2008) and $\epsilon_p \Phi$ which is a Newtonian cooling that mimics radiative cooling. When we refer to ϵ throughout the manuscript, this includes both ϵ_p and ϵ_w. Note that the inverse of ϵ can be interpreted as a dissipation timescale.

We use this model (equations B.3) in numerical form, discretised with centered differences in space and a Runge-Kutta integrator in time and apply a forcing $\overline{Q}$ derived from the precipitation changes in global climate models, assuming that all condensation leads to precipitation (Gill, 1982):

$$\overline{Q} = \frac{L_v P}{\rho c_p h} = -\frac{L_v P}{c_p h}\frac{\partial \Phi}{\partial p}, \tag{B.4}$$

where L_v is the latent heat of varpourisation, ρ is typical mid-tropospheric density, which is related to the vertical gradient in geopotential $\frac{\partial \Phi}{\partial p} = -\frac{1}{\rho} \approx -2.6 m^2 s^{-2} Pa^{-1}$ for the 400-150 hPa layer, c_p is the specific heat capacity of dry air, and $h = 6500$ m is the height over which the heating is distributed (the approximate height difference between 400 hPa and 150 hPa). Here we have also assumed that all of the temperature anomalies that arise due to convective heating anomalies are realised in this layer.

For P we use precipitation changes between a warm and a cold climate simulated by different global climate models. This means that u,v and Φ also represent the changes between the two climates. Because all terms in the Gill model are linear, this approach is equivalent to simulating the warm and cold climates explicitly with the Gill model and then taking the difference between these simulations. Simulations with the Gill model using the microphysical heating rates from the PJ simulations instead of precipitation yielded similar results and are therefore not discussed.

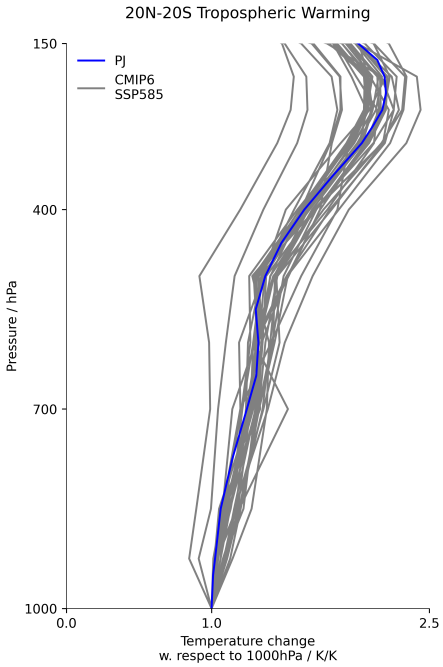

Figure B.2: Ratio of tropical mean (20°N-20°S) temperature change at different pressure levels and the 1000 hPa temperature change in CMIP6 models and PJ simulations. Changes are calculated as difference between the early and late period in CMIP6 SSP585 models (gray) and the warm and cold PJ simulation (blue).

B.3 Tropical Tropospheric Warming Patterns and Precipitation Changes in Global Climate Models

The warming in the tropical upper troposphere is amplified with respect to the surface (Figure B.2) and at first glance is broadly horizontally uniform, especially compared to higher latitudes. However, the CMIP6 models show a stronger warming in the Eastern Pacific compared to the rest of the tropics in the multi-model ensemble mean (Figure B.1a). Most individual models show considerably stronger deviations, in many cases more than 2 K horizontal difference between the regions of strongest and weakest warming, and the regional patterns differ from model to model. The storm-resolving PJ simulations (Figure B.1b) show horizontal anomalies from the mean tropospheric warming on a similar magnitude, with the strongest warming in the western Pacific. For example, the warming in the western Pacific, south of the equator, is around 2 K stronger than the warming over the neighbouring maritime continent. This anomalous warming is also reflected in the geopotential layer thickness

$$\Phi = \int \frac{R\, T_v}{p} dp, \tag{B.5}$$

where T_v is the virtual temperature and p is pressure. The 400 hPa to 150 hPa layer thickness (Figure B.1 e-f) shows very similar patterns to the 300 hPa temperatures. Generally, in regions where the layer thickness increases above average, upper tropospheric warming is also above average. Upper tropospheric layer thickness anomalies and SST anomalies regionally coincide to some degree (Figure B.1c and d), similar to the case of the recently observed temperature anomalies in the Pacific (Kamae et al., 2015). However, the correlation between SST anomalies and upper tropospheric temperature anomalies 20°N-20°S is only at 0.4 in the PJ simulations and on average 0.2 in the CMIP6 simulations

with a maximum value of 0.5. The strong warming over land surfaces (not shown) does not translate into stronger upper tropospheric warming.

The most likely mechanism by which SST anomalies and upper tropospheric temperatures are connected is through deep convection, which releases latent heating in the troposphere. Indeed, changes in precipitation (Figure B.3a) seem to roughly resemble the SST warming pattern (Figure B.1d). An increase in precipitation could either be related to an increase of humidity that occurs due to the warmer SSTs, and is transported by the mean circulation to the regions of deep convection. This can be characterised as thermodynamic changes in convection (Held and Soden, 2006). Alternatively, precipitation changes could be related to dynamic changes triggered by the SST pattern (Lindzen and Nigam, 1987), where an increase in moisture convergence would be associated with an increase of horizontal convergence of the winds or increased moisture advection. To understand which of these processes is more important we adopt the methodology of Seager et al., 2010 to decompose the precipitation changes into components that are driven by thermodynamic, dynamic, and transient eddy processes, as well as a nonlinear term. For simplicity we focus on the PJ simulations. At steady state, the changes in precipitation ΔP are related to changes in the mass weighted vertically integrated moisture flux convergence and changes evaporation ΔE:

$$\Delta P \approx \Delta E - \Delta \int_{p=p_s}^{p=0} \nabla \cdot (\mathbf{u} q) \frac{dp}{g}, \tag{B.6}$$

where $\mathbf{u}$ is the horizontal wind vector, q is specific humidity, and g is the gravitational acceleration. Δ denotes differences between the warm and cold PJ simulations. The mass-weighted integral on the right hand side quantifies the change in atmospheric moisture convergence between the simulations. The dynamic changes are related to changes in the winds $\Delta\mathbf{u}$

$$\Delta P_{\text{dyn}} = - \int_{p=p_s}^{p=0} \nabla \cdot (\Delta\mathbf{u}\, q) \frac{dp}{g}, \tag{B.7}$$

while the thermodynamic changes are related to changes in the specific humidity Δq

$$\Delta P_{\text{th}} = - \int_{p=p_s}^{p=0} \nabla \cdot (\mathbf{u}\, \Delta q) \frac{dp}{g}. \tag{B.8}$$

All the above terms are calculated with monthly mean data. Other terms like the transient eddy term, the nonlinear term and the residual are small (not shown), in accordance with earlier studies (Seager et al., 2010), and are not discussed further.

In the PJ simulations, ΔP_{dyn} dominates the other terms (Figure B.3). The most prominent precipitation changes, such as the strong increase east of Australia, and the distinctive pattern in the Atlantic are reflected in ΔP_{dyn}. The thermodynamic changes ΔP_{th} are typically smaller in magnitude and mostly opposed to the dynamic changes, which broadly agrees with earlier results (Seager et al., 2010; Bony et al., 2013). Over land, the thermodynamic changes ΔP_{th} are slightly stronger than the dynamic changes ΔP_{dyn}, likely because the availability of moisture plays a larger role compared to over oceans. We conclude that precipitation changes in the PJ simulations are coupled to circulation changes. Note that there is no monocasual relationship in which a change in one causes a change in the other, but not vice-versa.

Thus, the SST warming pattern triggers shifts in convective activity and thereby changes circulation and precipitation. If upper tropospheric warming is indeed related

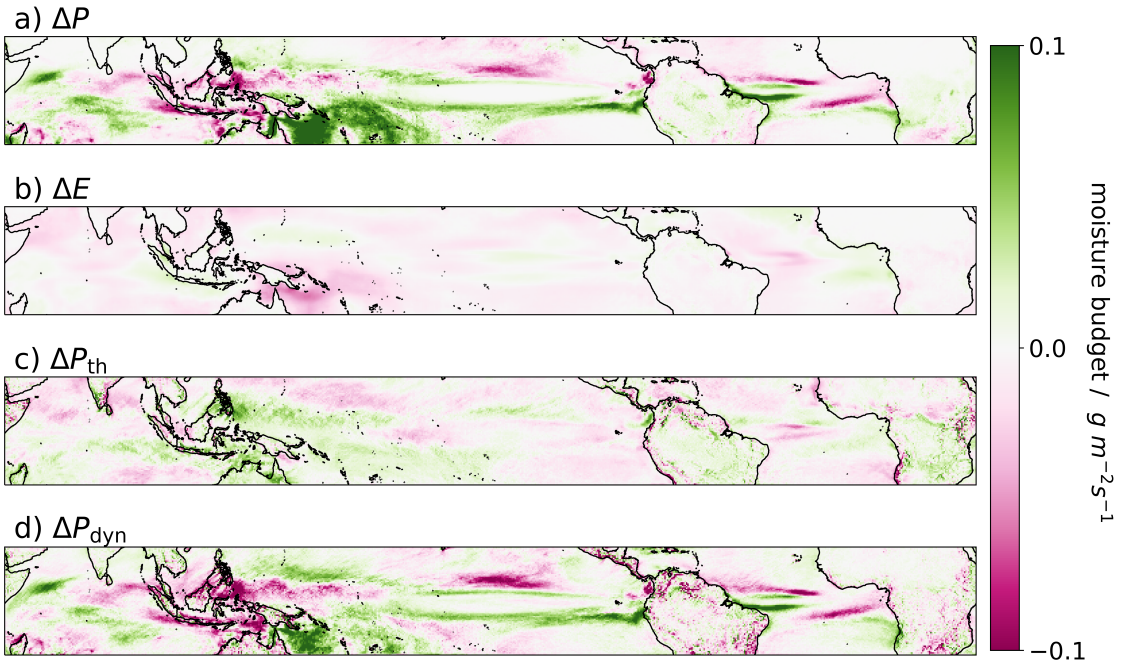

Figure B.3: Precipitation changes (ΔP, a) in the PJ Simulations decomposed into thermodynamic (ΔP_{th}, c) and dynamic (ΔP_{dyn}, d) changes. b) shows evaporation changes (ΔE). The signs are such that they are positive for atmospheric moisture loss.

to the changes of convective heating, as the next section will demonstrate, then the upper tropospheric warming pattern does not follow a simple thermodynamic argument, but is coupled to circulation changes.

B.4 Interpreting the warming pattern using the Gill model

This section compares the layer thickness pattern produced by the Gill model to the layer thickness anomalies in the global climate models. The Gill model produces a non-dimensionalised layer thickness, which we present redimensionalised, and compare to the 400-150 hPa layer thickness anomalies in the global climate models. These are the pressure levels at which our method works best, likely because the bulk of the additional tropospheric warming due to the latent heat release happens at these altitudes (Figure B.2). We also briefly discuss the comparison to the 700-200 hPa layer thickness, which is closer to the standard configuration of $p_{\text{b}} = 750$ and $p_{\text{t}} = 250$ hPa (Matsuno, 1966). Since it is not clear what value ϵ should have, we perform an ensemble of Gill simulations with different combinations of ϵ_{p} and ϵ_{w}. We only use those Gill simulations that converge to a stable solution, which is usually the case for sufficiently large ϵ. The numerical Gill model implemented here can reproduce the analytical solutions of Gill, 1980 accurately, for example the response to asymmetrical forcing (Figure B.4). Positive forcing (heating) induces an increase in layer thickness north of the equator, that extends to the west as a Rossby wave and to the east along the equator as a Kelvin wave.

As demonstrated in the previous section, the convective heating changes are connected to circulation changes in the PJ simulations. This coupling of convective heating and circulation is also represented in the Gill model to some extent, as a positive convective heating is balanced by convergence in the lower layer and divergence in the upper layer. Because the convective heating is prescribed, one might interpret the Gill model in such

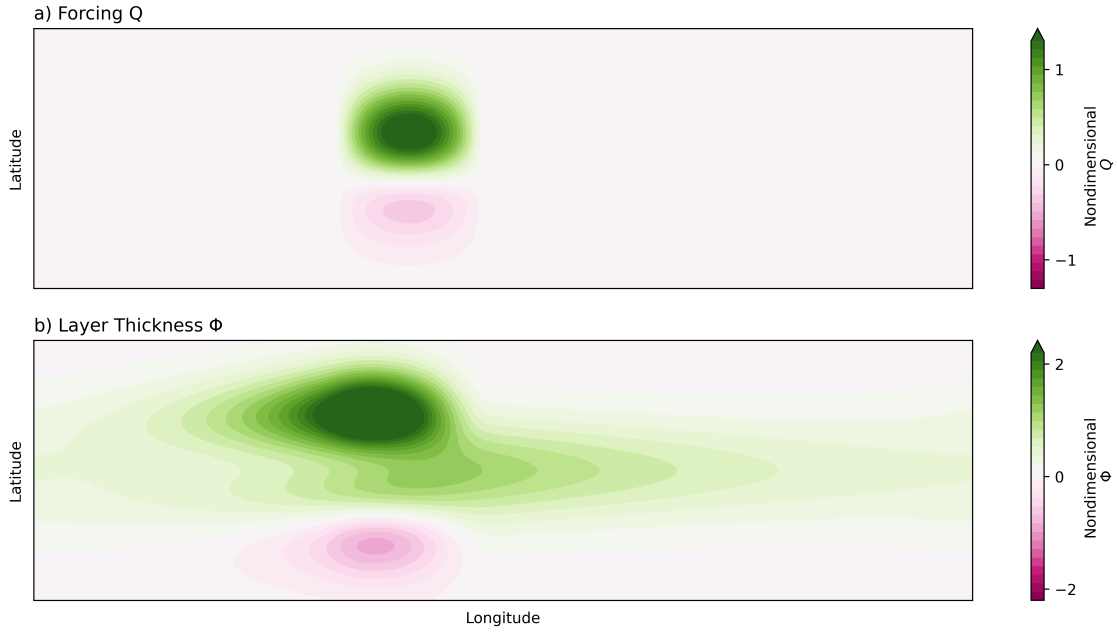

Figure B.4: Idealised asymmetric forcing (a) and the corresponding layer thickness solution produced by the numerical Gill model (b). For this idealised forcing there are analytical solutions (Gill, 1980). Positive forcing induces positive tropospheric layer thickness changes, corresponding to negative surface pressure anomalies in other interpretations of the Gill model (Gill, 1980).

a way that the circulation reacts to the convective heating in a clear cause-and-effect relationship. In reality, the circulation changes and precipitation changes cannot be easily disentangled into cause and effect. The fact that circulation and convective heating seems strongly coupled in both the Gill model and the PJ simulations, increases our confidence that the Gill model can adequately reproduce these mechanisms.

B.4.1 *Storm Resolving Perpetual January Simulations*

Having verified our implementation of the model against the analytic solutions, we now present layer thickness anomalies produced by Gill simulations forced with the PJ precipitation changes for different values of ϵ (Figure B.5). The Gill model layer thickness has a broadly similar magnitude as the layer thickness anomalies in the PJ simulations, suggesting that the behaviour is well described by the balances retained in the Gill model. The magnitude depends on many assumptions (for example the ones made in equation B.2), and therefore we focus primarily on how well the spatial patterns match. In all Gill simulations, the strong increase in layer thickness east of Australia, where the precipitation changes are most pronounced, is reproduced. The below average tropospheric warming over the maritime continent is also captured well. For $\epsilon = 0.2$ the layer thickness perturbation across large parts of the Pacific resembles the PJ layer thickness changes closely. For stronger dissipation ($\epsilon = 1.2$), the layer thickness perturbations are more localised and less smeared out. This results in a less realistic pattern in the eastern Pacific, but other, more small scale features of the warming patterns can be reproduced, such as the small patch of above average warming in the equatorial western Atlantic. For a small ϵ_p, but larger ϵ_w (Figure B.5d) the widespread Pacific warming and the below average warming over the maritime continent are reproduced well, but features on smaller scales

are less well represented. Overall, the numerical Gill model can reproduce the strong Pacific warming and the weak maritime continent warming well, as well as some of the more local warming patches for larger dissipation.

The dissipation terms have a considerable influence on the pattern: A large thermal dissipation $\epsilon_p \Phi$ balances the convective heating Q in the thermodynamic equation and therefore the layer thickness pattern Φ will tend to resemble the pattern of convective heating Q for the case of large ϵ_p. Thus, ϵ_p controls how far a signal can travel before it dissipates. The momentum dissipation $\epsilon_w u$ can help sustain strong zonal gradients of Φ even close to the equator, which can be seen qualitatively in Figure B.5d, which shows a case of large ϵ_w. Larger values for ϵ_w are associated with larger layer thickness gradients along the equator at all longitudes (Figure B.5e), inhibiting the homogenisation of the layer thickness anomalies through gravity waves. Therefore one can also think of the dissipation terms as determining a basin of influence for a given convective forcing. In reality, the processes represented by the dissipation terms are not horizontally invariant, and a larger dissipation in the Atlantic, compared to the Pacific, might explain the more localised response to the convective heating there.

We evaluate the performance of the Gill model in explaining the behaviour of the PJ simulations more quantitatively by calculating the Pearson correlation coefficients between the layer thickness patterns (Figure B.6). In the case of $\epsilon_p = \epsilon_w$ (Figure B.6a) the Gill simulations perform best for ϵ between 0.2 and 0.3, and indeed the simulation with $\epsilon = 0.2$ (Figure B.5), that corresponds to a dissipation timescale of approximately 1 day, shows good agreement with the PJ warming pattern. This is close to the original value of $\epsilon = 0.1$ used by Gill, 1980. Correlations with the 700-200 hPa layer thickness anomalies in the PJ simulations are similar, but overall a bit weaker. This is probably because the bulk of the additional tropospheric warming due to the increased convective heating is realised in the 400-150 hPa layer (Figure B.2). For the case of $\epsilon_p \neq \epsilon_w$ a slightly higher correlation can be found for $\epsilon_p \approx 0.1$ and $\epsilon_w \approx 0.3$ (Figure B.6b). Note that the correlation between SST anomalies and upper tropospheric warming anomalies (Figure B.1) is only at 0.4, while some of the Gill simulations have correlations of almost 0.9, illustrating the added insight provided by the Gill model. Using mutual information (Datseris and Parlitz, 2022) as a measure of correlation, which also takes non-linear, non-monotonic dependencies between two variables into account, yielded very similar results.

Finally, more idealised experiments that only use precipitation changes from one region as forcing can further illustrate the basins of influence that determine how far a convective heating signal is communicated before it dissipates. Figure B.7 presents cases where the Gill model is only forced with precipitation changes in the west Pacific and Atlantic respectively. The west Pacific forcing alone can explain almost all of the widespread Pacific warming, which is evocative of the Kelvin wave response east of the forcing in the idealised solution (Figure B.4). However, the pattern in the Atlantic is not reproduced, illustrating that the signal dissipates before it can reach the Atlantic. In contrast, the Atlantic layer thickness changes can be reproduced quite well by the local precipitation changes. Thus for $\epsilon = 0.2$ the basin of influence of western Pacific convection does not reach into the Atlantic (and vice-versa). Because the momentum dissipation helps sustain zonal gradients, the contributions from smaller terms to the momentum balance and thermodynamic equation, represented here through ϵ, are responsible for shaping these basins of influence, such that regional changes in convective heating can have regionally confined effects on the temperature pattern.

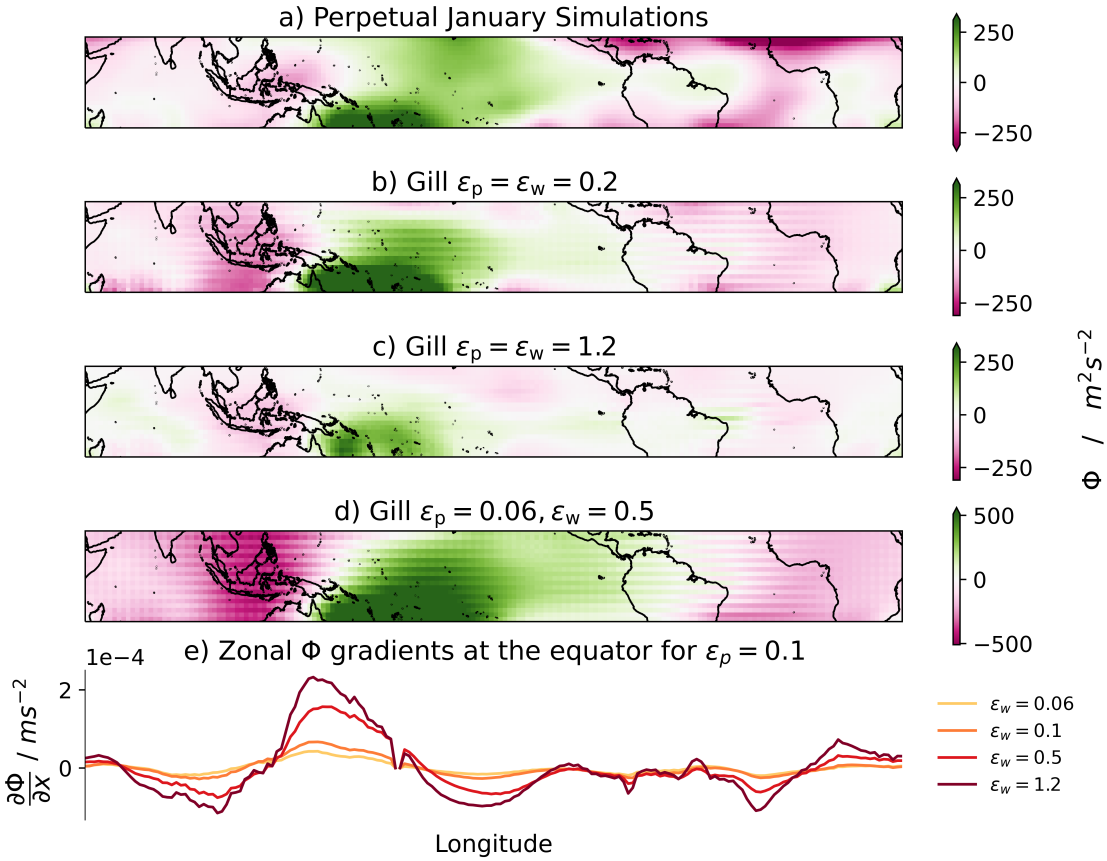

Figure B.5: Panel a) shows anomalies from the tropical (20°N-20°S) average layer thickness changes from the PJ simulation (as Figure B.1e), and panels b-d show anomalies from the tropical (20°N-20°S) average layer thickness produced by the Gill model forced by the PJ precipitation changes. Panel e) shows zonal layer thickness gradients for different Gill simulations.

B.4.2 *CMIP6*

We repeat the above analysis for all CMIP6 models using the SSP585 simulations. For each CMIP6 model, the convective heating Q is calculated with the precipitation changes between the 2080-2099 and 2015-2034 periods and used as forcing for an ensemble of numerical Gill simulations with varying values for ϵ. The correlation coefficient between the upper tropospheric layer thickness change from the respective CMIP6 model and all corresponding Gill simulations is given in Figure B.8 for the June, July, August (JJA) and December, January, February (DJF) seasons. For every CMIP6 model bar two in the DJF case, a corresponding Gill simulation with a layer thickness correlation coefficient higher than 0.5 exists, which we take as the threshold to indicate a skilful Gill simulation. For JJA results are overall similar, as there are only 4 CMIP6 models for which a skilful Gill simulation does not exist. In most instances, the $\epsilon = 0.1$ simulation (shown as orange dot) appears at the upper end of the distribution. For annual means (not shown) correlations are worse, although the Gill model is linear and the sum of the terms for individual seasons should be equivalent to the annual mean forcing. This suggests that the processes represented by the dissipation terms vary seasonally (Bao et al., 2022), and thus an annual mean dissipation term is less skilful at describing the relevant mechanisms. Similar to the PJ results, the 700-200hPa layer thickness shows smaller correlations, and for only

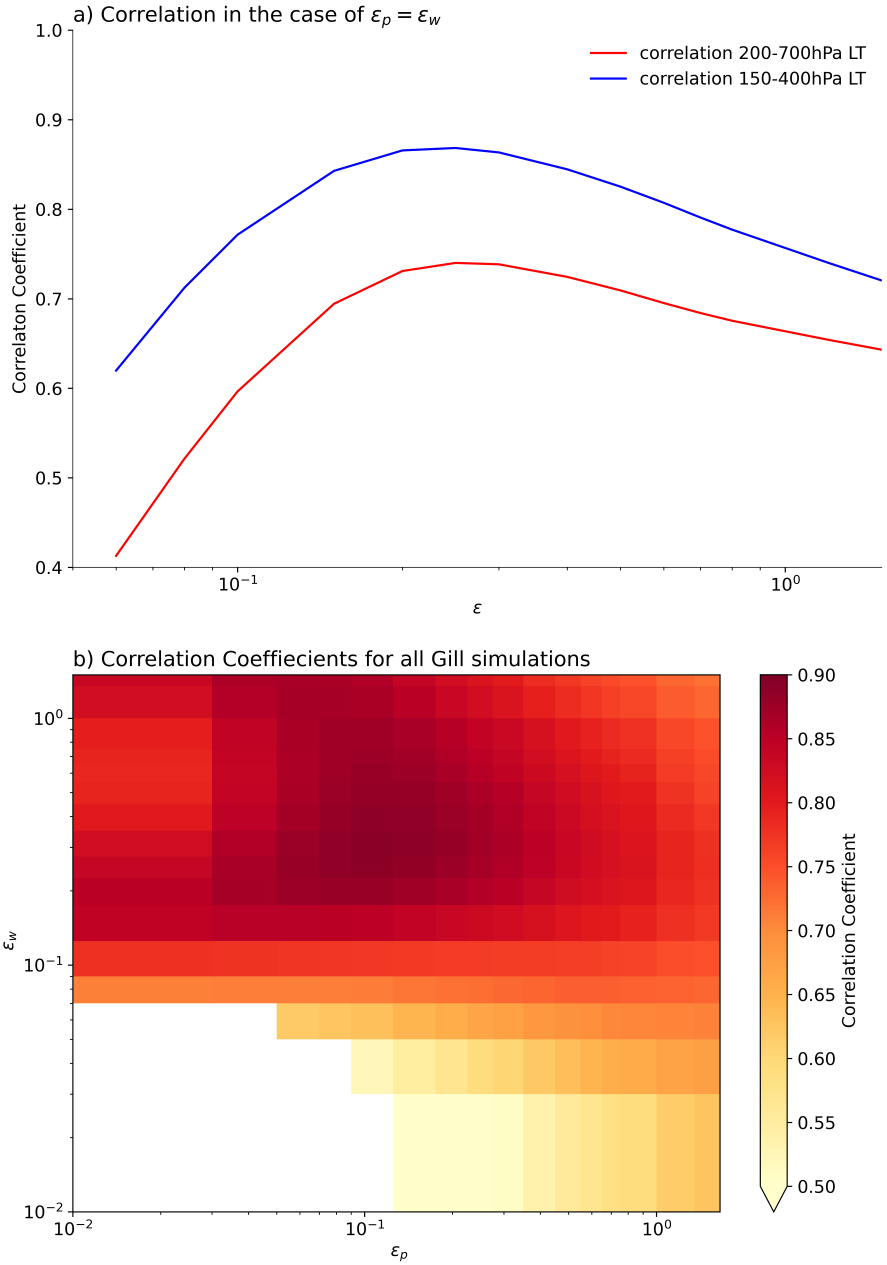

Figure B.6: Correlation coefficient between the PJ layer thickness and Gill simulations forced by precipitation changes. a) Correlation between 700-200 hPa and 400-150 hPa layer thickness changes in the PJ simulation and the Gill simulation for the case of $\epsilon_p = \epsilon_w$. b) Correlation coefficients between PJ 400-150 hPa layer thickness changes and the Gill simulation for all cases of ϵ_p and ϵ_w. White space denotes simulations that did not converge and thus are not considered. Correlations are calculated from 20°S to 10°N, since the northern hemisphere is the winter hemisphere.

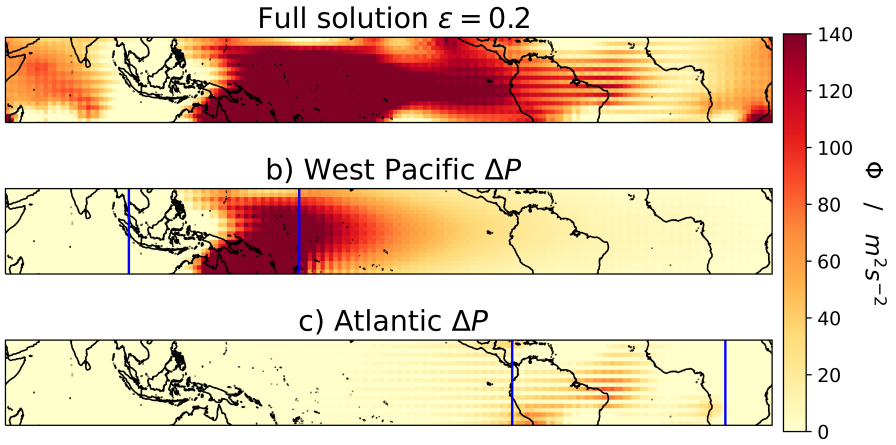

Figure B.7: Numerical Gill simulations forced by precipitation changes over the whole tropics (a), precipitation changes only in the West Pacific (100 to 180°E, marked by blue lines, panel b) and Atlantic (-80 to 20 °E, marked by blue lines, panel c) precipitation changes. All simulations are done with $\epsilon_p = \epsilon_w = 0.2$.

about half of the CMIP6 models a Gill simulation with a correlation larger than 0.5 exists (not shown).

Finally, we use the Gill simulations of the CMIP6 ensemble to assess which is the most skilful value for ϵ to simulate upper tropospheric warming (Figure B.9). The values of ϵ_p that achieve the highest correlation generally lie between 0.02 (corresponding to a dissipation timescale of 10 days) and 0.3 (18 hours). The ϵ_w distribution seems to center around slightly smaller values of 0.02 (10 days) to 0.1 (2 days). The distribution of cases with highest mutual information instead of the highest Pearson correlation coefficient is very similar. Lin et al., 2008 discussed eddy momentum flux and advection as possible processes that are parameterised by ϵ_w which have equivalent dissipation timescales of 5 to 10 days, and this is in agreement with most CMIP6 models here, although some show slightly smaller dissipation timescales (i.e. higher values of ϵ_w). In the PJ simulations the highest correlations are achieved between $\epsilon_w = 0.2$ and $\epsilon_w = 0.5$, which is at the higher end of the ϵ_w distribution for the CMIP6 models. Whether this is just a statistical outlier, or due to a fundamental difference between CMIP-type models and the storm resolving model is unclear. In the case of ϵ_p, radiative cooling, which acts on a timescale of a couple of days, seems represented with a realistic magnitude, although the range of optimal ϵ_p is quite large. Horizontal temperature advection, here represented through $\epsilon_p \Phi$, has also been shown to have a substantial contribution to the thermodynamic equation in some parts of the upper troposphere (Bao et al., 2022). The distribution of the most skilful thermal dissipation values also shows a considerable seasonality, again highlighting that the underlying processes represented through $\epsilon_p \Phi$ vary seasonally.

In the case of no thermal dissipation $\epsilon_p = 0$, for almost all CMIP6 models there is no corresponding Gill simulation that converges (not shown). We also tested simulations for $\epsilon_p = 0$ that have a zonally compensated forcing, which has been interpreted as the WTG configuration of the Gill model (Bretherton and Sobel, 2003), because in this configuration the thermal dissipation is implicitly included in Q and does not depend on Φ. In this case the simulations still usually only converge for $\epsilon_w \geq 0.1$. There is no CMIP6 model for which a corresponding Gill simulation in the WTG configuration shows the highest correlation.

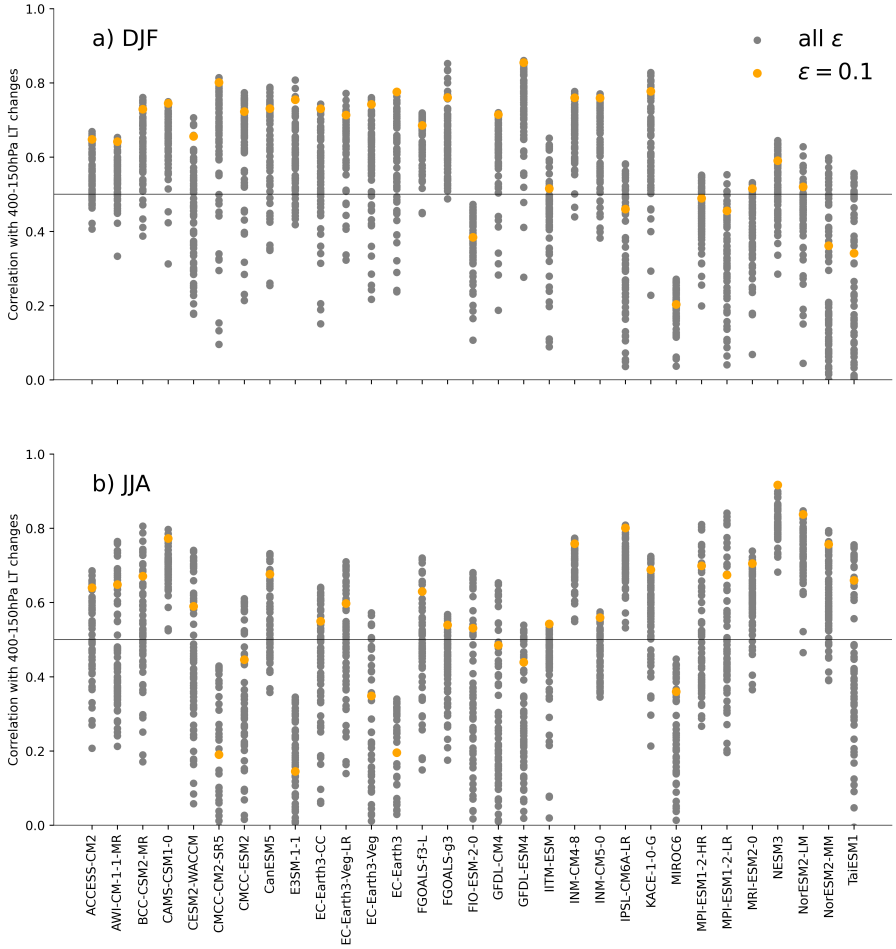

Figure B.8: Correlation of Gill simulations for a range of ϵ_p and ϵ_w values with the 400-150 hPa layer thickness anomalies in every CMIP6 SSP585 model (grey dots). Orange dots show the simulations with $\epsilon_p = \epsilon_w = 0.1$. Results are shown for the December, January, February (DJF, a) period and the June, July, August (JJA, b) period. Correlations are calculated for 20N-10S for JJA and 10N-20S for DJF.

The fact that there are a range of suitable values for ϵ points towards different physics and different large scale momentum balances in the CMIP6 models. We conclude that the best estimate for the thermal dissipation timescale is approximately 1-5 days and for the momentum dissipation timescale 2-10 days, which is realistic (Lin et al., 2008), further increasing our confidence in the patterns produced by the Gill model. The original values of $\epsilon = 0.1$ (2 days) used by Gill, 1980 are a good first estimate.

B.5 DISCUSSION AND CONCLUSION

Climate model projections of tropical upper tropospheric warming, while broadly uniform, show horizontal differences of 2 K or more, which could have implications for different aspects of tropical circulation (Sohn et al., 2016; Trabing et al., 2019). We show that SST changes trigger both changes in precipitation and circulation which in turn shape the upper tropospheric warming pattern. We demonstrate this causal mechanism by forcing a numerical Gill model with precipitation changes and thereby reproduce the different warming patterns across different models. Thus, the leading order balance that is responsible for the warming pattern is given by the Gill model. The dissipation term

controls how localised the response to convective heating is and thereby determines a basin of influence. The momentum dissipation in particular helps to sustain layer thickness gradients at the equator. In CMIP6 models the optimal value of ϵ corresponds to dissipation time scales of 1-10 days, implying different large scale momentum balances across CMIP6 models. Although the dissipation is a crude parameterisation for processes like advection, eddy momentum flux (Sardeshmukh and Held, 1984; Lin et al., 2008) and radiative cooling, it is essential for reproducing the main features of the warming pattern, illustrating that these processes are important for shaping the tropospheric warming pattern.

While the overall signal is well reproduced by the simple Gill model, there are certain limitations: There is no vertical dimension, and thus the convective heating is assumed to be evenly distributed across the layer. However, some of the convective heating changes might be more relevant for the mid- and lower troposphere, in the Indian ocean for example the 700-200 hPa layer thickness changes in the PJ simulations indicate a stronger relative increase compared to the 400-150 hPa case. This is also reproduced in the Gill simulations to some extent (the $\epsilon = 1.2$ case in Figure B.5), suggesting a stronger influence of mid-level convection in this region. Furthermore, the dissipation parameter likely varies horizontally across the domain, which could explain why some features of the warming pattern are more localised in some areas (like the Atlantic in the PJ simulations) and more "smeared out" (i.e. a less dissipated wave signal) in other areas. Adding more complexity, like including an advection term, or more realistic radiative cooling, could improve results even further but defeats the purpose of understanding the leading order balance. For some cases, the values for ϵ_w are slightly larger (i.e. represent shorter dissipation timescales) compared to the results of Lin et al., 2008, but it is not clear whether this is due to the inadequacy of our method, due to biases in CMIP6 models, or due to biases in the reanalysis data used by Lin et al., 2008. The circulation produced by the Gill model also matches the climate models' circulation changes (in this case the wind shear between 400 hPa and 150 hPa, not shown) well, although correlations are slightly lower compared to those of the layer thickness changes. Climate models often show jet-like anomalies of zonal wind in the upper troposphere that are related to extratropical geopotential changes (Rotstayn et al., 2013), which the Gill model cannot capture.In addition, vertical momentum transport through convection acts as a torque and thereby can have substantial impacts on upper tropospheric circulation (Shaw and Boos, 2012), which is likely not adequately represented by the dissipation parameters here.

Gill simulations using the WTG configuration of $\epsilon_p = 0$, with a zonally compensated forcing (Bretherton and Sobel, 2003), do not perform well overall. However, because these simulations only converge for high enough ϵ_w, they are only meaningful to some degree. In any case, the purpose of the WTG framework is not to study temperature gradients (or warming gradients) themselves, but instead facilitate the simulation and understanding of other aspects of tropical circulation [e.g. Bretherton and Sobel, 2002], and thus it is not surprising that this configuration might not work well. In fact, in the upper troposphere, horizontal temperature advection can also substantially impact temperatures in some regions (Bao et al., 2022), which would here be represented by $\epsilon_p \Phi$. A more extreme version of assuming temperature gradients are weak, is to set the layer thickness gradients to zero in the momentum equations. In that case the winds quickly dissipate and the thermodynamic equation is left with the balance $\Phi \epsilon_p = Q$, which means that the warming pattern coincides with the pattern of forcing Q.

Finally, if the precipitation changes were mainly of thermodynamic nature, then the strongest warming would happen roughly over the existing convective hotspots and

should be easy to predict. This can also be illustrated in the thermodynamic equation in the Gill model: If the circulation did not change, which means $u = v = 0$ in our configuration of the Gill model, and precipitation changes were purely related to thermodynamic processes, then the warming pattern Φ would be given directly by the forcing Q (assuming steady state): $\Phi\epsilon_p = Q$, where Q should be only derived from ΔP_{th}. This case results in a correlation of 0.03 between the Gill layer thickness and the layer thickness in the PJ simulations, illustrating the need to understand the coupling of precipitation and circulation for the warming pattern. These dynamical precipitation changes are strongly influenced by the SST pattern, which in turn differs considerably across climate models, and consequently upper tropospheric warming patterns also differ across climate models. This makes the problem more complex but is in agreement with past studies that have related SSTs (and their coupling to convection) to mean upper tropospheric warming (Fueglistaler et al., 2015; Tuel, 2019) and the local cooling in the upper tropospheric West Pacific in recent decades (Kamae et al., 2015). While climate models still have considerable problems simulating realistic tropical SSTs and precipitation, with our study we demonstrate that once climate models improve this aspect of tropical climate, projections of upper tropospheric warming patterns should also improve and become more consistent across different models.

ACKNOWLEDGEMENTS

The authors would like to thank C. Stephan, J. Bao and G. Datseris for valuable discussion and feedback. The research is supported by public funding to the Max Planck Society. H. Schmidt acknowledges support from the German Federal Ministry of Education and Research within the SOCTOC project of the ROMIC2 programme.

DATA AVAILABILITY STATEMENT

Code to run the numerical Gill model is available here https://github.com/pkeil7/numerical_gill . CMIP6 data are available at DKRZ or from the Earth System Grid Federation (ESGF) (https://esgf-node.llnl.gov/projects/cmip6/). The perpetual January simulations are available upon request to the corresponding author paul.keil@mpiment.mpg.de or Dian Putrasahan dian.putrasahan@mpimet.mpg.de.

APPENDIX

Derivation of Thermodynamic equation

We start with the thermodynamic equation in pressure coordinates [for example equation 3.6 in Holton and Hakim, 2013], but ignore horizontal temperature advection:

$$\frac{\partial T}{\partial t} + wT\frac{\partial \ln(\theta)}{\partial p} = \overline{Q}, \tag{B.9}$$

where T is the Temperature, w is the vertical velocity, θ is potential temperature, p is the pressure, and $\overline{Q}$ is the heating rate. With $\frac{\partial \Phi}{\partial p} = -\frac{1}{\rho}$ and $p = \rho RT$, where ρ is the density and R is the gas constant one obtains

$$-\frac{\partial}{\partial t}\frac{\partial \Phi}{\partial p} - w\frac{\partial \Phi}{\partial p}\frac{\partial \ln(\theta)}{\partial p} = \frac{R\overline{Q}}{p}. \tag{B.10}$$

We evaluate this equation on a set of vertical layers (typically $p_0 = 0\,\mathrm{hPa}$, $p_1 = 250\,\mathrm{hPa}$, $p_2 = 500\,\mathrm{hPa}$, $p_3 = 750\,\mathrm{hPa}$, $p_4 = 1000\,\mathrm{hPa}$), where Φ, u and v are defined on p_1 and p_3, and w is defined on p_0, p_2 and p_4. Assuming that the stability parameter $S = \frac{\partial \Phi}{\partial p}\frac{\partial log(\theta)}{\partial p}$ and the heating rate $\overline{Q}$ are vertically constant, equation B.10 can be vertically integrated. Using the corresponding subscripts for each pressure layer one obtains

$$-\frac{\partial(\Phi_1 - \Phi_3)}{\partial t} - w_2 S(p_1 - p_3) = R\overline{Q}\ln\left(\frac{p_1}{p_3}\right). \tag{B.11}$$

We use the continuity equation

$$\nabla \cdot \mathbf{v} = -\frac{\partial w}{\partial p}, \tag{B.12}$$

and assume $w_0 = w_4 = 0$ to obtain

$$\nabla \cdot \mathbf{v_1} = \frac{w_2}{p_0 - p_2}; \quad \nabla \cdot \mathbf{v_3} = -\frac{w_2}{p_2 - p_4}. \tag{B.13}$$

This can be used to derive an expression for w_2,

$$w_2 = -\frac{\nabla \cdot (\mathbf{v_3} - \mathbf{v_1})}{\frac{1}{p_2 - p_4} + \frac{1}{p_0 - p_2}}, \tag{B.14}$$

which we substitute into equation B.11 to get the final thermodynamic equation:

$$\frac{\partial \Phi_\mathrm{d}}{\partial t} + Sa\left(\frac{\partial u_\mathrm{d}}{\partial x} + \frac{\partial v_\mathrm{d}}{\partial y}\right) = R\overline{Q}\ln\left(\frac{p_3}{p_1}\right), \tag{B.15}$$

where we define the layer thickness between the first and the third layer $\Phi_\mathrm{d} = \Phi_1 - \Phi_3$ and the wind shear $u_\mathrm{d} = u_1 - u_3$ and $v_\mathrm{d} = v_1 - v_3$. These subscripts are dropped in the main part of the manuscript. The parameter a is related to the chosen pressure levels

$$a = \frac{p_1 - p_3}{\frac{1}{p_2 - p_4} + \frac{1}{p_0 - p_2}} \tag{B.16}$$

which reduces to $a = \frac{(p_1 - p_3)^2}{2}$ for the case of equidistant layers as used in Matsuno, 1966. If not otherwise stated, we use $p_0 = 0\,\mathrm{hPa}$, $p_1 = 150\,\mathrm{hPa}$, $p_2 = 275\,\mathrm{hPa}$, $p_3 = 400\,\mathrm{hPa}$, $p_4 = 1000\,\mathrm{hPa}$, because our main focus is on the upper troposphere. For convenience we use $p_\mathrm{t} = p_1$ and $p_\mathrm{b} = p_3$ in the main manuscript.

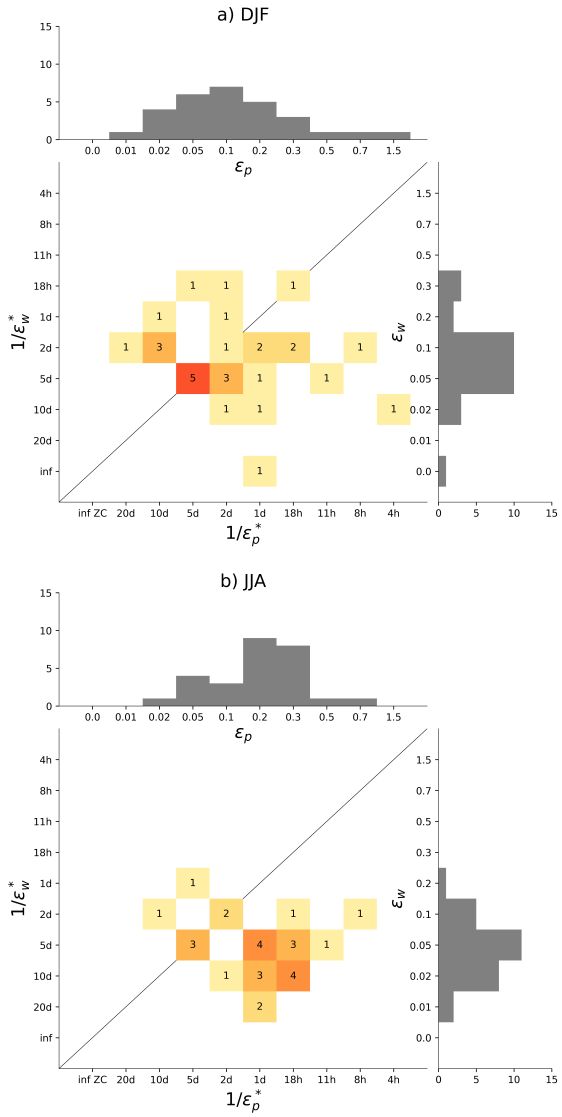

Figure B.9: Histogram of cases with highest correlation. This plot counts the amount of cases in which certain ϵ_p and ϵ_w values achieve the best correlation for every CMIP6 model, given there is a Gill simulation that exceeds a correlation of 0.5. Results are shown for the December, January, February (DJF, a) period and the June, July, August (JJA, b) period. The dissipation is shown in its non-dimensional value for the histogram plots, and the corresponding timescale (the inverse of the dimensional dissipation value ϵ^*) is given on the lowermost and leftmost axis. Here d refers to day and h to hour. "inf" refers to the infinite timescale for $\epsilon_p = 0$. For the case $\epsilon_p = 0$, the forcing Q is zonally compensated (indicated by "ZC"), following Bretherton and Sobel, 2003.

BIBLIOGRAPHY

Baba, Yuya and Marco A. Giorgetta (2019). "Tropical Variability Simulated in ICON-A With a Spectral Cumulus Parameterization". *Journal of Advances in Modeling Earth Systems* 12.1. ISSN: 19422466. DOI: 10.1029/2019MS001732.

Bao, Jiawei, Vishal Dixit, and Steven C Sherwood (2022). "Zonal temperature gradients in the tropical free troposphere". *Journal of Climate*, pp. 1–28.

Bao, Jiawei and Bjorn Stevens (2021). "The elements of the thermodynamic structure of the tropical atmosphere". *Journal of the Meteorological Society of Japan. Ser. II*.

Bao, Jiawei, Bjorn Stevens, Lukas Kluft, and Diego Jiménez-de-la-Cuesta (2021). "Changes in the tropical lapse rate due to entrainment and their impact on climate sensitivity". *Geophysical Research Letters* 48.18, e2021GL094969.

Bayr, Tobias, Dietmar Dommenget, Thomas Martin, and Scott B. Power (2014). "The eastward shift of the Walker Circulation in response to global warming and its relationship to ENSO variability". *Climate Dynamics* 43.9-10, pp. 2747–2763. ISSN: 14320894. DOI: 10.1007/s00382-014-2091-y.

Becker, Tobias and Cathy Hohenegger (2021). "Entrainment and Its Dependency on Environmental Conditions and Convective Organization in Convection-Permitting Simulations". *Monthly Weather Review* 149.2, pp. 537–550. ISSN: 0027-0644. DOI: 10.1175/mwr-d-20-0229.1.

Becker, Tobias, Bjorn Stevens, and Cathy Hohenegger (2017). "Imprint of the convective parameterization and sea-surface temperature on large-scale convective self-aggregation". *Journal of Advances in Modeling Earth Systems* 9, pp. 1488–1505.

Betts, Alan K (1982). "Saturation point analysis of moist convective overturning". *Journal of the Atmospheric Sciences* 39.7, pp. 1484–1505.

Bony, Sandrine, Gilles Bellon, Daniel Klocke, Steven Sherwood, Solange Fermepin, and Sébastien Denvil (2013). "Robust direct effect of carbon dioxide on tropical circulation and regional precipitation". *Nature Geoscience* 6.6, pp. 447–451. ISSN: 17520894. DOI: 10.1038/ngeo1799.

Bretherton, C. S. and P. K. Smolarkiewicz (1989). "Gravity waves, compensating subsidence and detrainment around cumulus clouds". *Journal of the Amospheric Sciences* 46.6, pp. 740–759. ISSN: 0022-4928. DOI: 10.1175/1520-0469(1989)046<0740:GWCSAD>2.0.CO;2.

Bretherton, Christopher S and Adam H Sobel (2002). "A simple model of a convectively coupled Walker circulation using the weak temperature gradient approximation". *Journal of climate* 15.20, pp. 2907–2920.

– (2003). "The Gill model and the weak temperature gradient approximation". *Journal of the Atmospheric Sciences* 60.2, pp. 451–460. ISSN: 00224928. DOI: 10.1175/1520-0469(2003)060<0451:TGMATW>2.0.CO;2.

Charney, Jule G (1963). "A note on the large-scale motions in the tropics". *J. Atmos. Sci.* 20, pp. 607–609.

Po-Chedley, Stephen, Benjamin D. Santer, Stephan Fueglistaler, Mark D. Zelinka, Philip J. Cameron-Smith, Jeffrey F. Painter, and Qiang Fu (2021). "Natural variability contributes to model–satellite differences in tropical tropospheric warming". *Proceedings of the National Academy of Sciences of the United States of America* 118.13, pp. 1–7. ISSN: 10916490. DOI: 10.1073/pnas.2020962118.

Po-Chedley, Stephen, Tyler J. Thorsen, and Qiang Fu (2015). "Removing diurnal cycle contamination in satellite-derived tropospheric temperatures: Understanding tropical tropospheric trend discrepancies". *Journal of Climate* 28.6, pp. 2274–2290. ISSN: 08948755. DOI: 10.1175/JCLI-D-13-00767.1.

Crueger, T., M. A. Giorgetta, R. Brokopf, M. Esch, S. Fiedler, C. Hohenegger, et al. (2018). "ICON-A, The Atmosphere Component of the ICON Earth System Model: II. Model Evaluation". *Journal of Advances in Modeling Earth Systems* 10.7, pp. 1638–1662. ISSN: 19422466. DOI: 10.1029/2017MS001233.

Datseris, George and Ulrich Parlitz (2022). *Nonlinear Dynamics: A Concise Introduction Interlaced with Code*. Springer Nature.

Dias, PL Silva, Wayne H Schubert, and Mark DeMaria (1983). "Large-scale response of the tropical atmosphere to transient convection". *J. Atmos. Sci* 40.11, pp. 2689–2707.

Emanuel, Kerry (2020). "The relevance of theory for contemporary research in atmospheres, oceans, and climate". *AGU Advances* 1.2, e2019AV000129.

Emanuel, Kerry A, J David Neelin, and Christopher S Bretherton (1994). "On large-scale circulations in convecting atmospheres". *Quarterly Journal of the Royal Meteorological Society* 120.519, pp. 1111–1143.

Eyring, Veronika, Sandrine Bony, Gerald A. Meehl, Catherine A. Senior, Bjorn Stevens, Ronald J. Stouffer, and Karl E. Taylor (2016). "Overview of the Coupled Model Intercomparison Project Phase 6 (CMIP6) experimental design and organization". *Geoscientific Model Development* 9.5, pp. 1937–1958. ISSN: 19919603. DOI: 10.5194/gmd-9-1937-2016.

Fiedler, Stephanie, Traute Crueger, Roberta D'Agostino, Karsten Peters, Tobias Becker, David Leutwyler, Laura Paccini, Jörg Burdanowitz, Stefan A Buehler, Alejandro Uribe Cortes, et al. (2020). "Simulated tropical precipitation assessed across three major phases of the coupled model intercomparison project (CMIP)". *Monthly Weather Review* 148.9, pp. 3653–3680.

Flannaghan, T. J., S. Fueglistaler, I. M. Held, S. Po-Chedley, B. Wyman, and M. Zhao (2014). "Tropical temperature trends in atmospheric general circulation model simulations and the impact of uncertainties in observed SSTs". *Journal of Geophysical Research* 119.23, pp. 13, 327–13, 337. ISSN: 21562202. DOI: 10.1002/2014JD022365.

Folkins, Ian (2002). "Origin of lapse rate changes in the upper tropical troposphere". *Journal of the Atmospheric Sciences* 59.5, pp. 992–1005. ISSN: 00224928. DOI: 10.1175/1520-0469(2002)059<0992:OOLRCI>2.0.CO;2.

Free, Melissa, Dian J. Seidel, James K. Angell, John Lanzante, Imke Durre, and Thomas C. Peterson (2005). "Radiosonde atmospheric temperature products for assessing climate (RATPAC): A new data set of large-area anomaly time series". *Journal of Geophysical Research Atmospheres* 110.22, pp. 1–12. ISSN: 01480227. DOI: 10.1029/2005JD006169.

Fu, Qiang, Syukuro Manabe, and Celeste M. Johanson (2011). "On the warming in the tropical upper troposphere: Models versus observations". *Geophysical Research Letters* 38.15, pp. 1–6. ISSN: 00948276. DOI: 10.1029/2011GL048101.

Fueglistaler, S., A. E. Dessler, T. J. Dunkerton, I. Folkins, Q. Fu, and P. W. Mote (2009). "Tropical tropopause layer". *Reviews of Geophysics* 47.1, pp. 1–31. ISSN: 87551209. DOI: 10.1029/2008RG000267.

Fueglistaler, S., C. Radley, and I. M. Held (2015). "The distribution of precipitation and the spread in tropical upper tropospheric temperature trends in CMIP5/AMIP simulations". *Geophysical Research Letters* 42.14, pp. 6000–6007. ISSN: 19448007. DOI: 10.1002/2015GL064966.

Gill, A. E. (1980). "Some simple solutions for heat-induced tropical circulation". *Quarterly Journal of the Royal Meteorological Society* 106.449, pp. 447–462. ISSN: 1477870X. DOI: 10.1002/qj.49710644905.

– (1982). "Studies of moisture effects in simple atmospheric models: The stable case". *Geophysical & Astrophysical Fluid Dynamics* 19.1-2, pp. 119–152.

Giorgetta, M. A., R. Brokopf, T. Crueger, M. Esch, S. Fiedler, J. Helmert, et al. (2018). "ICON-A, the Atmosphere Component of the ICON Earth System Model: I. Model Description". *Journal of Advances in Modeling Earth Systems* 10.7, pp. 1613–1637. ISSN: 19422466. DOI: 10.1029/2017MS001242.

Gutjahr, Oliver, Dian Putrasahan, Katja Lohmann, Johann H Jungclaus, Jin-Song von Storch, Nils Brüggemann, Helmuth Haak, and Achim Stössel (2019). "Max planck institute earth system model (MPI-ESM1. 2) for the high-resolution model intercomparison project (HighResMIP)". *Geoscientific Model Development* 12.7, pp. 3241–3281.

Haimberger, Leopold, Christina Tavolato, and Stefan Sperka (2012). "Homogenization of the global radiosonde temperature dataset through combined comparison with reanalysis background series and neighboring stations". *Journal of Climate* 25.23, pp. 8108–8131. ISSN: 08948755. DOI: 10.1175/JCLI-D-11-00668.1.

Hann, J. (1874). "Die Gesetze der Temperatur-Aenderung in aufsteigenden Luftströmungen und einige der wichtigsten Folgerungen aus denselben." *Zeitschrift der Österreichischen Gesellschaft für Meteorologie* 9, pp. 321–329.

Held, Isaac M and Brian J Soden (2006). "Robust responses of the hydrological cycle to global warming". *Journal of climate* 19.21, pp. 5686–5699.

Hersbach, Hans, Bill Bell, Paul Berrisford, Shoji Hirahara, András Horányi, Joaquín Muñoz-Sabater, et al. (2020). "The ERA5 global reanalysis". *Quarterly Journal of the Royal Meteorological Society* 146.730, pp. 1999–2049. ISSN: 1477870X. DOI: 10.1002/qj.3803.

Hertz, Heinrich (1884). "Graphische Methode zur Bestimmung der adiabatischen Zustandsänderung feucher Luft." *Meteorologische Zeitschrift* 1, pp. 421–431.

Hohenegger, Cathy, Peter Korn, Leonidas Linardakis, René Redler, Reiner Schnur, Panagiotis Adamidis, Jiawei Bao, Swantje Bastin, Milad Behravesh, Martin Bergemann, et al. (2022). "ICON-Sapphire: simulating the components of the Earth System and their interactions at kilometer and subkilometer scales". *Geoscientific Model Development Discussions*, pp. 1–42.

Holton, JR and GJ Hakim (2013). *An introduction to dynamic meteorology. Waltham, MA*. Academic Press.

Kamae, Youichi, Hideo Shiogama, Masahiro Watanabe, Masayoshi Ishii, Hiroaki Ueda, and Masahide Kimoto (2015). "Recent slowdown of tropical upper tropospheric warming associated with Pacific climate variability". *Geophysical Research Letters* 42.8, pp. 2995–3003. ISSN: 19448007. DOI: 10.1002/2015GL063608.

Kelvin, Lord (1890). "On the Convective Equilibrium of Temperature in the Atmosphere." *Read before the Literary and Philosophical Society of Manchester 1862, Published in Mathematical and Phyiscal Papers, Volume III. Elasiticity, Heat, Electro-Magnestism* Appendix E, pp. 255–260.

Lau, Ka-Ming and Hock Lim (1982). "Thermally driven motions in an equatorial β-plane: Hadley and Walker circulations during the winter monsoon". *Monthly Weather Review* 110.5, pp. 336–353.

Lee, Sukyoung, Cian Woods, and Rodrigo Caballero (2019). "Relation Between Arctic Moisture Flux and Tropical Temperature Biases in CMIP5 Simulations and Its Fin-

gerprint in RCP8.5 Projections". *Geophysical Research Letters* 46.2, pp. 1088–1096. ISSN: 19448007. DOI: 10.1029/2018GL080562.

Lin, Jia Lin, Brian E. Mapes, and Weiqing Han (2008). "What are the sources of mechanical damping in Matsuno-Gill-type models?" *Journal of Climate* 21.2, pp. 165–179. ISSN: 08948755. DOI: 10.1175/2007JCLI1546.1.

Lindzen, Richard S and Sumant Nigam (1987). "On the role of sea surface temperature gradients in forcing low-level winds and convergence in the tropics". *Journal of Atmospheric Sciences* 44.17, pp. 2418–2436.

Lu, Jianhua and Ming Cai (2010). "Quantifying contributions to polar warming amplification in an idealized coupled general circulation model". *Climate Dynamics* 34.5, pp. 669–687. ISSN: 09307575. DOI: 10.1007/s00382-009-0673-x.

Mamalakis, Antonios, Imme Ebert-Uphoff, and Elizabeth A Barnes (2022). "Neural network attribution methods for problems in geoscience: A novel synthetic benchmark dataset". *Environmental Data Science* 1.

Manabe, Syukuro and Robert F. Strickler (1964). *Thermal Equilibrium of the Atmosphere with a Convective Adjustment*.

Manabe, Syukuro and Richard T. Wetherald (1967). *Thermal Equilibrium of the Atmosphere with a Given Distribution of Relative Humidity*.

Matsuno, Taroh (1966). "Quasi-Geostrophic Motions in the Equatorial Area". *Journal of the Meteorological Society of Japan. Ser. II* 44.1, pp. 25–43. ISSN: 0026-1165. DOI: 10.2151/jmsj1965.44.1_25.

Mauritsen, Thorsten, Bjorn Stevens, Erich Roeckner, Traute Crueger, Monika Esch, Marco Giorgetta, et al. (2012). "Tuning the climate of a global model". *Journal of Advances in Modeling Earth Systems* 4.8, pp. 1–18. ISSN: 19422466. DOI: 10.1029/2012MS000154.

Mitchell, D. M., P. W. Thorne, P. A. Stott, and L. J. Gray (2013). "Revisiting the controversial issue of tropical tropospheric temperature trends". *Geophysical Research Letters* 40.11, pp. 2801–2806. ISSN: 00948276. DOI: 10.1002/grl.50465.

Miyawaki, Osamu, Zhihong Tan, Tiffany A. Shaw, and Malte F. Jansen (2020). "Quantifying Key Mechanisms That Contribute to the Deviation of the Tropical Warming Profile From a Moist Adiabat". *Geophysical Research Letters* 47.20. ISSN: 0094-8276. DOI: 10.1029/2020gl089136.

Möbis, Benjamin and Bjorn Stevens (2012). "Factors controlling the position of the Intertropical Convergence Zone on an aquaplanet". *Journal of Advances in Modeling Earth Systems* 4.11, pp. 1–16. ISSN: 19422466. DOI: 10.1029/2012MS000199.

Nordeng, T. E. (1994). "Extended version of the convective parameterization scheme at ECMWF and their impact on the mean and transient activity of the model in the tropics". *ECWF internal report*.

Oort, Abraham H (1983). *Global atmospheric circulation statistics, 1958-1973*. 14. US Department of Commerce, National Oceanic and Atmospheric Administration.

Plant, Robert S and Jun-Ichi Yano (2016). *Parameterization of atmospheric convection*. World Scientific.

Putrasahan, DA, Oliver Gutjahr, Helmut Haak, Johann H Jungclaus, Katja Lohmann, MJ Roberts, and J-S von Storch (2021). "Effect of resolving ocean eddies on the transient response of global mean surface temperature to abrupt 4xCO2 forcing". *Geophysical Research Letters* 48.8, e2020GL092049.

Reichler, Thomas and Junsu Kim (2008). "How well do coupled models simulate today's climate?" *Bulletin of the American Meteorological Society* 89.3, pp. 303–311. ISSN: 00030007. DOI: 10.1175/BAMS-89-3-303.

Retsch, MH, C Jakob, and MS Singh (2022). "Identifying Relations Between Deep Convection and the Large-Scale Atmosphere Using Explainable Artificial Intelligence". *Journal of Geophysical Research: Atmospheres* 127.3, e2021JD035388.

Rodwell, Mark J. and Brian J. Hoskins (1996). "Monsoons and the dynamics of deserts". *Quarterly Journal of the Royal Meteorological Society* 122.534, pp. 1385–1404. ISSN: 00359009. DOI: 10.1256/smsqj.53407.

Romps, David M. (2010). "A direct measure of entrainment". *Journal of the Atmospheric Sciences* 67.6, pp. 1908–1927. ISSN: 00224928. DOI: 10.1175/2010JAS3371.1.

Romps, David M. and Zhiming Kuang (2010). "Do undiluted convective plumes exist in the upper tropical troposphere?" *Journal of the Atmospheric Sciences* 67.2, pp. 468–484. ISSN: 00224928. DOI: 10.1175/2009JAS3184.1.

Rotstayn, LD, Mark Andrew Collier, Stephen John Jeffrey, J Kidston, JI Syktus, and KK Wong (2013). "Anthropogenic effects on the subtropical jet in the Southern Hemisphere: aerosols versus long-lived greenhouse gases". *Environmental Research Letters* 8.1, p. 014030.

Santer, B. D., T. M.L. Wigley, C. Mears, F. J. Wentz, S. A. Klein, D. J. Seidel, et al. (2005). "Atmospheric science: Amplification of surface temperature trends and variability in the tropical atmosphere". *Science* 309.5740, pp. 1551–1556. DOI: 10.1126/science.1114867.

Santer, Benjamin D., John C. Fyfe, Giuliana Pallotta, Gregory M. Flato, Gerald A. Meehl, Matthew H. England, et al. (2017a). "Causes of differences in model and satellite tropospheric warming rates". *Nature Geoscience* 10.7, pp. 478–485. ISSN: 17520908. DOI: 10.1038/ngeo2973.

Santer, Benjamin D., Susan Solomon, Giuliana Pallotta, Carl Mears, Stephen Po-Chedley, Qiang Fu, et al. (2017b). "Comparing tropospheric warming in climate models and satellite data". *Journal of Climate* 30.1, pp. 373–392. ISSN: 08948755. DOI: 10.1175/JCLI-D-16-0333.1.

Sardeshmukh, Prashant D and Isaac M Held (1984). "The vorticity balance in the tropical upper troposphere of a general circulation model". *Journal of the atmospheric sciences* 41.5, pp. 768–778.

Seager, Richard, Naomi Naik, and Gabriel A. Vecchi (2010). "Thermodynamic and dynamic mechanisms for large-scale changes in the hydrological cycle in response to global warming". *Journal of Climate* 23.17, pp. 4651–4668. ISSN: 08948755. DOI: 10.1175/2010JCLI3655.1.

Shaw, Tiffany A and William R Boos (2012). "The tropospheric response to tropical and subtropical zonally asymmetric torques: Analytical and idealized numerical model results". *Journal of the atmospheric sciences* 69.1, pp. 214–235.

Sherwood, S C, J R Lanzante, and C L Meyer (2005). "Radiosonde daytime biases and late-20th century warming". *Science* 309.5740, pp. 1556–1559.

Sherwood, Steven C. and Nidhi Nishant (2015). "Atmospheric changes through 2012 as shown by iteratively homogenized radiosonde temperature and wind data (IUKv2)". *Environmental Research Letters* 10.5. ISSN: 17489326. DOI: 10.1088/1748-9326/10/5/054007.

Simmons, Adrian, Cornel Soci, Julien Nicolas, Bill Bell, Paul Berrisford, Rossana Dragani, Johannes Flemming, Leo Haimberger, Sean Healy, and Hans Hersbach (2020). "Technical Memo ECMWF". January.

Singh, Martin S. and Paul A. O'Gorman (2013). "Influence of entrainment on the thermal stratification in simulations of radiative-convective equilibrium". *Geophysical Research Letters* 40, pp. 4398–4403.

Sobel, Adam H and Christopher S Bretherton (2000). "Modeling tropical precipitation in a single column". *Journal of climate* 13.24, pp. 4378–4392.

Sobel, Adam H, Johan Nilsson, and Lorenzo M Polvani (2001). "The weak temperature gradient approximation and balanced tropical moisture waves". *Journal of the atmospheric sciences* 58.23, pp. 3650–3665.

Sohn, Byung Ju, Sukyoung Lee, Eui Seok Chung, and Hwan Jin Song (2016). "The role of the dry static stability for the recent change in the Pacific Walker circulation". *Journal of Climate* 29.8, pp. 2765–2779. ISSN: 08948755. DOI: 10.1175/JCLI-D-15-0374.1.

Stevens, Bjorn, Claudia Acquistapace, Akio Hansen, Rieke Heinze, Carolin Klinger, Daniel Klocke, et al. (2020). "The added value of large-eddy and storm-resolving models for simulating clouds and precipitation". *Journal of the Meteorological Society of Japan* 98.2, pp. 395–435. ISSN: 00261165. DOI: 10.2151/jmsj.2020-021.

Stevens, Bjorn, Masaki Satoh, Ludovic Auger, Joachim Biercamp, Christopher S. Bretherton, Xi Chen, et al. (2019). "DYAMOND: the DYnamics of the Atmospheric general circulation Modeled On Non-hydrostatic Domains". *Progress in Earth and Planetary Science* 6.1. ISSN: 21974284. DOI: 10.1186/s40645-019-0304-z.

Stevens, Bjorn and A Pier Siebesma (2020). *Clouds as Fluids*. Cambridge University Press. DOI: 10.1017/9781107447738.003.

Stone, P. H. and J. H. Carlson (1979). *Atmospheric lapse rate regimes and their parameterization*. DOI: 10.1175/1520-0469(1979)036<0415:ALRRAT>2.0.CO;2.

Suárez-Gutiérrez, Laura, Chao Li, Peter W. Thorne, and Jochem Marotzke (2017). "Internal variability in simulated and observed tropical tropospheric temperature trends". *Geophysical Research Letters* 44.11, pp. 5709–5719. ISSN: 19448007. DOI: 10.1002/2017GL073798.

Thorne, Peter W., John R. Lanzante, Thomas C. Peterson, Dian J. Seidel, and Keith P. Shine (2011). "Tropospheric temperature trends: History of an ongoing controversy". *Wiley Interdisciplinary Reviews: Climate Change* 2.1, pp. 66–88. ISSN: 17577799. DOI: 10.1002/wcc.80.

Thorne, Peter W., D. E. Parker, B. D. Santer, M. P. McCarthy, D. M.H. Sexton, M. J. Webb, J. M. Murphy, M. Collins, H. A. Titchner, and G. S. Jones (2007). "Tropical vertical temperature trends: A real discrepancy?" *Geophysical Research Letters* 34.16, pp. 1–5. ISSN: 00948276. DOI: 10.1029/2007GL029875.

Thorne, Peter W., David E. Parker, Simon F.B. Tett, Phil D. Jones, Mark McCarthy, Holly Coleman, and Philip Brohan (2005). "Revisiting radiosonde upper air temperatures from 1958 to 2002". *Journal of Geophysical Research D: Atmospheres* 110.18, pp. 1–17. ISSN: 01480227. DOI: 10.1029/2004JD005753.

Tiedtke, M. (1989). *A comprehensive mass flux scheme for cumulus parameterization in large-scale models*. DOI: 10.1175/1520-0493(1989)117<1779:ACMFSF>2.0.CO;2.

Trabing, Benjamin C., Michael M. Bell, and Bonnie R. Brown (2019). "Impacts of radiation and upper-tropospheric temperatures on tropical cyclone structure and intensity". *Journal of the Atmospheric Sciences* 76.1, pp. 135–153. ISSN: 15200469. DOI: 10.1175/JAS-D-18-0165.1.

Tuel, A. (2019). "Explaining Differences Between Recent Model and Satellite Tropospheric Warming Rates With Tropical SSTs". *Geophysical Research Letters* 46.15, pp. 9023–9030. ISSN: 19448007. DOI: 10.1029/2019GL083994.

Webster, Peter J (1972). "Response of the tropical atmosphere to local, steady forcing". *Monthly Weather Review* 100.7, pp. 518–541.

Wu, Guoxiong, Bian He, Yimin Liu, Qing Bao, and Rongcai Ren (2015). "Location and variation of the summertime upper-troposphere temperature maximum over South

Asia". *Climate Dynamics* 45.9-10, pp. 2757–2774. ISSN: 14320894. DOI: 10.1007/s00382-015-2506-4. URL: http://dx.doi.org/10.1007/s00382-015-2506-4.

Wu, Yutian, Mingfang Ting, Richard Seager, Huei Ping Huang, and Mark A. Cane (2011). "Changes in storm tracks and energy transports in a warmer climate simulated by the GFDL CM2.1 model". *Climate Dynamics* 37.1, pp. 53–72. DOI: 10.1007/s00382-010-0776-4.

Xu, Kuan-Man and Kerry A Emanuel (1989). "Is the tropical atmosphere conditionally unstable?" *Monthly Weather Review* 117.7, pp. 1471–1479.

Zelinka, Mark D. and Dennis L. Hartmann (2010). "Why is longwave cloud feedback positive?" *Journal of Geophysical Research Atmospheres* 115.16, pp. 1–16. ISSN: 01480227. DOI: 10.1029/2010JD013817.

Zhou, Chunlüe, Junhong Wang, Aiguo Dai, and Peter W. Thorne (2021). "A new approach to homogenize global subdaily radiosonde temperature data from 1958 to 2018". *Journal of Climate* 34.3, pp. 1163–1183. ISSN: 08948755. DOI: 10.1175/JCLI-D-20-0352.1.

Zhou, Wenyu and Shang Ping Xie (2019). "A conceptual spectral plume model for understanding tropical temperature profile and convective updraft velocities". *Journal of the Atmospheric Sciences* 76.9, pp. 2801–2814. ISSN: 15200469. DOI: 10.1175/JAS-D-18-0330.1.

VERSICHERUNG AN EIDES STATT

Hiermit erkläre ich an Eides statt, dass ich die vorliegende Dissertationsschrift selbst verfasst und keine anderen als die angegebenen Quellen und Hilfsmittel benutzt habe

Hamburg, 7. Oktober 2022

Paul Peter Keil

Hinweis / Reference

Die gesamten Veröffentlichungen in der Publikationsreihe des MPI-M
„Berichte zur Erdsystemforschung / Reports on Earth System Science“,
ISSN 1614-1199

sind über die Internetseiten des Max-Planck-Instituts für Meteorologie erhältlich:
https://mpimet.mpg.de/forschung/publikationen

All the publications in the series of the MPI -M
„Berichte zur Erdsystemforschung / Reports on Earth System Science“,
ISSN 1614-1199

are available on the website of the Max Planck Institute for Meteorology:
https://mpimet.mpg.de/en/research/publications